DE-4898-F

Final Report
PERIOD September 1980 — March 1982

Ceramic Heat Exchanger Technology Development

Prepared for the United States
Department of Energy

SOLAR
TURBINES
INCORPORATED

Printed in the United States of America

Available from

National Technical Information Service
U. S. Department of Commerce
5285 Port Royal Road
Springfield, Virginia 22161
Price: Printed Copy $_____; Microfische $2.25

DE-4898-F

Final Report
PERIOD September 1980 — March 1982

Ceramic Heat Exchanger Technology Development

Michael E. Ward
Alan H. Campbell

Prepared for the United States
Department of Energy
Under Contract No. DE-ACOI-80ETB712

SR82-R-4553-30
Date Published Nov 1982

SOLAR
TURBINES
INCORPORATED
SUBSIDIARY OF CATERPILLAR TRACTOR CO.
P.O. Box 80966, San Diego, CA 92138

50272-101

REPORT DOCUMENTATION PAGE	1. REPORT NO. DE-4898-F	2.	3. Recipient's Accession No.

4. Title and Subtitle

CERAMIC HEAT EXCHANGER TECHNOLOGY DEVELOPMENT

5. Report Date
November 1982

6.

7. Author(s)
Michael E. Ward and Alan H. Campbell

8. Performing Organization Rept. No.
SR82-R-4898-30

9. Performing Organization Name and Address
Solar Turbines Incorporated
2200 Pacific Highway
San Diego, California 192138

10. Project/Task/Work Unit No.

11. Contract(C) or Grant(G) No.
(C)DE-AC01-80ET-13712
(G)

12. Sponsoring Organization Name and Address
U.S. Department of Energy
1000 Independence Avenue, S.W.
Washington, DC 20582

13. Type of Report & Period Covered
Final
Sept. 1980-March 1982

14.

15. Supplementary Notes
DOE Project Manger, Stanley J. Dapkunas
Fossil Energy Division (GTN)

16. Abstract (Limit: 200 words)

Technology for pressurized, high-temperature, ceramic-tube heat exchangers is being established by materials evaluation, design, and fabrication studies followed by rig tests. Candidate ceramic materials have been surveyed for strength, environmental stability with coal ash, and other design properties. Design and fabrication studies of joining methods were responsible for selection of the chosen heat exchanger configuration. A full-length, twenty-eight tube, 4.56 m (15 ft) ceramic-tube heat exchanger with a 11.43 cm (4.5 in.) diameter ceramic header has been successfully tested with a 1505 K (2250°F) outlet temperature at 689 kPa (100 psi). Hot side gas temperature during this test was 1643 K (2500°F). This module has been operated for approximately 125 hours.

17. Document Analysis a. Descriptors

Ceramic Heat Exchanger, Indirect Fired, Gas Turbine, Coal Fired Gas Turbine, Heat Transfer, Silicon Carbide

b. Identifiers/Open-Ended Terms

Ceramics, Gas Turbine, Heat Exchanger

c. COSATI Field/Group

18. Availability Statement	19. Security Class (This Report)	21. No. of Pages
RELEASE UNLIMITED	UNCLASSIFIED	96
	20. Security Class (This Page) UNCLASSIFIED	22. Price

(See ANSI-Z39.18) See Instructions on Reverse

OPTIONAL FORM 272 (4-77)
(Formerly NTIS-35)
Department of Commerce

TABLE OF CONTENTS

Section		Page
	SUMMARY	1
1	INTRODUCTION	5
2	TECHNICAL DESCRIPTION	9
	2.1 Ceramic Ball-Socket Mechanical Joint (Spherical Joint)	9
	2.1.1 Objective	9
	2.1.2 Ball and Socket Joint Tests	20
	2.1.3 Stress Model	23
	2.2 Axial Finned Tubing	23
	2.2.1 Finned Tubing	24
	2.2.2 Assumptions Inherent With Simplified Constraints	25
	2.2.3 General Differential Equation	25
	2.2.4 Longitudinal Fin of Rectangular Profile	27
	2.2.5 Longitudinal Fin of Triangular Profile	29
	2.2.6 Longitudinal Fin of Concave Parabolic Profile	30
	2.2.7 Optimum Shapes of Longitudinal Fins	31
	2.2.8 Rectangular Profile	31
	2.2.9 Triangular Profile	33
	2.2.10 Concave Parabolic Profile	33
	2.2.11 Comparison of Optimum Longitudinal Fins	34
	2.2.12 Analysis	36
	2.2.13 Discussion of Results	46
	2.2.14 Test Samples	51
	2.2.15 Conclusions	51
	2.2.16 Thermal Shock Tests	55
	2.3 Endurance Test of the Ceramic Heat Exchanger	57
	2.3.1 Test Results	66
3	CONCLUSIONS	75
	REFERENCES	77
	APPENDIX A - Fin Equations	79
	APPENDIX B - Modified Bessel Function Approximation	87
	APPENDIX C - Outside Heat Transfer Coefficient Changes With Fin/Tube Geometry	91

LIST OF FIGURES

Figure		Page
1	Indirect Exhaust Coal Fired Combined Cycle	6
2	Separately Fired Cogeneration System	7
3	Ball and Socket Joint (Maximum Angle of Rotation)	11
4	Ball and Socket Joint (Contact Area Calculation Variables)	12
5	Ball and Socket Joint (Cut Back Surfaces)	13
6	Ball and Socket Joint (Design Calculation Results)	14
7	Ball and Socket Joint (Design Calculation Results)	15
8	Ball and Socket Joint (Design Calculation Results)	15
9	Ball and Socket Joint (Design Calculation Results)	16
10	Ball and Socket Joint (Design Calculation Results)	16
11	Ball and Socket Joint (Mismatches in Radii)	17
12	Ball and Socket Joint (Solution to Mismatches in Radii)	17
13	Ball and Socket Joint (Solution to Mismatches in Radii)	18
14	Ball and Socket Joint (Solution to Mismatches in Radii)	18
15	Ball and Socket Joint (Hertzian Contact Stress)	19
16	Ball and Socket Joint (Maximum Angle of Rotation)	20
17	Ball and Socket Joint (Test Specimen)	21
18	Ball and Socket Joint (Pneumatic Controlled Grinding Fixture)	21
19	Ball and Socket Joint (Test Fixture)	22
20	Ball and Socket Joint (Socket Portion After Failure Resulting from a 11,325 kgf (25,000 lbf) Compressive Load)	22
21	Finite Element Stress Model of a Ball and Socket Joint	23

LIST OF FIGURES (Continued)

Figure		Page
22	Typical Extended Surfaces	24
23	Longitudinal Fin With Arbitrary Profile: (a) Coordinate System, (b) Fin Profile Area, (c) Fin Cross-Sectional Area	26
24	Terminology and Coodinate System, Longitudinal Fin of Rectangular Profile	27
25	Longitudinal Fin of Triangular Profile	29
26	Longitudinal Fin of Concave Parabolic Profile	30
27	Computer Model	37
28	Fin/Tube Temperature for Calculating Thermal Stresses	45
29	Thermal Stress Nomenclature	47
30	Outside Circumferential Temperature Differences as a Function of Rectangular or Triangular Longitudinal Fin Geometry	50
31	Change in Tubular Weight for Rectangular Fins	52
32	Change in Tubular Weight for Triangular Fins	53
33	Triangular Finned Test Sample	54
34	Rectangular Fin Test Sample	55
35	Square Finned Ceramic Tube (NC 430 SiC)	56
36	Triangular Finned Ceramic Tube (SC-1 SiC)	57
37	Square Finned Ceramic Tube (Thermal Shock Test Without Susceptor)	58
38	Triangular Finned Ceramic Tube (Thermal Shock Test Without Susceptor)	59
39	Square Finned Ceramic Tube (Thermal Shock Test With Susceptor)	60
40	Triangular Finned Ceramic Tube (Thermal Shock Test With Susceptor)	61
41	Square Finned Ceramic Tube (Thermal Shock Test)	62
42	Axial Counter-Flow Heat Exchanger Concept	63

LIST OF FIGURES (Continued)

Figure		Page
43	Ceramic Header	645
44	4.57 Meter (15 ft) Ceramic Tube	64
45	Metal Header (Top View)	65
46	Metal Header (Side View With Bellows)	66
47	The 4.57 Meter (15 Ft)Ceramic Tube Heat Exchanger Module	67
48	The 4.57 Meter (15 ft) Ceramic Tube Heat Exchanger Module	68
49	Initial Module Tests	69
50	Thermal Transient Plot	69
51	New Test Facility	71
52	Ceramic Heat Exchanger Endurance Test (Test Conditions)	72
53	Ceramic Header After Tests Above the Melting Point of Silicon	73
54	Ceramic Header After Tests Above the Melting Point of Silicon	74

LIST OF TABLES

Tables		Page
1	Composite Cost of Energy in $ Per Million Btu for USA	5
2	Longitudinal Fins - Properties of Optimum Fins With Simplified Constraints	35
3	Longitudinal Rectangular Fin [h_i = 85.2 w/m^2·k (15 Btu/hr ft^2 °F)]	38
4	Longitudinal Rectangular Fin [h_i = 255.5 w/m^2·k (45 Btu/hr/ft^2/°F)]	39
5	Longitudinal Rectangular Fin [h_i = 425.8 w/m^2·k (75 Btu/hr/ft^2/°F)]	40
6	Longitudinal Triangular Fin [h_i = 85.2 w/m^2·k (15 Btu/hr/ft^2/°F)]	41
7	Longitudinal Triangular Fin (h_i = 255.5 w/m^2·k (45 But/hr/ft^2/°F)]	42
8	Longitudinal Triangular Fin (h_i = 425.8 w/m^2·k (75 Btu/hr/ft^2/°F)]	43
9	Comparison of Thermal Stresses in Rectangular and Triangular Fins	48
10	Comparison of Rectangular and Triangular Fins on Heat Exchanger Matrix Weight	54

SUMMARY

Modern, high efficiency gas turbine engines have been designed to operate on clean fuels that do not cause corrosion, fouling or erosion of the hot turbine section. The range of fuels has been extended to a very limited extent by careful control or neutralization of potential corrosive agents such as sodium and vanadium. Economic factors are forcing examination of lower grade fuels.

Earlier attempts to direct-fire a gas turbine with coal were terminated in the early 1960's because of the erosion and fouling that occurred. More recent work on direct firing has been through Pressurized Fluid Bed Combustion (PFBC) where the coal is burnt in a fluidized bed with limestone to fix the sulfur to meet environmental requirements. Two factors limit the acceptability of this solution. The first is that the outlet gas temperature is limited to 1227°K (1750°F) by factors such as clinkering in the bed and sulfur capture efficiencies. The second is uncertainty that conventional cleaning by multiple cyclones will maintain adequate cleanliness on a continuous basis.

An alternative approach to firing a gas turbine with dirty fuels is indirect firing. The gas turbine's compressor discharge air is passed through one or more tubular heat exchangers (metallic, ceramic, or hybrid) fired externally by a coal combustor.

An indirect-fired gas turbine requires development and matching of a large number of components. These components would include manifolds, trim combustors, coal burners and controls. When the problem areas were examined by a critical path type of analysis, it was concluded that the ceramic heat exchanger to heat high pressure air from 977°K (1300°F) up to the turbine inlet temperature was the critical barrier to the system. It was further concluded that work on other components should not be started until a ceramic heat exchanger module had been operated to simulate the high pressure high temperature service conditions expected in an indirectly coal fired open cycle gas turbine. A tubular ceramic heat exchanger was selected as most likely to meet the range of requirements expected for a coal-fired unit.

Endurance Test of the Full Size Ceramic Heat Exchanger Module

The ceramic heat exchanger module, designed and tested for only a few hours on a previous DOE contract (EF-77-C-01-2556), was moved to a new test facility. A new outer shell was constructed with a fiber backed refractory lining. The 4.57 meter (15 ft) long ceramic tubes' ball and socket joints were refurbished. The tubes were installed in the new shell and readied for endurance testing.

The test was concluded after 118 hours. The unit was running steady with very little deviation except for what resulted from the test facility. After the system was running steady, leakage was immeasurable. The only leakage in the tube to header joints that occurred was when a thermal cycle occurred. The tube bundle would either expand or contract depending upon the thermal cycle characteristic and the metal header would not totally follow the tube bundle. This was caused by the sealing slide gates between the metal shell and the metal header. Binding in this slide gate would prevent the smooth movement of the metal header. Periodic manual adjustment of the metal header was needed during the test.

During the 118 hour endurance test, no damage to the ceramics was seen. Inspection of the header, tubing and joints after the test revealed that all were in good condition. Ceramic material temperatures, verified by radiation pyrometry, ranged from 1561°K (2350°F) for the ceramic header to 1477°K (2200°F) for the ceramic tubes at the hot end.

Ball and Socket Joints (Spherical Joints)

The objective of this analysis was to define the relevant geometric parameters required for the development of a spherical joint. A detailed analysis was made of this type of joint. Several general conclusions were made with specific recommendations. To allow for the necessary rotational movement in the joint and at the same time minimize contact stresses, a spherical diameter of 4.4 to 8.9 cm (1.75 to 3.5 in.) should be utilized. Tube ends should be ground as closely as possible to the same radii. Because of growth differences in the joint caused by temperature profiles, the radii of each mating surface should be within 0.0317 cm (0.0125 in.) for a 2.54 cm (1 in.) OD tube with a 2.54 cm (1 in.) radius. The contact point of the seat should be moved away from the edges of the socket portion of the joint. This can be accomplished by making the contour of the tube end in a three part grinding procedure. The socket portion of the joint would then have a given radius with a flat on either side. The edges between flat and curve can be smoothed by lapping. If initially the radius of the tube end is identical or nearly identical to that of the nipple, the contact point will occur near the center of the nipple seat curvature. If the respective radii grow apart with a temperature difference increase, contact should still occur far from the edges.

Sample spherical joints were manufactured for mechanical strength testing. These joints were manufactured using a pneumatic control grinding fixture. These joints were placed in a specially designed fixture to permit axial loading of the joint while internal air pressure was applied. These joints were prepared with four different spherical surfaces to investigate the effect (if any) of spherical radius on joint strength. These results were encouraging since the maximum compressive load (axial load) on any ball and socket joint in the actual heat exchanger design would not exceed 22.68 kgf (50 lbs) where the average failure load for a 2.54 cm (1 in.) radius joint in these tests was 11,340 kgf (25,000 lbs).

Axial Finned Tubing

The test module has proven that a bare tube pressurized ceramic heat exchanger is feasible. The fact that fifteen-foot long ceramic tubes had to be used to transfer the necessary heat did present some difficulties, especially in material handling. Solar recommends that the same facility be used to investigate the possibliity of a hybrid metal/ceramic tube design. The metal tubes would extend from the metal header for approximately five feet then mate directly to axial finned ceramic tubes. These ceramic axial finned tubes would extend for ten feet to a ceramic tubular header.

An investigation into possible axial finned tube geometries was completed. Two possible finned geometries were identified. A square finned tube sintered silicon carbide segment was purchased from Norton. A triangular finned tube sintered silicon carbide segment was purchased from Coors. Both axial finned ceramic tube specimens were indirectly heated with an induction coil with and without a susceptor. The square fin tube developed circumferential hairline fractures. At no time did the triangular finned tubes develop any fracture. The fractures in the square finned tube were a function of its geometry, square cornered at the fin tip and base.

Recommendations

At the conclusion of the present work of retubing the ceramic heat exchanger with axial finned tubing, Solar Turbines Incorporated feels that with the technology that the company has acquired since the early 1970's in the use of structural ceramics, Solar would be in a position to enter into a ceramic heat exchanger prototype development project ending with a proof-of-concept test of a pressurized full size ceramic heat exchanger in an environment suitable for siliconized silicon carbide materials.

1

INTRODUCTION

Modern, high efficiency gas turbine engines have been designed to operate on clean fuels that do not cause corrosion, fouling or erosion of the hot turbine section. The range of fuels has been extended to a very limited extent by careful control or neutralization of potential corrosive agents such as sodium and vanadium. Economic factors are forcing examination of lower grade fuels, as illustrated in Table 1.

Table 1

Composite Cost of Energy in $ Per Million Btu for USA
(Energy User News, March 9, 1981)

Fuel	March 1981	March 1980	% Increase
Electricity	14.40	12.48	15
Gasoline	12.63	10.32	22
Distillate oil	8.83	7.01	26
Residual oil	5.87	4.60	28
Coal	1.42	1.36	5

Noteworthy is the more rapid rise in costs of petroleum-based energy than electricity and coal; the need to broaden the range of fuels used in the gas turbine is clear.

Earlier attempts to direct fire a gas turbine with coal were terminated in the early 1960's because of the erosion and fouling that occurred. More recent work on direct firing has been through the PFBC where the coal is burnt in a fluidized bed with limestone to fix the sulfur to meet environmental requirements (Ref. 1). Two factors limit the acceptibility of this solution. The first is that the outlet gas temperature is limited to 1227°K (1750°F) by factors such as clinkering in the bed and sulfur capture efficiencies. The second is uncertainty that conventional cleaning by multiple cyclones will maintain adequate cleanliness on a continuous basis. All tests run to date have involved some cool-down of the PFBC off-gases resulting from duct losses which in turn required partial reheating by a "clean" fuel such as natural gas or diesel oil. Further, there appears to be evidence that a PFBC will be more effective in very large sizes (e.g., larger than 70 MW).

An alternate approach to firing a gas turbine with dirty fuels is indirect firing. Figure 1 shows a schematic of such a system. The gas turbine's compressor discharge air is passed through one or more tubular heat exchangers fired externally by a coal combustor. The system includes heat recovery from the exhaust by a waste heat boiler and steam turbine using a once-through cycle demonstrated at Solar Turbines Incorporated. Particular importance is attached to the operation of the "gas" turbine on clean air. Analyses suggest that at least 28°K (50°F) higher inlet temperature may be possible by avoidance of combustion pattern factors and avoidance of accelerated corrosion or fouling. After expansion through the turbine, the warm air is then used to supply the combustion air to the coal combustor. It is evident that this clean and warm air [700°K (800°F)] could be used for other purposes if desired. Figure 2 shows some of these alternatives.

Requirements of Indirect-Fired System

An indirect-fired gas turbine requires development and matching of a large number of components. These components would include manifolds, trim combustors, coal burners and controls. When the problem areas were examined by a critical path type of analysis it was concluded that the ceramic heat exchanger to heat high pressure air from 978°K (1300°F) up to the turbine inlet temperature was the critical barrier to the system. It was further concluded that work on other components should not be started until a ceramic heat exchanger module had been operated to simulate the high pressure high temperature service conditions expected in an indirectly coal fired open cycle gas turbine. A tubular ceramic heat exchanger was selected as most likely to meet the range of requirements expected for a coal-fired unit.

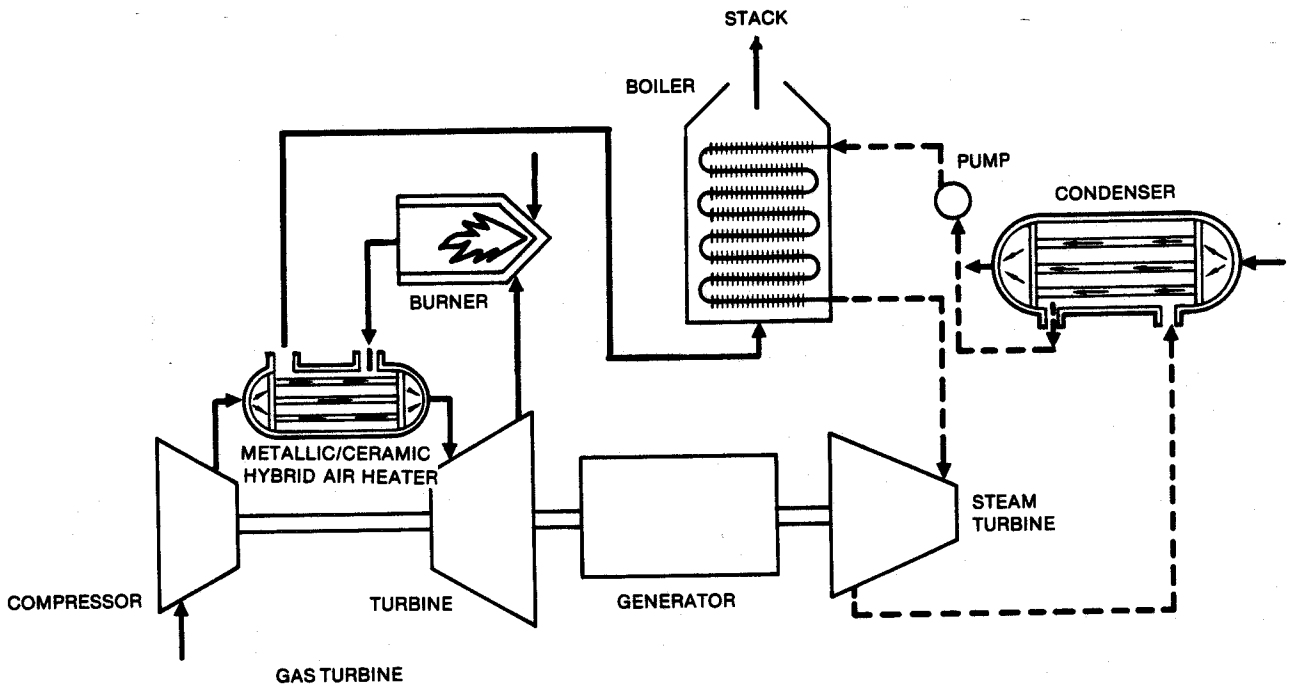

Figure 1. Indirect Exhaust Coal Fired Combined Cycle

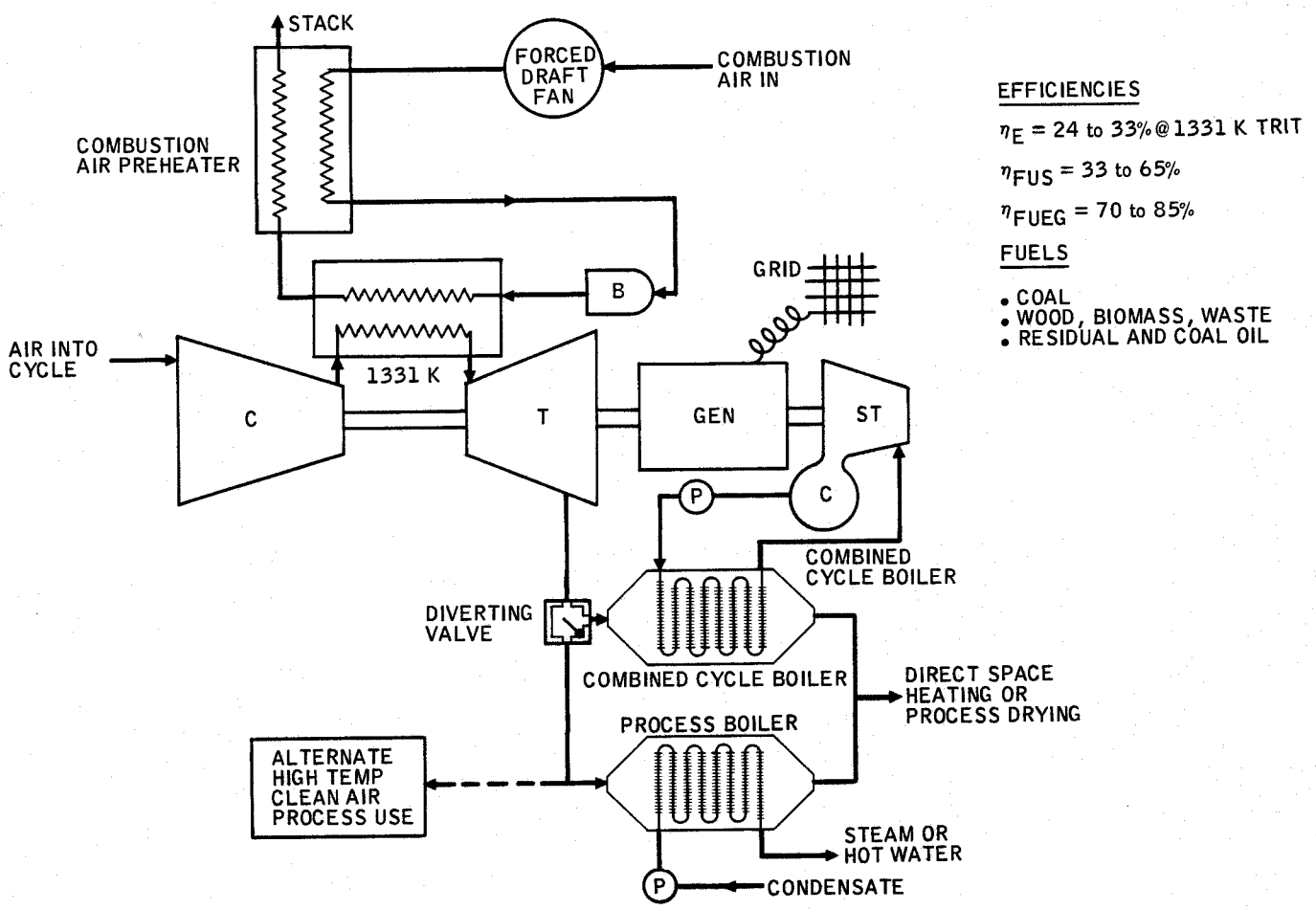

Figure 2. Separately Fired Cogeneration System

2

TECHNICAL DESCRIPTION

2.1 CERAMIC BALL-SOCKET MECHANICAL JOINT (SPHERICAL JOINT)

2.1.1 Objective

The objective of this analysis was to define the relevant geometric parameters required for the development of a spherical joint. In particular, the effects of spherical radius and tube and nipple I.D. and O.D. on joint contact area were examined.

The definition of the optimum spherical joint is one in which stresses due to compressive loading are minimized and mechanical integrity (i.e., sealing) is maintained though all motions experienced during heat exchanger operation. To evaluate joint design geometries, contact areas were calculated for several "design" angles of rotation or misalignment. The "optimum" joint would be one in which the maximum contact area could be maintained (thus minimizing contact stress) with the maximum allowable angle of rotation.

The following assumptions were made to define the spherical joint problem.

Assumptions:

1. There are two sources of misalignment prior to assembly of the tube bundle and header;

   a) Bowing in the tube created during the casting process.

   b) Angular displacement of the tube end with respect to the center span joint due to (a) or misalignment during joint brazing.

2. After assembly, tube ends and nipples match with equal spherical radii which are ground and lapped prior to assembly.

3. Movement within the joint is constrained to rotation about the spherical center of the tube end and is due only to thermal gradients in the tube bundle.

4. Sufficient compressive force exists in the joint so as to keep the spherical surfaces in contact at all times (i.e., only sliding of one surface with respect to the other takes place).

5. The purpose of the spherical joint is to allow a limited amount of rotation (to be determined in this analysis) and prevent translational motion of the tube end.

6. The following criteria were chosen for determining the maximum allowable angle of rotation of the tube end:

   a) The flow path through the tube ID cannot be obstructed or occuluded.

   b) Positive contact area between tube and nipple must be maintained.

   c) Tube ID < nipple I.D.

   d) Tube OD $\leq$ nipple O.D.

7. Tube end and nipple are at the same temperature during operation.

Calculation Procedures:

The initial calculation made was that of maximum allowable angle of rotation (identified as sigma, σ). Sigma is a function of tube ID, nipple ID and spherical radius. The maximum angle as shown in Figure 3 is reached just before the tube ID becomes occluded.

$$\sigma = \theta_2 - \theta_1 = \text{Arc sin}(Y/R) - \text{Arc sin}(X/R)$$

The calculation for contact area is shown in Figure 4.

Contact Area $\cong 2\pi Rh$ where R $\sim$ spherical radius

$h = h_1 - h_2$ where $h_1 = \sqrt{R^2 - y^2}$

$h_2 = R \sin(\theta + \phi)$

$\phi = \text{Arc cos}(D/2R)$ D $\sim$ tube diameter

It should be noted that contact area is a function of the chosen spherical radius and the design angle θ. Once θ is set the nipple must be cut back as shown in Figure 5 so there is no interference between the outer tube wall and spherical seat as rotation takes place through the chosen range of motion. Figure 5 depicts cases in which the spherical radius ranges from 1.27 to 2.54 cm (1/2 to 1 in.). For each case the contact area at maximum allowable angle of rotation ($\theta = \phi$) is shown.

A second parameter designated as sphere depth can be calculated. The sphere depth is an indicator of the grinding and lapping required to manufacture the joint. It is also an indicator of the joint's ability to withstand lateral loads which would tend to unseat the tube.

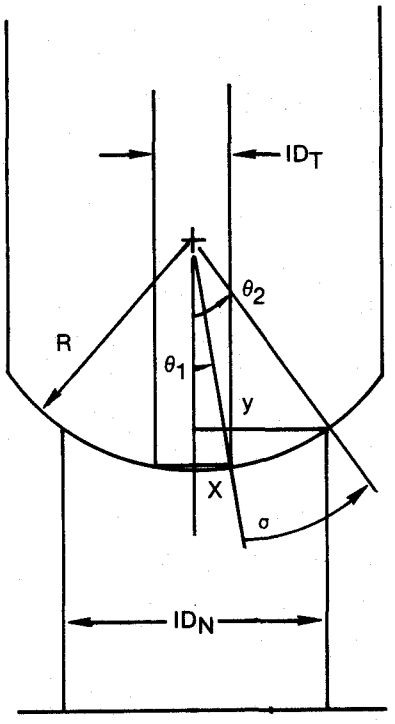

Figure 3. Ball and Socket Joint (Maximum Angle of Rotation)

Results:

The results are shown grapically in Figures 6 through 10 and can be summarized as follows:

- As the design angle of rotation increases the contact area decreases.
- For a given spherical radius, as the ratio of tube ID to nipple ID approaches one, allowable design angle decreases (contact area increases).
- As the spherical radius increases contact area decreases for any given design angle.
- Spherical depth and maximum angle of rotation also decrease as spherical radius increases.

Discussion:

The results of this analysis are based solely on geometrical factors and the constraints outlined in the section on assumptions.

As stated in Section 2.1.1, the optimum joint would have maximum contact area with large design angle of rotation. The results indicate that large design

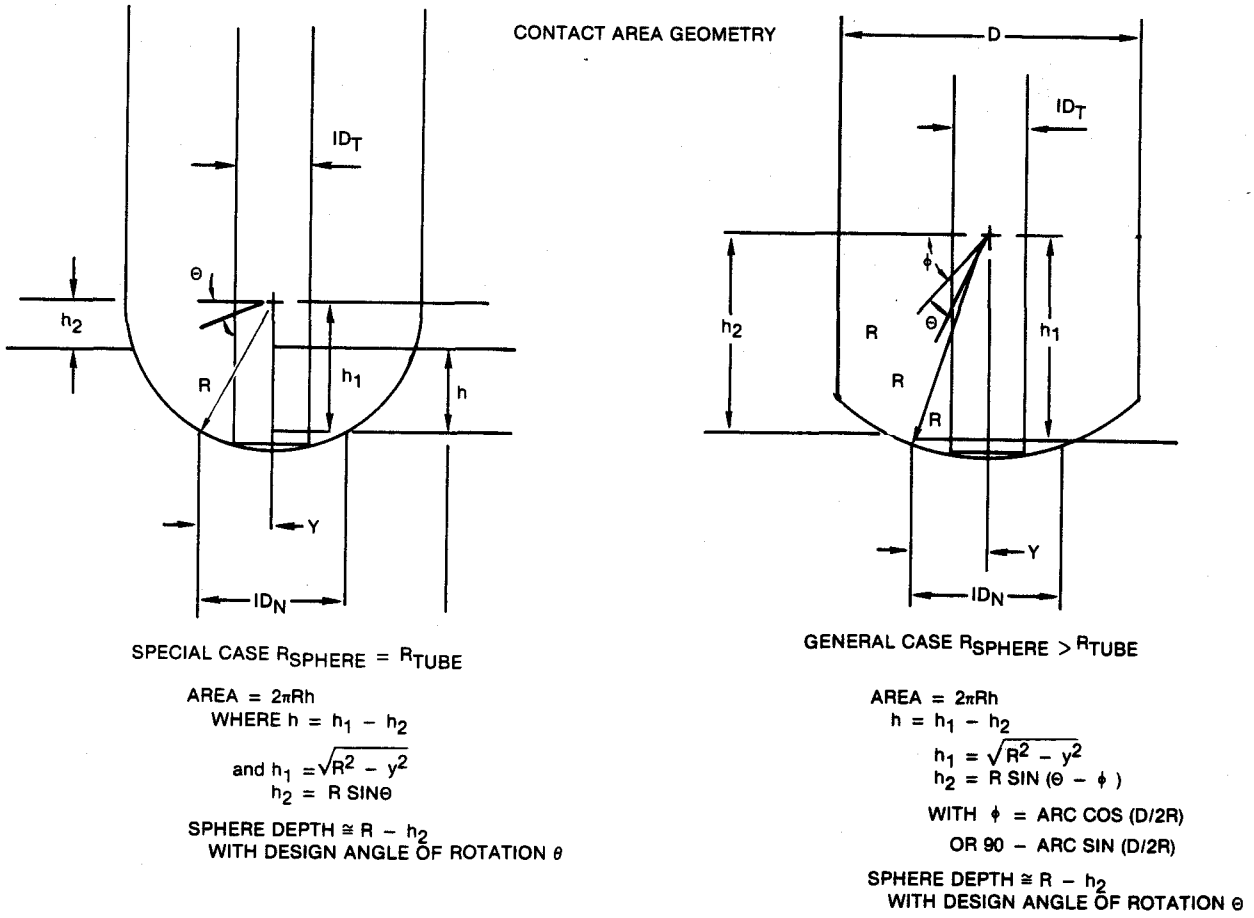

Figure 4. Ball and Socket Joint (Contact Area Calculation Variables)

angles of rotation result in a decreased contact area. Therefore, a tradeoff is required for choosing the proper joint geometry. An expected angle of rotation can be chosen and the tube and nipple IDs selected for maximum contant area or a required contact area can be calculated based on stress criteria and the tube and nipple IDs chosen for maximum allowable design angle of rotation.

At this point it may be relevant to discuss the validity of some of the initial assumptions. The most questionable assumptions are numbers 2 and 7. If the grinding and lapping operation is not "perfect" the spherical radius of the tube end will be slightly different from that of the nipple seat. This will also be the case if the temperature of the tube end is different from that of the nipple seat. The result of possible mismatches in radii are illustrated in Figure 11. In either case the result is line contact between the spherical surfaces. From the point of view of joint stability (i.e., resisting lateral loads) Case 1 is preferable. However, sealing in the joint in these cases is not dependent upon the validity of assumption No. 3. If rotation of the tube end does not take place with respect to the spherical center, the line of contact will lift off the seat during the rotation, resulting in leakage. If assumption No. 3 is valid then contact will be

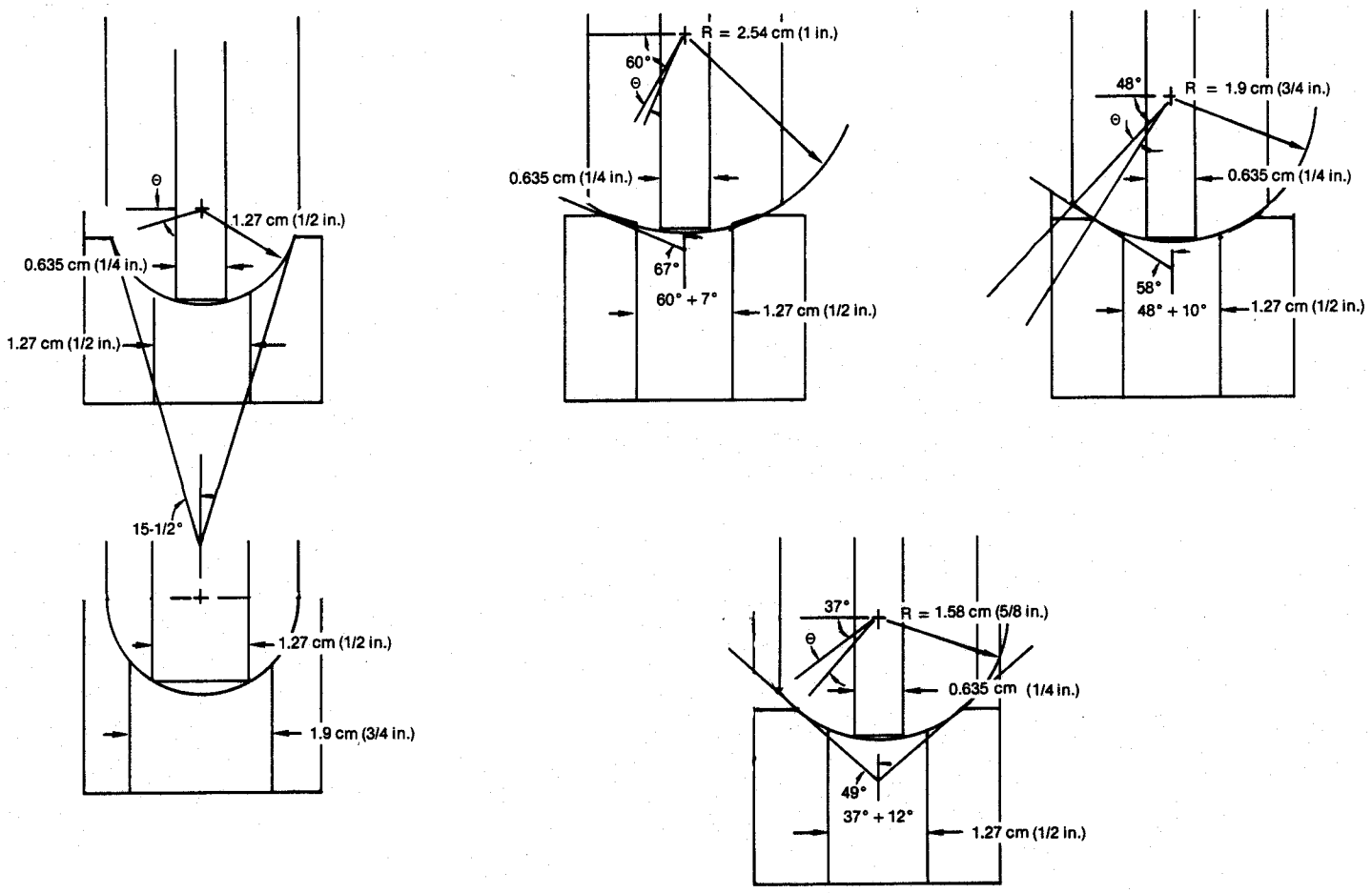

Figure 5. Ball and Socket Joint (Cut Back Surfaces)

maintained through the same allowable angle of rotation as calculated previously. (Note: Assumption No. 3 will be valid because of the compressive loading applied during assembly which locks the joint in place.) (See Assumption No. 4.)

A mismatch in radii creates a new problem in the joint design. As shown in Figure 11 (cases 1 and 2) a stress concentration will be created along the line of contact.

Because it will be very difficult to avoid this problem in practice an attempt must be made to minimize the effect of this type of contact by proper design.

The first step is to move the contact point away from the edges of the nipple. This can be accomplished by making the contour of the tube end in a three part grinding procedure. The socket portion of the joint would be configured to have a radius sealing surface with a flat on either side (Figs. 12, 13 and 14). If initially the radius of the tube end is identical or nearly identical to that of the socket, the contact point will occur near the center of the socket seat curvature. If the respective radii grow apart at temperature, contact should still occur far from the edges.

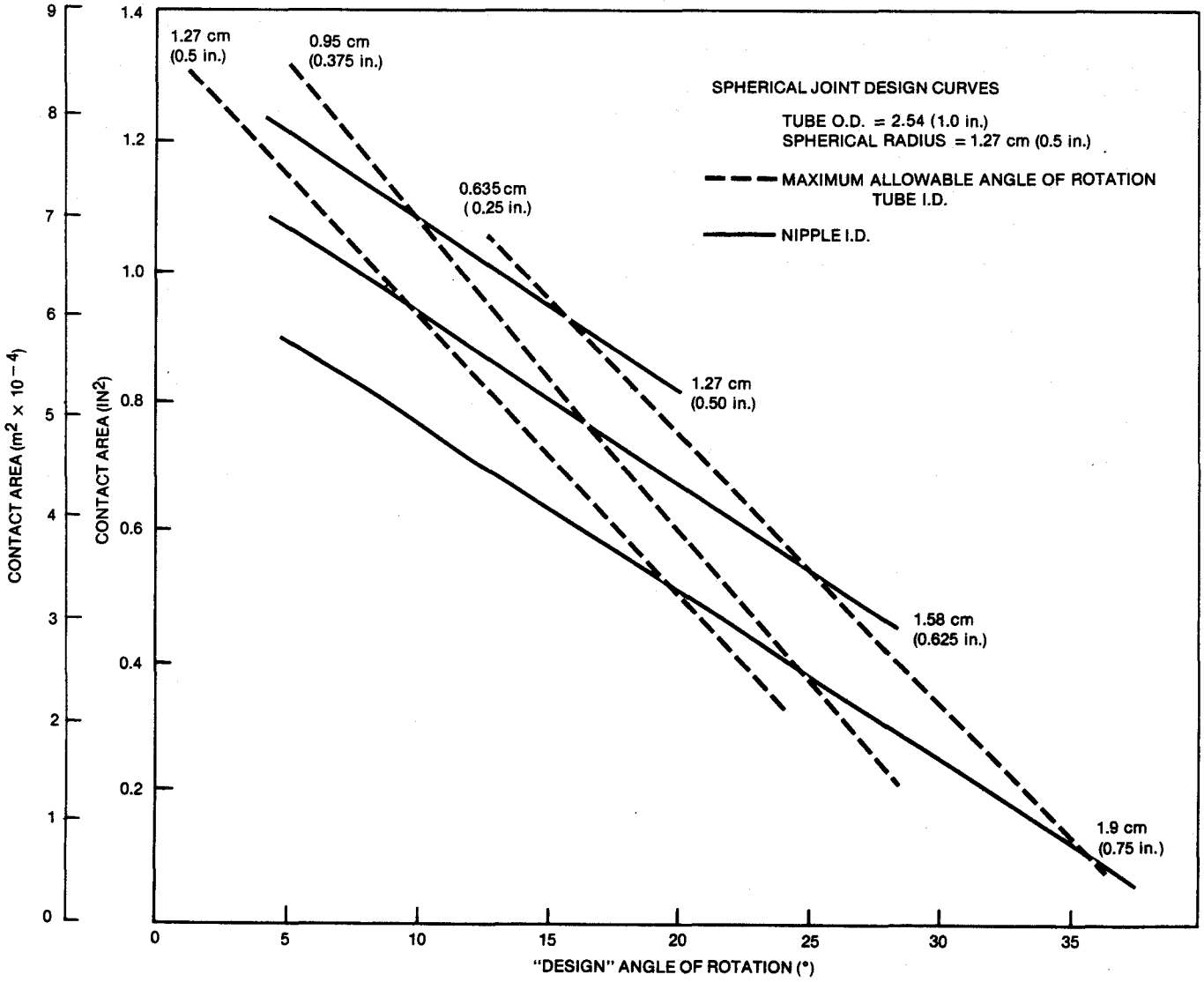

Figure 6. Ball and Socket Joint (Design Calculation Results)

With this geometry the joint stress can be approximated as the Hertzian contact stress developed with a sphere in a spherical cup. In this case, the stress level for a given material and load is a function of the spherical diameters and numerical difference in diameters as shown in Figure 15.

The following conclusions were made from this analysis:

1. Ideally if the spherical radii of tube end and socket could be made identical and would remain identical, stress levels would be very low with the designed loading (i.e., the load would bear on a contact area). In reality, radii will not be the same and line contact will exist.

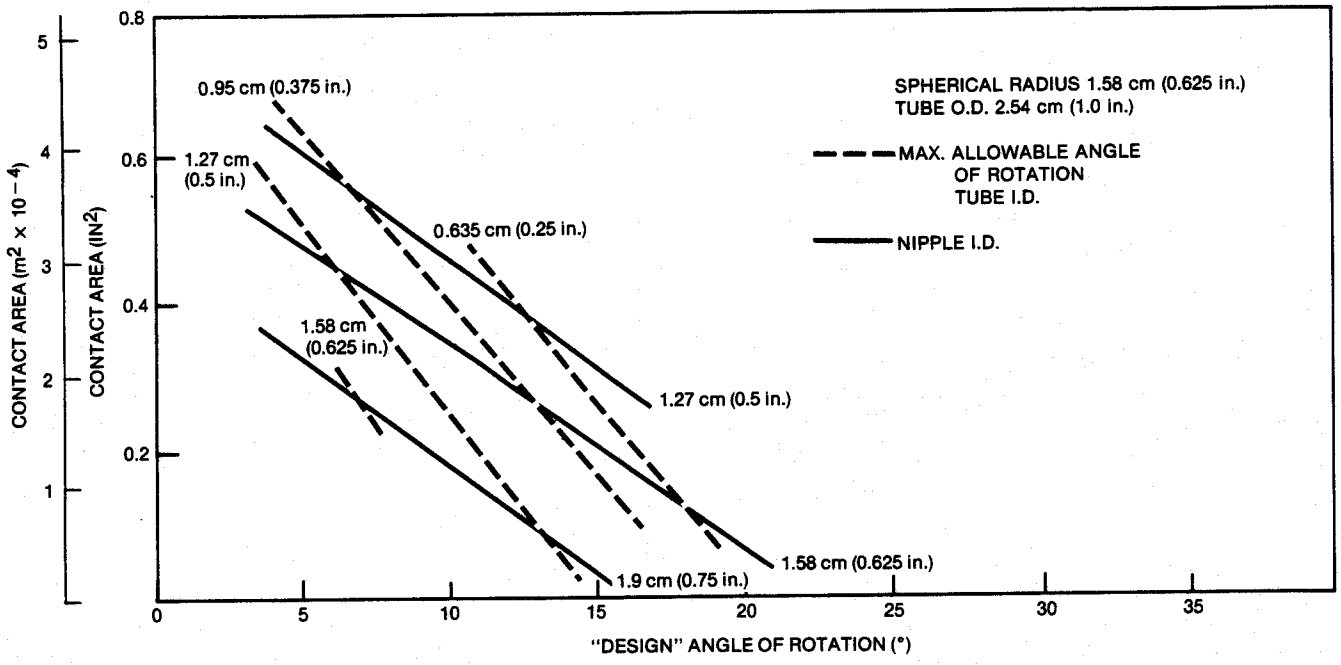

Figure 7. Ball and Socket Joint (Design Calculation Results)

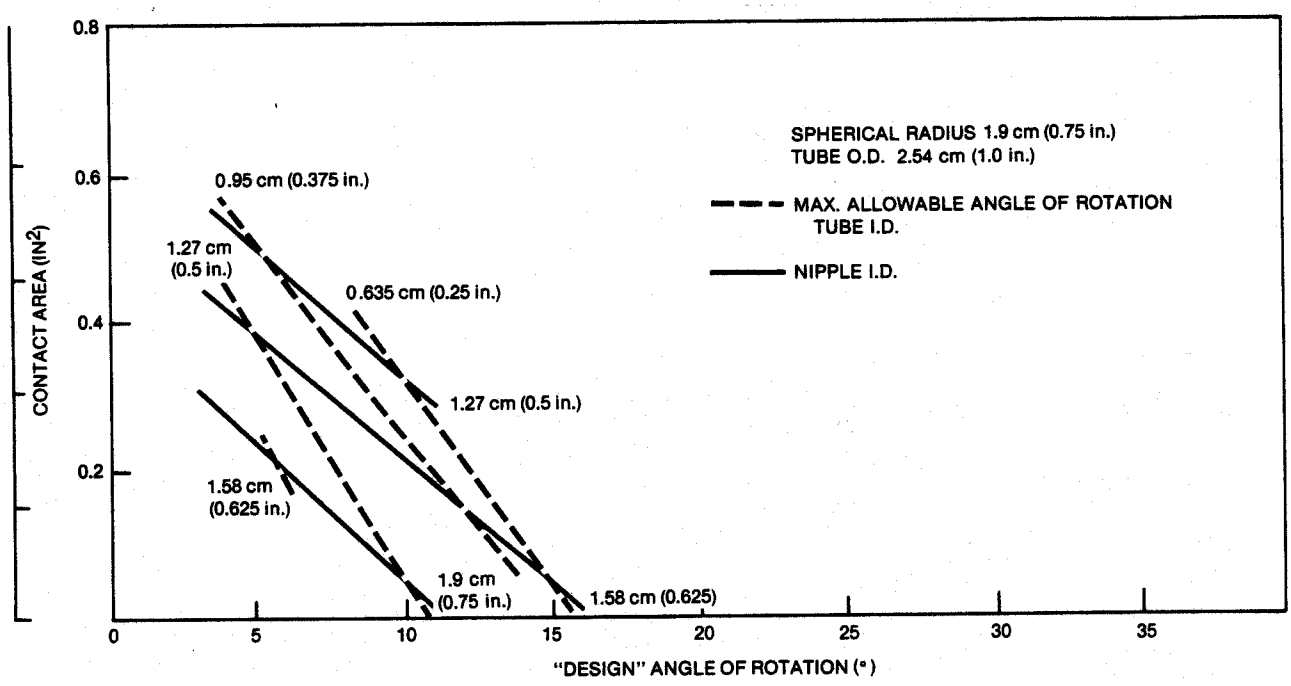

Figure 8. Ball and Socket Joint (Design Calculation Results)

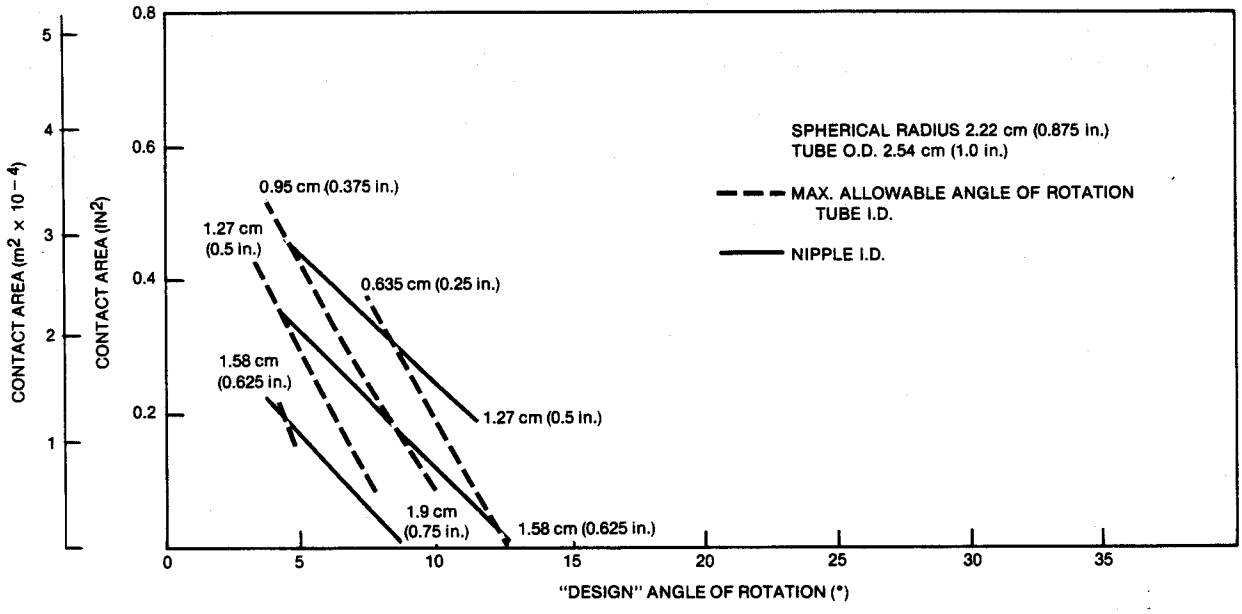

Figure 9. Ball and Socket Joint (Design Calculation Results)

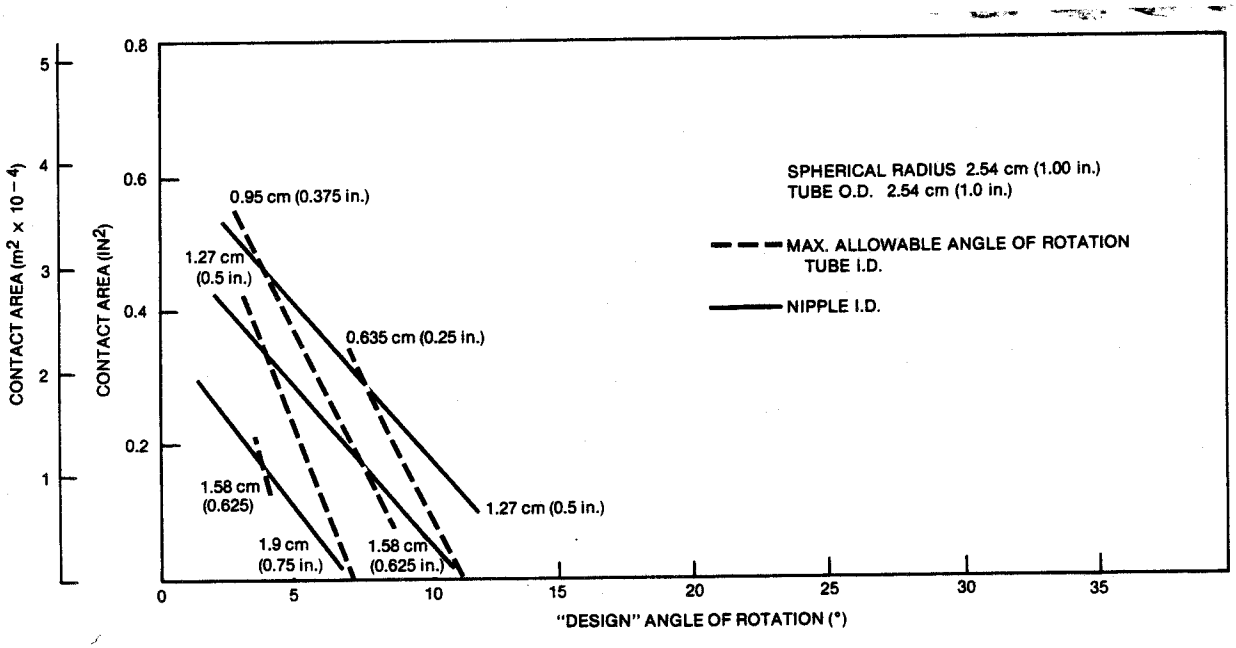

Figure 10. Ball and Socket Joint (Design Calculation Results)

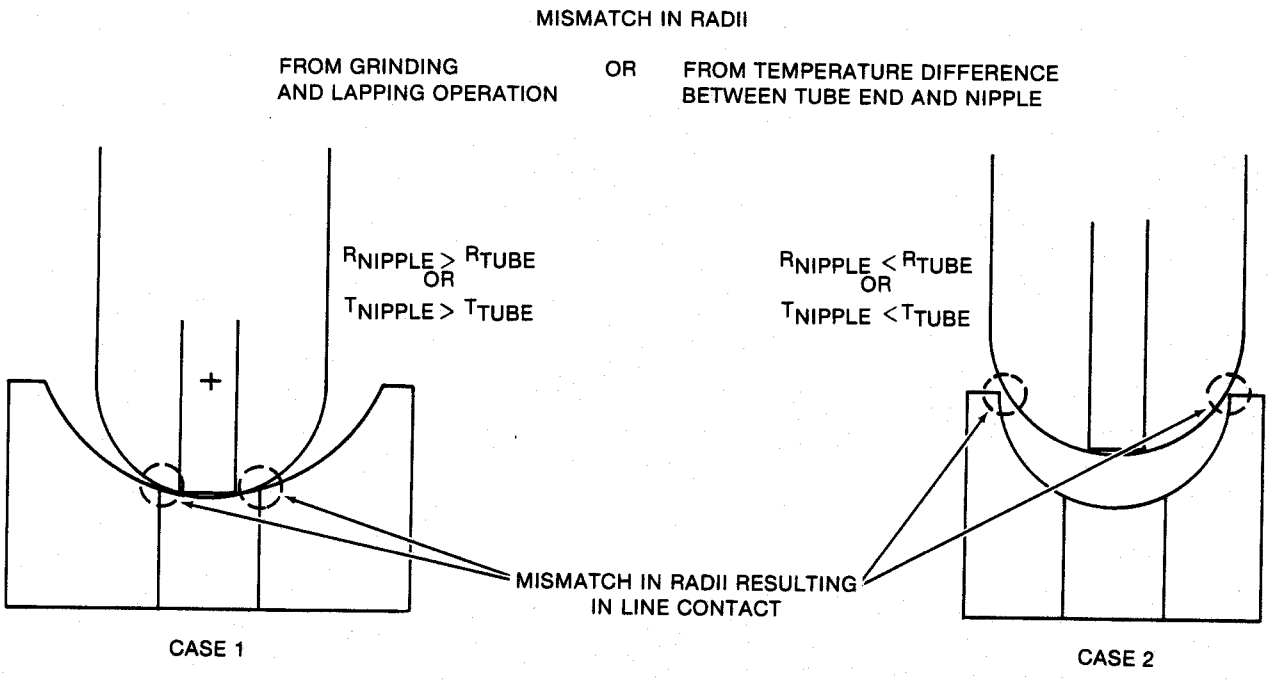

Figure 11. Ball and Socket Joint (Mismatches in Radii)

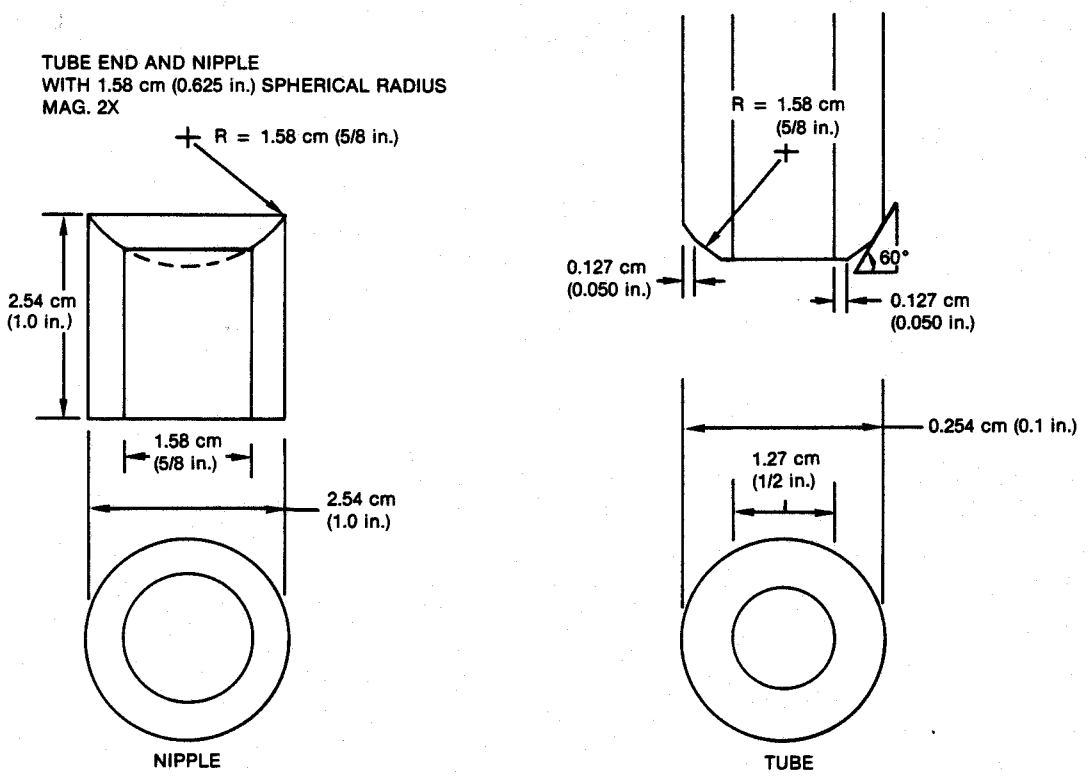

Figure 12. Ball and Socket Joint (Solution to Mismatches in Radii)

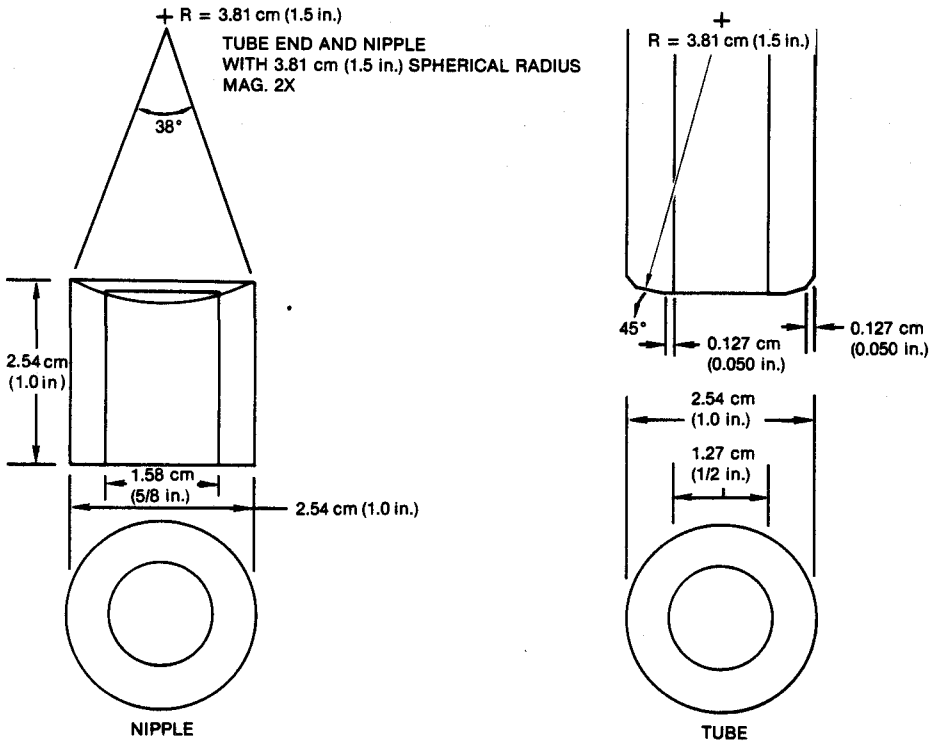

Figure 13. Ball and Socket Joint (Solution to Mismatches in Radii)

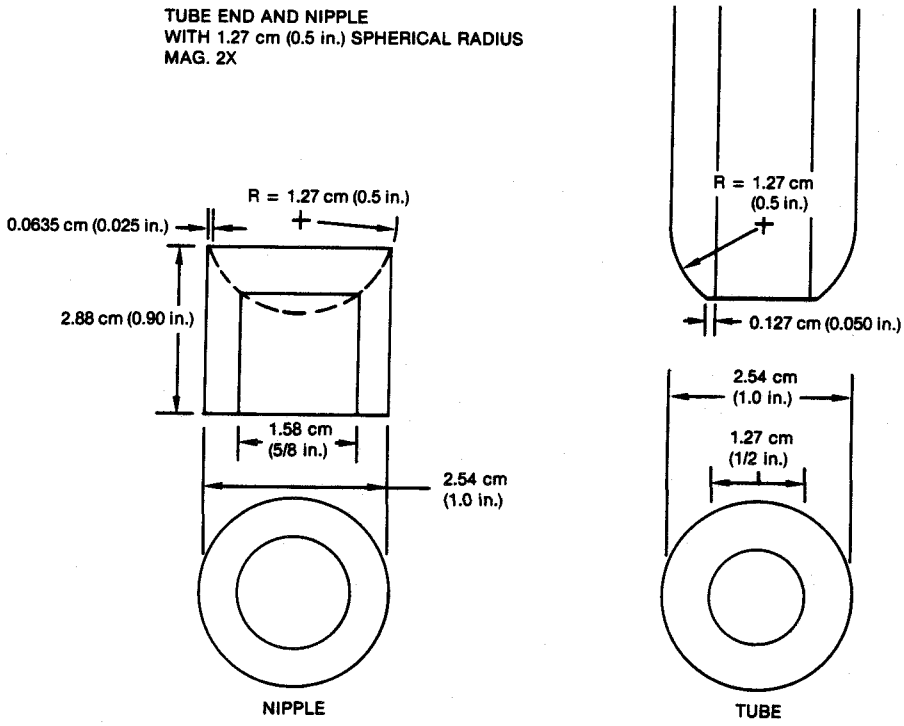

Figure 14. Ball and Socket Joint (Solution to Mismatches in Radii)

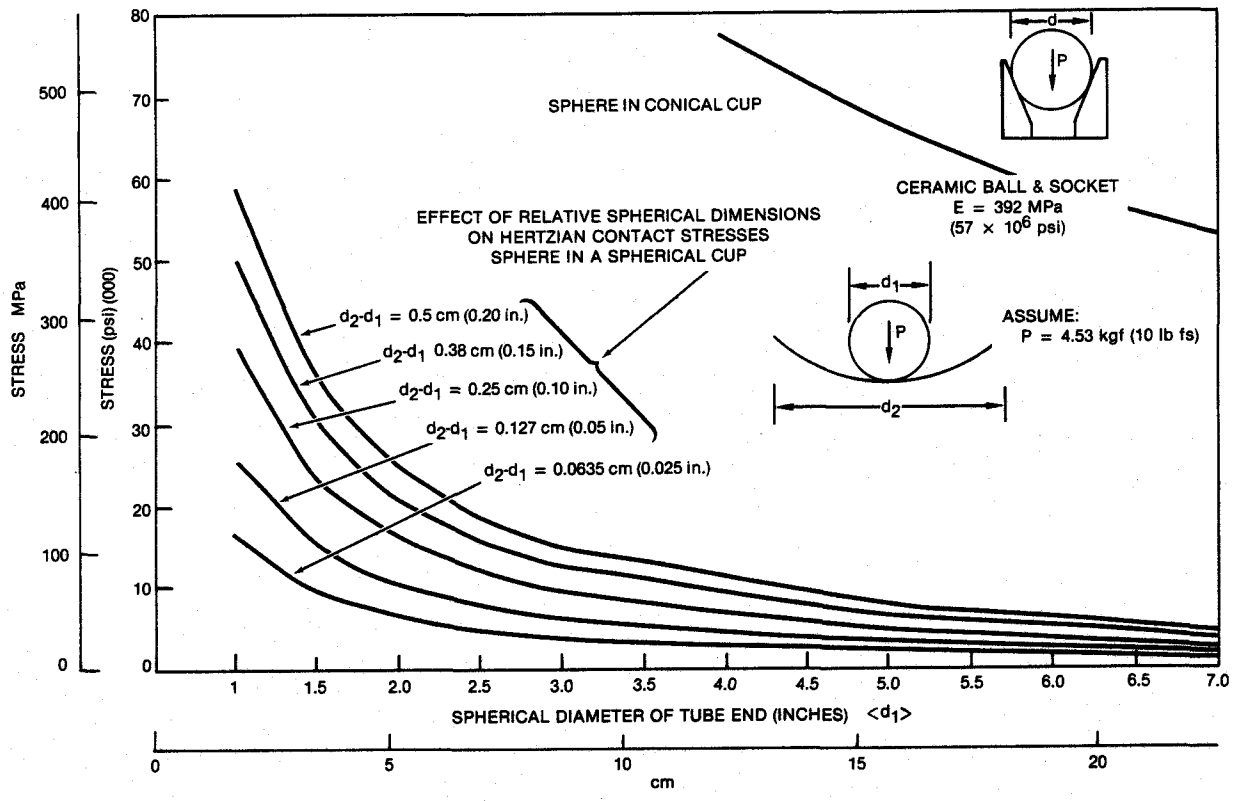

Figure 15. Ball and Socket Joint (Hertzian Contact Stress)

2. An extreme case of interest is when the spherical cup degenerates to a cone (i.e., $R \rightarrow \infty$). The Hertzian contact stress is then given by:

   $\sigma(ksi) = 0.616 \sqrt[3]{PE^2/d^2}$ where d = spherical diameter of tube end

   In this case calculated stresses are six to ten times greater than the spherical cup case for a given tube spherical diameter.

3. Although a compound contour is required to shift contact points away from nipple edges, the effect of edge loading can be minimized by using large spherical radii on both tube and nipple.

4. Large spherical radii also produce lower contact stresses and make radii differences less critical (see Fig. 15).

5. However, large radii restrict the allowable rotational movement within the joint. The ability to accommodate this movement is a prime function of the joint.

To allow for the necessary rotational movement in the joint and at the same time minimize contact stresses, a spherical diameter of 4.44-8.89 cm (1.75-3.5 in.) should be utilized (Fig. 16). Tube ends should be ground as closely as possible to the same radii. Because the growth in radii due to temperature

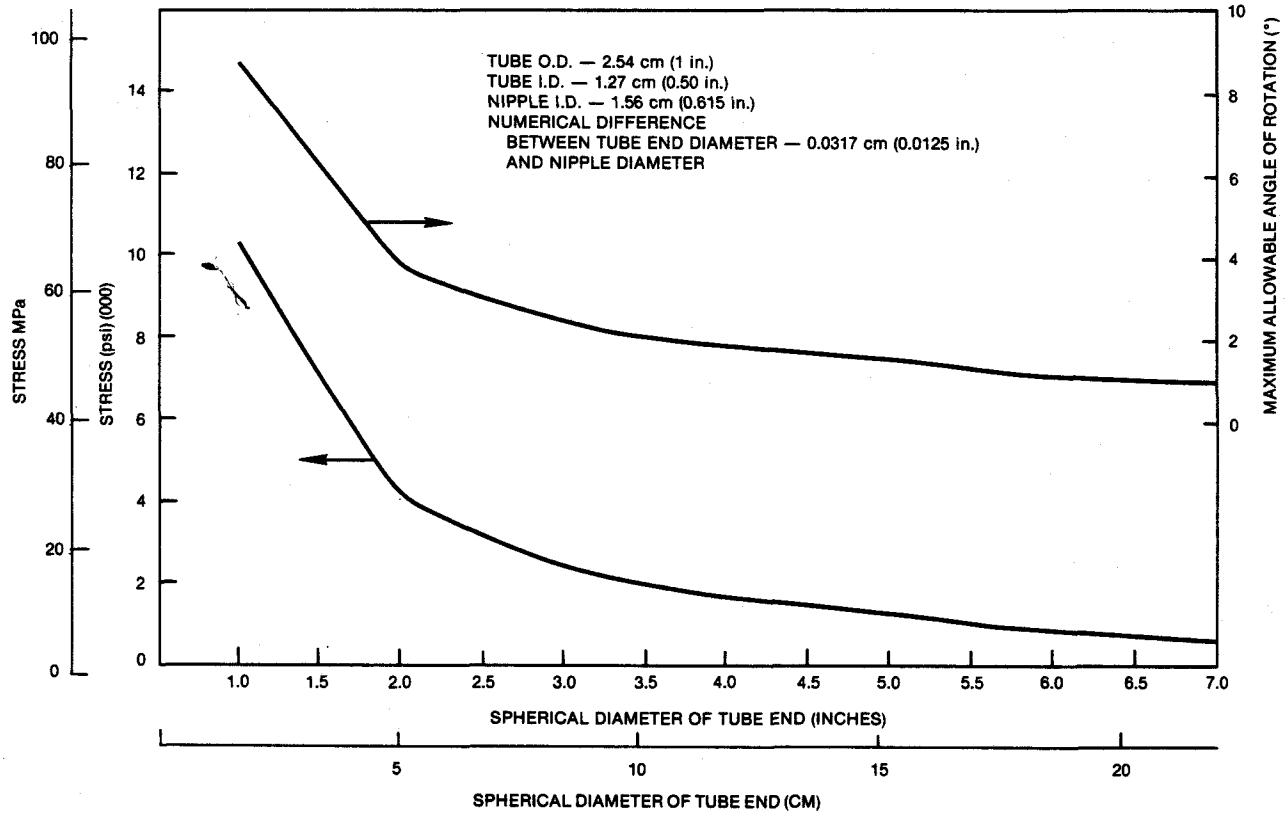

Figure 16. Ball and Socket Joint (Maximum Angle of Rotation)

is on the order of 10^{-4} cm, the grinding tolerances (D_2-d_1 as shown in Fig. 15) become significant. If the two spherical surfaces can be within 0.032 cm (0.0125 in.) or less, contact stresses can be held below 34,450 kPa (5,000 psi).

2.1.2 Ball and Socket Joint Tests

To verify the results of the analysis, a stress model was constructed using finite element analysis and a number of sample joints using various spherical diameters were mechanically tested to determine failure loads.

Sample spherical joints were manufactured typical to the one shown in Figure 17 for mechanical strength testing. These joints were manufactured using a pneumatic control grinding fixture shown in Figure 18. These joints were placed in a specially designed fixture (Fig. 19) to permit axial loading of the joint while internal air pressure was applied. These joints were prepared with four different spherical surfaces to investigate the effect of spherical radius on joint strength. The tests were performed only for comparison purposes. Statistical test sample quantities were not used.

The results of the compression testing are summarized below and in Figure 20.

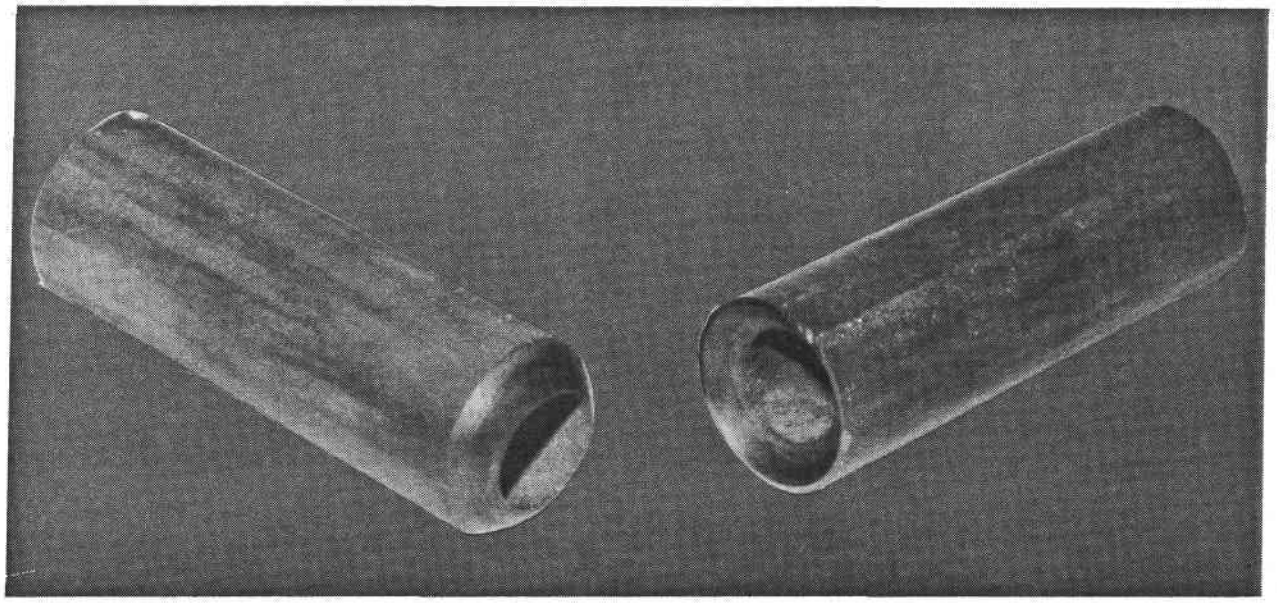

Figure 17. Ball and Socket Joint (Test Specimen)

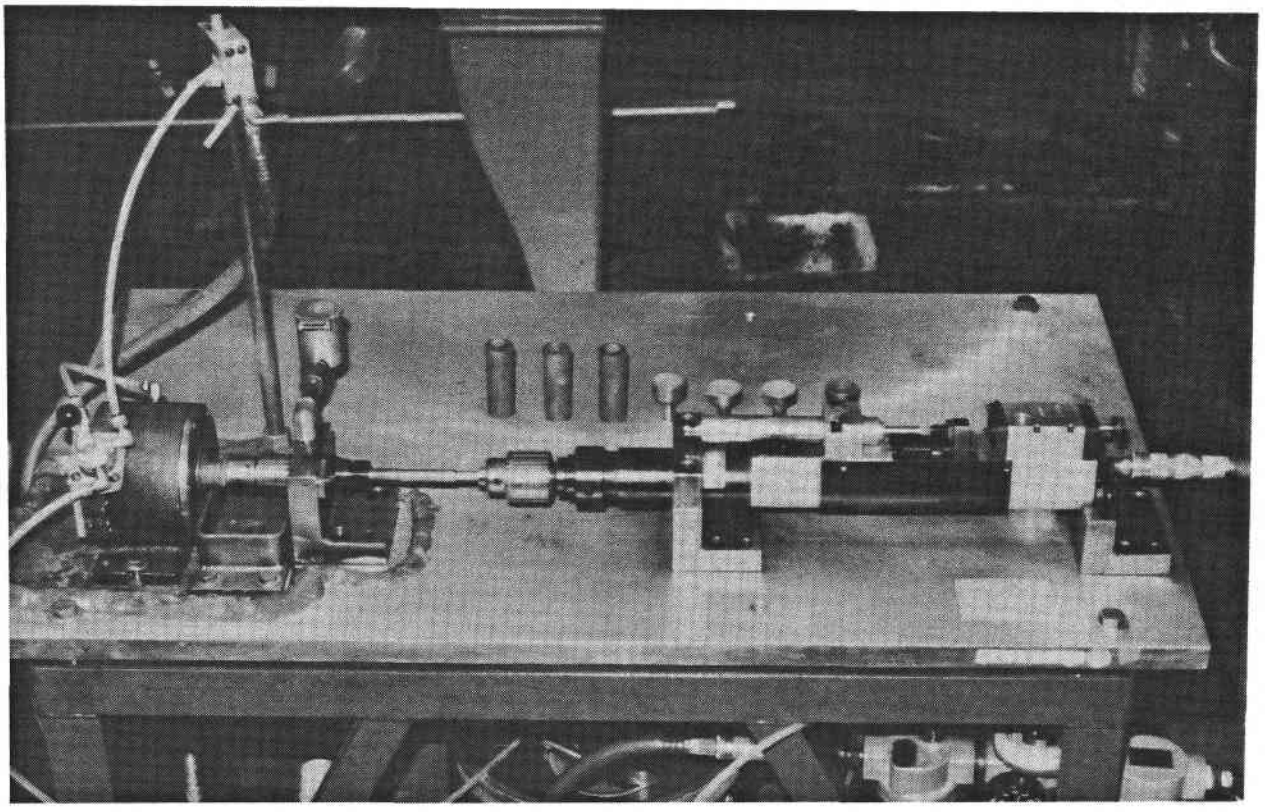

Figure 18. Ball and Socket Joint (Pneumatic Controlled Grinding Fixture)

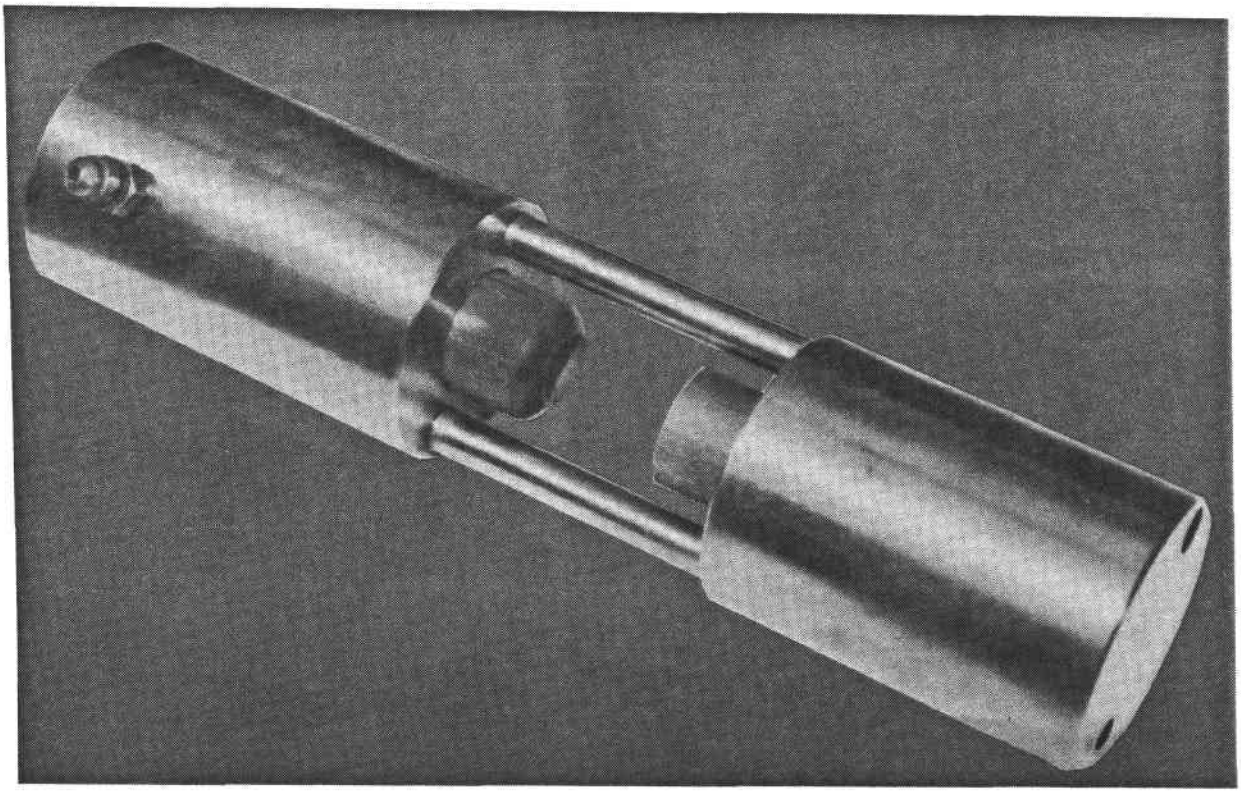

Figure 19. Ball and Socket Joint (Test Fixture)

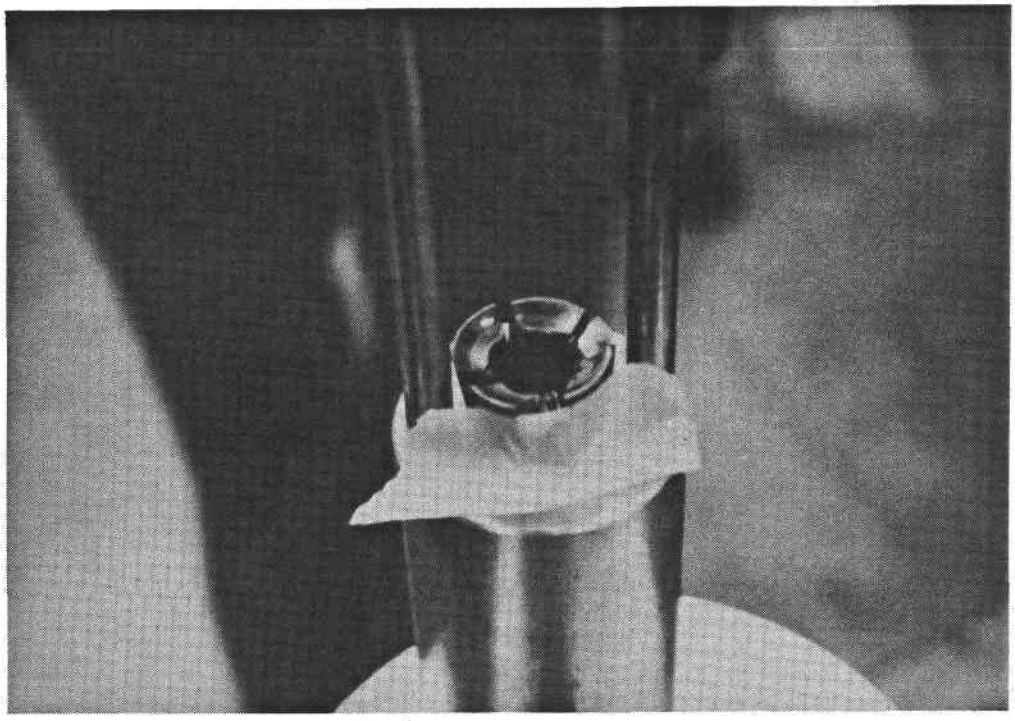

Figure 20. Ball and Socket Joint [Socket Portion After Failure Resulting Resulting From a 11,325 kgf (25,000 lbf) Compressive Load]

Spherical Joint Radius		Failure Load	
cm	(in.)	kgf	(lbf)
1.58	0.625	1359-2718	3000-6000
2.54	1.0	11,325	25,000
3.81	1.5	20,385	45,000
11.43	3.0	20,385+	45,000+

These results were very encouraging since the maximum compressive load (axial load) on any ball and socket joint in the actual heat exchanger design would not exceed 22.65 kgf (50 lbf).

2.1.3 Stress Model

A finite element stress model, shown in Figure 21 was constructed of a ball and socket joint. The results from the computer analysis of the failed joint test specimens indicate that failure was shear. These failure stresses averaged 172 MPa (25,000 psi).

2.2 AXIAL FINNED TUBING

Extended surfaces to improve heat transfer has long been practiced in heat exchanger technology. However, in the past, most of the analysis and applications have been directed towards placing metal fins onto metal tubes. The current investigation explores the possibilities of improving heat transfer of ceramic tubes by the use of ceramic finning.

A review of the governing differential equations which derive both the heat transfer and fin efficiencies in general and for three types of longitudinal

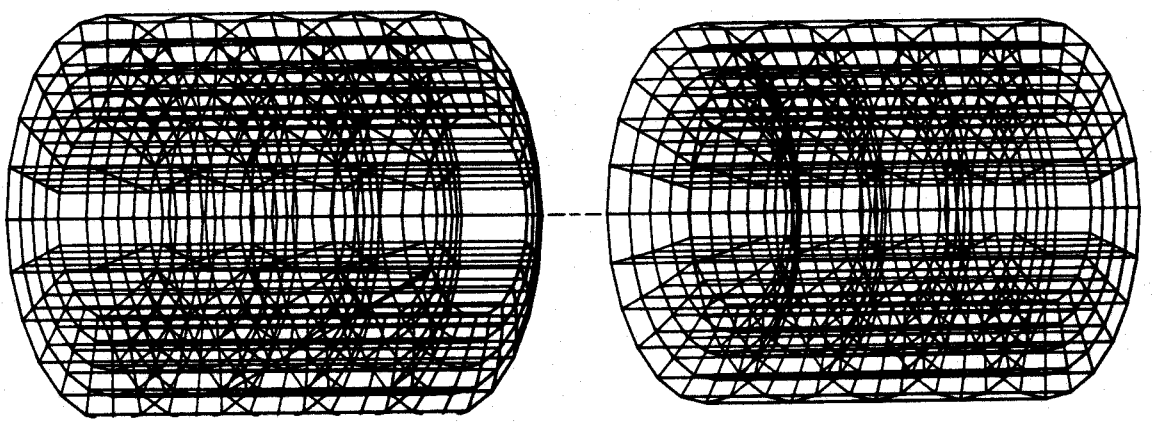

Figure 21. Finite Element Stress Model of a Ball and Socket Joint

fins; the rectangular, triangular, and concave parabolic profiles will be followed by more detailed analyses as well as an assessment of the induced thermal stresses. Spines and circular fins are far less attractive from an overall cost and manufacturing viewpoint and will not be considered at present. Also, longitudinal fins will be considered over circular finning because of the longitudinal flow used in the units as well as the ease of manufacture.

2.2.1 Finned Tubing

The optimum heat transfer occurs when the product of the heat transfer coefficient times the surface area (hA) are the same for both the inside and outside of the heat exchange surface. When one or the other is different, then enhancement of heat transfer can be obtained by increasing either the heat transfer coefficient (h) or the surface area (A) on the lesser side. Process or flow requirements generally do not allow freedom of selection of the heat transfer coefficient so that the most easily obtained solution is by increasing the surface area. The surface area is generally increased through finning. Various types of finning are shown in Figure 22 and are of three basic types: longitudinal fins (a, b, c, d); radial fins (e,f); and spines (g, h, i). Because of the ease of fabrication, only the longitudinal fins will be considered in the present analysis for use with ceramic tubes.

There are generally two types of approaches to solving the general differential fin equation. The first is by using simplified constraints which greatly simplify the resulting equations as well as easing their solution. The second approach is to use real constraints which account for the heat loss on the fin tip. The difference between the two solutions is usually negligible and amounts to usually a small (1-3%) error in the results. Therefore, all analyses will be performed using the simplified constraints to simplify the equations and obtain fast estimates for comparing alternative fin geometries.

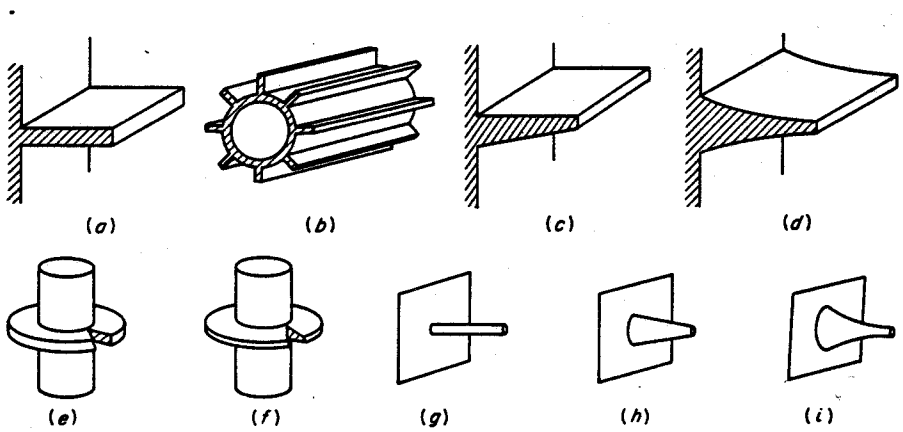

Figure 22. Typical Extended Surfaces

2.2.2 Assumptions Inherent With Simplified Constraints

The following are the assumptions used in the analyses:

1. Steady state heat flow
2. Constant homogeneous material and material thermal properties
3. Constant uniform heat transfer coefficient around fin
4. Uniform temperature of surrounding fluid
5. No temperature gradients across the fin width
6. Uniform temperature across the base of the fin
7. No contact resistance between fin and base
8. No heat sources within the fin
9. Negligible heat transfer through the outer fin edge compared to remainder of fin
10. Heat transfer is proportional to the temperature difference between the fin and surrounding fluid

Real constraints omit assumption #9 and account for the heat loss from the fin tip. Methods are also available to analyze fins with nonuniform heat transfer coefficients around the fin (assumption #3) but in either case the remainder of the assumptions are still applicable. Simplified constraints should not affect the results of fins with no edges at the tips, e.g., triangular and parabolic.

If fins with radiation heat input are to be analyzed, then assumptions 3 and 10 above must be modified. Number 3 because of varying view factors to the surroundings and number 10 because radiation heat transfer is proportional to the temperature raised to the fourth power.

2.2.3 General Differential Equation

Consider a longitudinal fin of arbitrary profile shown in Figure 23.

Let 'x' be the distance along the fins as measured from the fin tip. Further, let '$A(x) - f_1(x)$' be the fin cross section. The equations for the fin profile are $y = f_2(x)$ and $y = -f_2(x)$ for both upper and lower surfaces, respectively. Using these definitions, the generalized heat flow through the base of the fin by conduction can be shown to be

$$dq = K\, d/dx\, [f_1(x)\, dt/dx]\, dx \qquad (1)$$

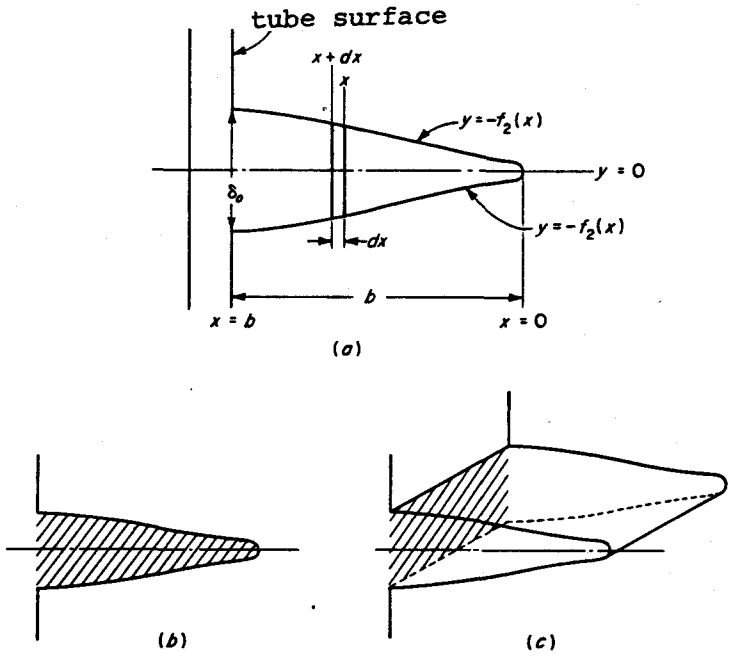

Figure 23. Longitudinal Fin With Arbitrary Profile: (a) Coordinate System, (b) Fin Profile Area, (c) Fin Cross-Sectional Area

If only steady state conditions are assumed, then the above heat flow through the base of the fin must be equal to the heat being transferred to the surrounding fluid by convection or

$$dq = 2h(t - t_s)dx \tag{2}$$

The temperature difference between the fin and its surrounding (t_s) is defined as

$$\theta = t - t_s$$

and since t_s is assumed constant then $d\theta = dt$. Equations (1) and (2) can now be combined to form the general differential equation shown below:

$$f_1(x)\ d^2\theta/dx^2 + df_1(x)/dx\ d\theta/dx - 2h\theta/k = 0 \tag{3}$$

or

$$2f_2(x)\ d^2\theta/dx^2 + 2df_2(x)/dx\ d\theta/dx - 2h\theta/k = 0 \tag{3a}$$

The fin profile is generally of the form

$$f_2(x) = \delta_o/2(x/b)^{(1-2m/1-m)} \tag{4}$$

where δ_o is the fin thickness at its base. The general boundary conditions are

$$\text{at } x = b \qquad \theta = \theta_o \tag{5}$$

$$\text{at } x = 0 \qquad d\theta/dx = 0 \tag{6}$$

2.2.4 Longitudinal Fin of Rectangular Profile

The profile function for the rectangular fin shown in Figure 24 is obtained by substituting n = 1/2 into equation (4) resulting in

$$f_2(x) = \delta_o/2 \tag{7}$$

From equation (7)

$$df_2(x)/dx = 0 \tag{8}$$

Then substituting equations (7) and (8) into (3a) result in the differential equation for the longitudinal rectangular fin, or

$$d^2\theta/dx^2 - dh\theta/k\delta_o = 0 \tag{9}$$

This is a second order differential equation with constant coefficients whose solution is

$$\theta = C_1 e^{mx} + C_2 e^{-mx} \tag{10}$$

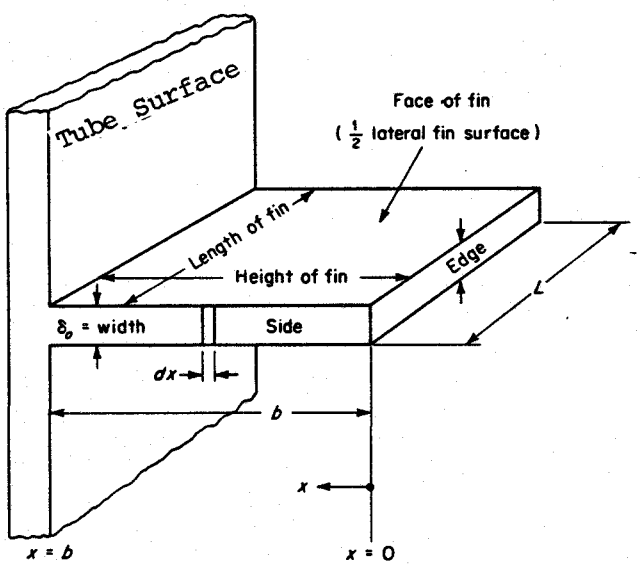

Figure 24. Terminology and Coordinate System, Longitudinal Fin of Rectangular Profile

where $m = (2h/k\delta_o)^{1/2}$

The constants C_1 and C_2 can be obtained by applying the boundary conditions (5) and (6). This yields a solution for the point wise temperature difference between the fin and the surrounding fluid.

$$\theta(x) = \theta_o \cosh mx/\cosh mb \tag{11}$$

The generalized heat flow through the base of the fin is given by

$$q_o = kA\, d\theta/dx|_{x=b} \tag{12}$$

For a unit length where $A = \delta_o x1$, then the derivative of equation (11) substituted into (12) yields

$$q_o = k\delta_o\, m\delta_o \sinh mb/\cosh mb$$

or

$$q_o = k\delta_o \theta m_1 \tanh mb \tag{13}$$

The fin temperature varies from the base to its tip thus reducing the heat transfer as the temperature difference between the fin and its surroundings decreases. The maximum heat transfer from the fin therefore occurs if the entire fin were at a constant base temperature. The ratio between the heat transfer of the fin with its actual temperature profile divided by the heat transfer of the fin if it were at a constant temperature equal to the base is defined as the fin efficiency η. This can be expressed as

$$\eta = \int_o^b \theta(x)dx/\theta_o b$$

where P is the perimeter of the fin.

The actual heat flow for the rectangular fin was given previously in equation (13). By definition, the ideal heat flow for a rectangular fin where $L >> \delta_o$ is

$$q_i = 2hb\theta_o$$

the fin efficiency may now be expressed as

$$\eta = \tanh mb/mb \tag{14}$$

where $m = (k\delta_o/2h)^{1/2}$ as before.

The heat transfer equation (13) and the fin efficiency equation are the basis of all comparisons and performance predictions for fins of different shapes and sizes.

The fin efficiency appears in the calculation of the overall heat transfer coefficient (U_i) of the surface as shown below

$$1/U_i = A_i/\eta_o h_o A_o + 1/h_i$$

where η_o is the surface efficiency defined by

$$\eta_o = 1 - A_f/A_o\ (1 - \eta_f)$$

where
U_i = overall heat transfer coefficient
A_i = inside surface area
A_o = outside surface area
A_f = fin area
h_o = outside heat transfer coefficient
h_i = inside heat transfer coefficient
η_f = fin efficiency

2.2.5 Longitudinal Fin of Triangular Profile

The triangular fin, shown in Figure 25 has the following profile function, with n = 0,

$$f_2(x) = \delta_o/2\ (x/b) \tag{15}$$

and

$$df_2(x)/dx = \delta_o/2b \tag{16}$$

The differential equation then becomes

$$x\ d^2\theta/dx^2 + d\theta/dx - m^2b\theta = 0 \tag{17}$$

The general solution for this equation is

$$\theta = C_1I_o(2m\sqrt{bx}) + C_2K_o(2m\sqrt{bx}) \tag{18}$$

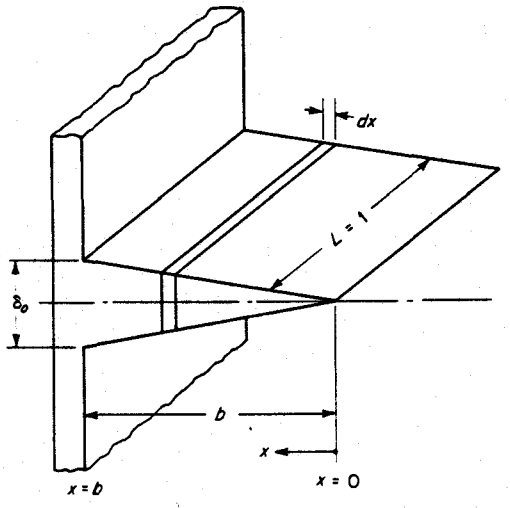

Figure 25. Longitudinal Fin of Triangular Profile

Applying the previous boundary conditions (5) and (6) yields

$$\theta = \theta_o I_o(2m\sqrt{bx})/I_o(2mb) \qquad (18a)$$

As before, the heat flow through the base of the fin can be calculated by substituting the above equation into the general heat flow equation (12) and simplifying

$$q_o = 2h\theta_o I_1(2mb)/mI_o(2mb) \qquad (19)$$

And similarly, the fin efficiency is

$$\eta = I_1(2mb)/mbI_o(2mb) \qquad (20)$$

2.2.6 Longitudinal Fin of Concave Parabolic Profile

The concave parabolic fin of Figure 26 is characterized by the following profile

$$n = \infty$$

thus $f_2(x) = \delta_o/2\ (x/b)^2$

and $df_2(x)/dx = \delta_o/b\ (x/b)$

Upon substituting and rearranging, the governing differential equation becomes

$$x^2\, d^2/dx^2 + 2x\, d/dx - m^2b^2\theta = 0 \qquad (21)$$

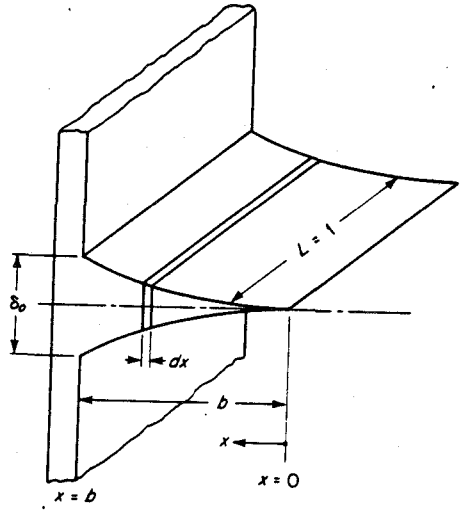

Figure 26. Longitudinal Fin of Concave Parabolic Profile

Similarly, it can be shown from the above that

$$q_o = k\delta_o\theta_o/2b\ [-1 + \sqrt{1 + (2mb)^2}] \tag{22}$$

and

$$\eta = 2/[1 + \sqrt{1 + (2mb)^2}] \tag{23}$$

$$\theta = \theta_o\ (x/b)^{P1}$$

where $P_1, P_2 = -1/2 \pm 1/2\ (1 + 4m^2b^2)^{1/2}$

The three fins analyzed above (rectangular, triangular and parabolic) will be the baseline for further comparisons. The rectangular fin because it is the type most commonly attached to a tube. The triangular because it is the type most commonly seen in extruded tubing with integral fins, and the parabolic because with $P_1 = 1$, it is the longitudinal fin of least material and can be used as a baseline for comparison.

2.2.7 Optimum Shapes of Longitudinal Fins

The optimum fin dimensions are those which dissipate the maximum amount of heat. Generally, a fin width or height can be given and the problem is to find the other dimension that will maximize the heat transfer. This implies that the heat flow through the base can be a maximum and the larger fins than the optimum will have decreased fin efficiency thereby reducing heat transfer below the maximum or smaller fins by having less surface area will not transfer as much heat as the optimum.

2.2.8 Rectangular Profile

For a rectangular fin profile the fin area $A_p = b\delta_o$. Let β_L be the optimizing parameter, then

$$\beta_L = mb = b\ (2h/k\delta_o)^{1/2} = A_p\ (2h/k)^{1/2}\ \delta_o^{-3/2} \tag{24}$$

The heat flow through the base can now be written as

$$q_o = k\delta_o\delta_o(2h/k\delta_o)^{1/2} \tanh A_p\ (2h/k)^{1/2}\ (1/\delta_o)^{3/2}$$

To maximize heat flow through the fin, differentiate the above equation with respect to δ_o and set equal to zero, or

$$dq_o/d\delta_o = 0$$

The resulting transcendental equation can be solved by trial and error

$$3\beta_L \operatorname{sech}^2 \beta_L = \tanh \beta_L$$

from which

$$\beta_L = 1.4192$$

is the solution. Therefore, the optimum rectangular fin becomes, by substitution that having a fin width of

$$\delta_o = 0.791\ (2hA_p^2/k)^{1/3} \tag{25}$$

or for the fin height

$$b = A_p/\delta_o = 1.267\ (kA_p/2h)^{1/3} \tag{26}$$

These are the optimum fin dimensions to transfer the greatest amount of heat for the least amount of fin material. Schneider (Ref. 2) shows that for a longitudinal rectangular fin, the optimum Nusselt number is

$$(Nu)_{opt} = (h\delta_o/2k)_{opt} = 1$$

This indicates that "for a Nu less than one, the fin will have a cooling effect and for Nu greater than one the fin will have an unfavorable insulating effect". The above equation can be re-written as

$$h \leq 2k/\delta_o$$

which means that when the surface conductance for the fin is just equal to or less than the unit internal conductance, then the fin is just becoming useful. When the converse is true, then the addition of fins will decrease the heat transfer and so defeat the purpose of the extended fins.

The above conclusions explain why extended surfaces are ideal for gases with low heat transfer coefficient (h), somewhat less effective for liquids with much larger heat transfer coefficient and almost totally ineffective for condensing vapors or boilers where the heat transfer coefficient is very large. This is expressed mathematically for gases as $Nu \ll 1$, for liquids $Nu \leq 1$ and for condensing vapors $Nu > 1$.

Eckert and Drake (Ref. 3) recommend using finned surfaces if the following condition is true

$$2k/h\delta_o > 5$$

or

$$h < dk/5\delta_o$$

This is similar to the conclusion of Schneider (Ref. 2) but favors a narrower range of h.

2.2.9 Triangular Profile

From before, the heat flow through the base of the triangular fin is

$$q_o = 2h\theta_o I_1(2mb)/mI_o(2mb)$$

If we define the optimizing parameter as

$$\beta_T = 2mb = 2b(2h/k\delta_o)^{1/2} \tag{27}$$

The fin profile is $A_p = \delta_o b/2$ then

$$\beta_T = 4A_p (2h/k)^{1/2} \delta_o^{-3/2}$$

and

$$\delta_o = [4A_p (h/k)^{1/2}/\beta_T]^{2/3}$$

As before, differentiating q_o with respect to δ_o and setting equal to zero results in a transcendental equation whose solution is

$$\beta_T = 2.6188$$

Substituting back into equation (27) gives an equation for the optimum fin width as

$$\delta_o = 1.328 [A_p^2(2h/k)]^{1/3} \tag{28}$$

and the optimum fin height

$$b = 2A_p/\delta_o = 1.506 [A_p k/2h]^{1/3} \tag{29}$$

2.2.10 Concave Parabolic Profile

Following the same procedure as in the previous solutions

$$q_o = k\delta_o\theta_o/2b [-1 + (1 + (2mb)^2)^{1/2}] \tag{30}$$

Defining the optimization parameter as

$$\beta_p = mb = b(2h/k\delta_o)^{1/2}$$

and the profile area as

$$A_p = \delta_o b/3$$

then

$$\beta_p = 2A_p (1h/k)^{1/2} \delta_o^{-3/2}$$

The differentiation and subsequent solution yield the following as a solution to the transcendental equation

$$\beta_p = \sqrt{2}$$

Then the optimum fin width becomes

$$\delta_o = 1.651 \left[A_p^2 (2h/k)\right]^{1/3} \tag{31}$$

and the optimum fin height is

$$b = 3A_p/b = 1.817 (A_p k/2h)^{1/3} \tag{32}$$

2.2.11 Comparison of Optimum Longitudinal Fins

A summary of the results for optimum fins is contained in Table 2.

Since the concave parabolic fin is the fin with least material, all comparisons will be referenced to it. From Table 2 it can be summarized that the heat transferred by the various fin types is as follows:

$$q_R = 2.00\ h^2 A_p k \theta_o^3 \quad \text{(rectangular)}$$

$$q_T = 2.875\ h^2 A_p k \theta_o^3 \quad \text{(triangular)}$$

$$q_p = 3.048\ h^2 A_p k \theta_o^3 \quad \text{(parabolic)}$$

If we assume that q and θ_o are the same for each case, as in a given heat exchanger design, then a relative comparison between fin types can be made. Comparing to a parabolic fin, the rectangular is

$$(A_p)_R/(A_p)_P = 3.048/2.000 = 1.52$$

and for the triangular fin

$$(A_p)_T/(A_p)_p = 3.048/2.875 = 1.06$$

Thus, for the same operating conditions (q, θ_o) the optimum rectangular fin requires 52 percent more volume (hence weight) than the optimum concave parabolic fin. Similarly, the optimum triangular fin requires only 6 percent more material than the optimum parabolic fin. For extrusion, the triangular fin is more compatible with present fabrication procedures than either the rectangular or parabolic profiles. The parabolic fin, with its pointed end, is susceptible to fracture during handling. Therefore, the triangular fin appears to be the most desired profile for application in ceramic finned tubing from performance, manufacturing and handling considerations.

These equations also show that the total weight of the fin is proportional to the profile area and to the specific weight of the material used.

Table 2

Longitudinal Fins - Properties of Optimum Fins
With Simplified Constraints

For Maximum Heat Flow

		Rectangular Profile	Triangular Profile	Parabolic Profile (Concave)
Profile Area	A_p =	$b\delta_o$	$b\delta_o/2$	$b\delta_o/3$
Optimum Thickness	δ_o =	$0.9929\ hb^2/k$	$1.1665\ h\ b^2/k$	$h\ b^2/k$
Optimum Height	b =	$1.0035(k\delta_o/h)^{1/2}$	$1.8852(k\delta_o/4h)^{1/2}$	$2.4495(k\delta_o/6h)^{1/2}$
Optimum mb	mb =	1.4192	1.3094	1.414
Alternate Forms				
Optimum Thickness	δ_o =	$0.791(2hA_p^2/k)^{2/3}$	$1.328[A_p^2(2h/k)]^{1/3}$	$1.651[A_p^2(2h/k)]^{1/3}$
Optimum Height	b =	$1.262(kA_p/2h)^{1/3}$	$1.506(A_pk/2h)^{1/3}$	$1.817(A_pk/2h)^{1/3}$
Heat Flow With Optimum	q_o =	$1.26(h^2A_pk)^{1/3}\theta_o$	$1.422\ (h^2A_pk)^{1/3}\theta_o$	$1.45(h^2A_pk)^{1/3}\theta_o$
$m = (2h/k\delta_o)^{1/2}$				

Weight = $f(\gamma/k)$

For example, consider the following materials*

Copper γ = 556 lb/ft^3, k = 225 Btu/hr/ft/°F, γ/k = 2.471

Aluminum γ = 169 lb/ft^3, k = 117 Btu/hr/ft/°F, γ/k = 1.444

Steel γ = 453 lb/ft^3, k = 25 Btu/hr/ft/°F, γ/k = 18.12

Ceramic γ = 193 lb/ft^3, k = 10 Btu/hr/ft/°F, γ/k = 19.3

The copper fin would require 13.7 percent of the weight of a steel fin for the same performance, the aluminum 8 percent and the ceramic 107 percent of the steel fin. The ceramic fins require substantially more weight than either the copper or aluminum fins but the reason that ceramic fins are used is because metallic fins cannot survive the temperature environment anticipated during use and, therefore, are not viable alternatives.

The basic equation also shows that the fin volume increases as the cube of the heat flow. Therefore, to double the heat transfer, tradeoffs between simply doubling the number of fins or by increasing the volume of the same number of fins by a factor of eight must be considered. In general, a large number of smaller fins is preferred over fewer but longer fins because the

*kg/m^3 = 16.01 (lbm/ft^3) and 2/(m·°K) = 1.73 (Btu/h·ft·°F)

spacing between tubes governs the external heat transfer coefficient. Thus as the fin height increases, the external heat transfer coefficient generally decreases (all other parameters held constant) and the governing hA product can remain about the same thus defeating the purpose of finning the tube in the first place. The ideal situation is to increase the heat transfer area while keeping the heat transfer coefficient constant and derive the maximum benefit from the additional expense at finning the tube.

2.2.12 Analysis

Heat Transfer

Of particular interest with ceramics are the thermal gradients generated within the fin/tube structure as a result of finning. These gradients produce thermal stresses within the tube and must be well below the already low allowables for ceramics to prevent crack formation and propagation.

In order to estimate the maximum magnitudes of these gradients, a simple computer program was developed based on the model shown in Figure 27. The temperature of the tube base below a fin can be compared with that of a plain tube in the same environment. The program selects a fin height and fin thickness then calculates temperature differences, heat flow, and weight difference in comparison to unfinned tubing for a given external heat transfer coefficient. The program automatically steps through a series of pre-selected fin heights, fin thickness, and external heat transfer coefficients. In addition, the program calculates the optimum fin thickness given the fin height as well as all the other associated parameters. Results are presented in Tables 3 through 8.

The overall increase (or decrease) in heat transfer is computed using the unfinned tube as a baseline. In addition, if the increased heat transfer is assumed directly proportional to tube length then an overall change in the core matrix weight for the heat exchanger can be estimated as shown in the tables.

The equations for approximating the base temperature under the fin as well as the fin tip temperature are given below:

Tube Wall Temperature:

$$T_{base} = t_c + h_o/(h_{io} + h_o) \times (T_c - t_c)$$

Fin Tip Temperature:

$$T_{tip} = \left[\frac{(T_{gas} - T_{base})}{\cosh mb}\right] \quad \text{(for longitudinal rectangular fin)}$$

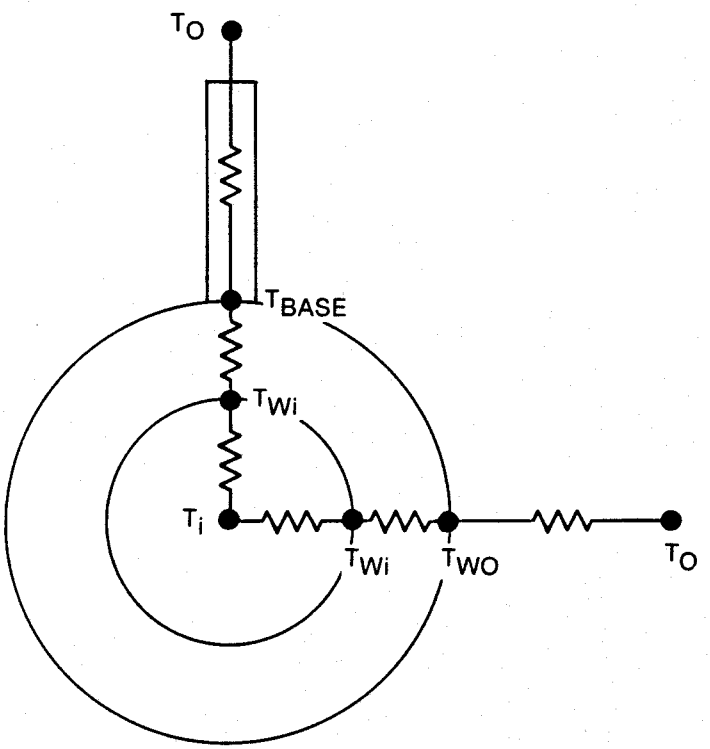

T_O = OUTSIDE FLUID
T_{BASE} = TUBE WALL UNDER FIN
T_{WO} = OUTER TUBE WALL (NOT UNDER FIN)
T_{Wi} = INNER TUBE WALL
T_i = INSIDE FLUID

Figure 27. Computer Model

$$T_{tip} = \left[\frac{(T_{gas} - T_{base})}{I_o\ (2mb)}\right] + T_{base} \quad \text{(for longitudinal triangular fin)}$$

where

h_{io} = h_i x A_i(surface inside)/A_o(surface outside)

h_o = heat transfer coefficient (outside)

h_i = heat transfer coefficient (inside)

T_{base} = tube wall temperature

T_{tip} = fin tip temperature

T_c = temperature of gas around fins

t_c = temperature of fluid inside tube

Table 3

Longitudinal Rectangular Fin
[h_i = 85.2 w/(m^2·K (15 Btu/hr/ft^2/°F)]

ΔT on Outside Wall (Fin-No Fin) (°F)	ΔT on Inside Wall (Fin-No Fin) (°F)	Fin Height (b) (inches)	Fin Thickness at Base (δo) (inches)	ΔQ With Fin Over Width δo (%)	ΔWeight per Foot of Tube With Finning (%)	Fin Efficiency (η_{fin}) (%)	Internal Heat Transfer Coefficient Btu/hr/ft^2/°F	ΔQ For Tube (%)	ΔWeight for Heat Exchanger Core (%)	STRESSES Radial Under Fin (S_1) (psi)	Inner Circumferential (S_2) (psi)	Fin Radial (S_3) (psi)	Outer Circumferential (S_4) (psi)	Radial Number Fin (S_5) (psi)
82.6	78.4	0.100	0.005	42.6	0.7	0.921	15	0.5	0.1	3308	7915	207	8944	2320
85.6	75.7	0.100	0.010	41.1	1.4	0.956	15	1.0	0.3	3275	7648	408	8642	2320
67.3	59.6	0.100	0.050	32.4	6.8	0.987	15	4.1	2.4	3072	6020	1634	6802	2320
59.4	52.6	0.100	0.075	28.6	10.2	0.990	15	5.5	4.2	2983	5311	2167	6001	2320
53.2	47.0	0.100	0.100	25.6	13.6	0.991	15	6.5	6.2	2913	4751	2588	5368	2320
43.9	38.8	0.100	0.150	21.1	20.4	0.992	15	8.1	10.7	2810	3921	3210	4430	2320
37.3	33.0	0.100	0.200	17.9	27.2	0.992	15	9.1	15.5	2737	3335	3648	3768	2320
28.7	25.4	0.100	0.300	13.8	40.7	0.991	15	10.5	25.9	2640	2562	4222	2894	2320
23.2	20.5	0.100	0.400	11.2	54.3	0.991	15	11.4	36.8	2575	2073	4582	2343	2320
87.1	77.0	0.100	0.007	41.9	1.0	0.944	15	0.8	0.2	3292	7782	307	8793	2320
89.9	79.5	0.200	0.005	43.2	1.4	0.757	15	0.6	0.8	3823	8034	93	9078	2320
88.3	78.1	0.200	0.010	42.5	2.7	0.855	15	1.1	1.6	3305	7891	198	8917	2320
77.4	68.5	0.200	0.050	37.2	13.6	0.960	15	4.7	8.2	3184	6919	927	7818	2320
71.9	63.6	0.200	0.075	34.6	20.4	0.970	15	6.6	12.4	3122	6424	1299	7258	2320
67.1	59.3	0.200	0.100	32.2	27.2	0.975	15	8.2	16.7	3068	5994	1622	6773	2320
59.1	52.3	0.200	0.150	28.4	40.7	0.980	15	10.9	25.5	2980	5284	2153	5971	2320
52.8	46.8	0.200	0.200	25.4	54.3	0.982	15	12.9	34.4	2910	4723	2572	5337	2320
43.5	38.5	0.200	0.300	20.9	81.5	0.983	15	16.0	52.5	2806	3890	3192	4396	2320
35.9	32.7	0.200	0.400	17.8	108.6	0.984	15	18.1	70.9	2732	3302	3627	3731	2320
82.5	73.1	0.200	0.030	39.7	8.1	0.940	15	3.0	4.8	3241	7378	582	8337	2320
90.2	79.8	0.300	0.005	43.4	2.0	0.600	15	0.6	1.5	3327	8063	52	9111	2320
89.1	78.8	0.300	0.010	42.8	4.1	0.735	15	1.1	2.9	3314	7964	121	8999	2320
81.3	72.0	0.300	0.050	39.1	20.4	0.920	15	5.0	14.4	3228	7269	636	8214	2320
77.1	68.3	0.300	0.075	37.1	30.6	0.941	15	7.1	21.0	3181	6894	917	7790	2320
73.3	64.9	0.300	0.100	35.3	40.7	0.952	15	9.0	28.0	3139	6556	1170	7408	2320
66.8	59.1	0.300	0.150	32.1	61.1	0.963	15	12.3	41.4	3065	5968	1610	6744	2320
51.3	54.2	0.300	0.200	29.5	81.5	0.968	15	15.0	54.3	3004	5475	1977	6187	2320
52.5	46.5	0.300	0.300	25.3	122.2	0.973	15	19.8	79.4	2906	4695	2557	5305	2320
45.9	40.6	0.300	0.400	22.1	163.0	0.975	15	22.5	103.8	2833	4105	2994	4638	2320
78.4	69.4	0.300	0.067	37.7	27.0	0.936	15	6.4	19.1	3195	7010	830	7921	2320
90.3	79.9	0.400	0.005	43.4	2.7	0.479	15	0.6	2.1	3328	8073	30	9122	2320
89.4	79.1	0.400	0.010	43.0	5.4	0.623	15	1.1	4.3	3318	7993	80	9031	2320
83.3	73.8	0.400	0.050	40.1	27.2	0.872	15	5.1	20.7	3250	7449	475	8417	2320
80.0	70.8	0.400	0.075	38.5	40.7	0.906	15	7.3	30.4	3212	7148	699	8077	2320
76.9	68.0	0.400	0.100	37.0	54.3	0.923	15	9.4	39.8	3178	6870	907	7763	2320
71.3	63.1	0.400	0.150	34.3	81.5	0.942	15	13.1	57.7	3116	6374	1277	7202	2320
66.5	58.8	0.400	0.200	32.0	108.6	0.951	15	16.3	74.7	3062	5943	1598	6715	2320
58.5	51.8	0.400	0.300	28.1	163.0	0.960	15	21.5	106.4	2973	5231	2126	5911	2320
52.2	46.2	0.400	0.400	25.1	217.3	0.964	15	25.6	136.1	2903	4668	2543	5274	2320
74.6	66.1	0.400	0.119	35.9	64.7	0.932	15	10.9	46.8	3153	6671	1055	7538	2320
90.4	80.0	0.500	0.005	43.4	3.4	0.393	15	0.6	2.8	3328	8076	18	9126	2320
89.6	79.3	0.500	0.010	43.1	6.8	0.529	15	1.1	5.6	3320	8006	54	9046	2320
84.5	74.8	0.500	0.050	40.6	34.0	0.820	15	5.2	27.0	3263	7554	372	8535	2320
81.7	72.3	0.500	0.075	39.3	50.9	0.865	15	7.5	39.6	3232	7302	558	8251	2320
79.1	70.0	0.500	0.100	38.0	67.9	0.890	15	9.7	51.7	3202	7067	732	7985	2320
74.3	65.7	0.500	0.150	35.7	101.9	0.917	15	13.6	74.3	3149	6638	1051	7501	2320
70.0	62.0	0.500	0.200	33.7	135.8	0.931	15	17.1	95.4	3101	6258	1333	7071	2320
62.8	55.6	0.500	0.300	30.2	203.7	0.945	15	23.1	133.7	3021	5611	1813	6340	2320
56.9	50.3	0.500	0.400	28.3	271.6	0.952	15	27.8	168.1	2955	5082	2203	5742	2320
71.1	63.0	0.500	0.188	24.2	126.4	0.928	15	16.2	89.7	3114	6359	1258	7185	2320

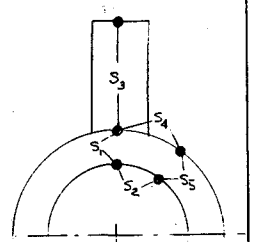

Table conversions to SI units:

°K = °F + 459.67/1.8

centimeter = 2.54 inches

w/(m^2·k) = 5.678 Btu/(h·ft^2·°F)

Table 4

Longitudinal Rectangular Fin
[h_i = 255.5 w/(m^2·k) (45 Btu/hr/ft^2/°F)]

ΔT on Outside Wall (Fin-No Fin) (°F)	ΔT on Inside Wall (Fin-No Fin) (°F)	Fin Height (b) (inches)	Fin Thickness at Base (δo) (inches)	ΔQ With Fin Over Width δo (%)	ΔWeight per Foot of Tube With Finning (%)	Fin Efficiency (η_{fin}) (%)	Internal Heat Transfer Coefficient Btu/hr/ft^2/°F	ΔQ For Tube (%)	ΔWeight for Heat Exchanger Core (%)	STRESSES Radial Under Fin (S_1) (psi)	Inner Circumferential (S_2) (psi)	Fin Radial (S_3) (psi)	Outer Circumferential (S_4) (psi)	Radial Number Fin (S_5) (psi)
147.4	106.0	0.100	0.005	102.1	0.7	0.921	45	1.3	-0.5	7936	10710	496	14885	3926
140.4	101.0	0.100	0.010	91.3	1.4	9.956	45	2.5	-1.2	7747	10204	965	14182	3926
101.9	73.3	0.100	0.050	70.6	6.8	0.987	45	9.0	-2.8	6699	7404	3563	10291	3926
86.9	62.6	0.100	0.075	60.32	10.2	0.990	45	11.5	-2.5	6292	6318	4570	8781	3926
75.8	54.5	0.100	0.100	52.5	13.6	0.991	45	13.4	-1.6	5989	5508	5319	7656	3926
60.3	43.4	0.100	0.150	41.8	20.4	0.992	45	16.0	1.2	5567	4381	6360	6089	3926
50.0	36.0	0.100	0.200	34.7	27.2	0.992	45	17.7	4.7	5287	3634	7047	5050	3926
37.2	26.8	0.100	0.300	25.8	40.7	0.991	45	19.7	13.0	4938	2702	7898	3756	3926
29.5	21.2	0.100	0.400	20.4	54.3	0.991	45	20.8	22.2	4729	2144	8401	2980	3926
125.8	90.5	0.100	0.022	87.2	3.0	0.978	45	5.0	-2.1	7348	9139	1954	12702	3926
150.5	108.3	0.200	0.005	104.3	1.4	0.757	45	1.3	0.0	8022	10938	225	15203	3926
146.8	105.6	0.200	0.010	101.7	2.7	0.855	45	2.6	0.1	7919	10664	474	14822	3926
122.4	88.1	0.200	0.050	84.8	13.6	0.960	45	10.8	1.3	7257	8894	2114	12362	3926
110.9	79.8	0.200	0.075	76.8	20.4	0.970	45	14.7	2.7	6943	8057	2889	11199	3926
101.3	72.9	0.200	0.100	70.2	27.2	0.975	45	17.9	4.4	6683	7363	3532	10234	3926
86.4	62.2	0.200	0.150	59.9	40.7	0.980	45	22.9	8.6	6277	6278	4535	8726	3926
75.3	54.1	0.200	0.200	52.2	54.3	0.982	45	26.6	13.3	5974	5469	5281	7601	3926
59.7	43.0	0.200	0.300	41.4	81.5	0.983	45	31.6	24.1	5552	4342	6316	6034	3926
49.4	35.6	0.200	0.400	34.3	108.6	0.984	45	34.9	35.8	5271	3593	6998	4994	3926
105.2	75.7	0.200	0.089	72.9	24.3	0.973	45	16.6	3.7	6788	7644	3273	10624	3926
151.3	108.9	0.300	0.005	104.9	2.0	0.600	45	1.3	0.7	8044	10996	125	15283	3926
148.7	107.0	0.300	0.010	103.0	4.1	0.735	45	2.6	1.3	7971	10803	290	15015	3926
130.9	94.2	0.300	0.050	90.7	20.4	0.920	45	11.6	6.5	7488	9512	1476	13220	3926
121.8	87.6	0.300	0.075	84.4	30.6	0.941	45	16.1	9.5	7241	8852	2087	12303	3926
113.9	81.9	0.300	0.100	78.9	40.7	0.952	45	20.1	12.5	7025	8277	2619	11504	3926
100.8	72.5	0.300	0.150	69.8	61.1	0.963	45	26.7	18.1	6668	7323	3502	10178	3926
90.3	65.0	0.300	0.200	62.6	81.5	0.968	45	31.9	23.6	6384	6563	4202	9122	3926
74.7	53.8	0.300	0.300	51.8	122.2	0.973	45	39.6	34.3	5959	5430	5244	7547	3926
63.6	45.8	0.300	0.400	44.1	163.0	0.975	45	44.9	44.8	5658	4624	5980	6427	3926
90.1	64.8	0.300	0.201	62.4	81.9	0.968	45	32.0	23.7	6378	6549	4216	9102	3926
151.6	109.1	0.400	0.005	105.1	2.7	0.479	45	1.3	1.3	8051	11015	73	15309	3926
149.4	107.5	0.400	0.010	103.6	5.4	0.623	45	2.6	2.7	7992	10859	192	15093	3926
135.4	97.4	0.400	0.050	93.8	27.2	0.872	45	11.9	12.0	7609	9837	1113	13672	3926
127.9	92.0	0.400	0.075	88.7	40.7	0.906	45	16.9	16.9	7407	9295	1613	12919	3926
121.2	87.2	0.400	0.100	84.0	54.3	0.923	45	21.4	21.3	7225	8810	2061	12245	3926
109.7	79.0	0.400	0.150	76.1	81.5	0.942	45	29.1	28.8	6912	7975	2832	11084	3926
100.2	72.1	0.400	0.200	69.5	108.6	0.951	45	35.4	34.8	6653	7283	3471	10122	3926
85.3	61.4	0.400	0.300	59.1	163.0	0.960	45	45.2	44.2	6248	6200	4467	8617	3926
74.2	53.4	0.400	0.400	51.4	217.3	0.964	45	52.4	51.1	5945	5391	5207	7494	3926
78.6	56.5	0.400	0.357	54.5	194.2	0.963	45	49.6	48.4	6064	5709	4917	7935	3926
151.7	109.1	0.500	0.005	105.1	3.4	0.393	45	1.3	2.0	8053	11021	44	15319	3926
149.8	107.8	0.500	0.010	103.8	6.8	0.529	45	2.6	4.0	8002	10884	131	15128	3926
138.0	99.3	0.500	0.050	95.7	34.0	0.820	45	12.2	17.6	7682	10029	875	13940	3926
131.7	94.8	0.500	0.075	91.3	50.9	0.865	45	17.4	24.6	7510	9570	1296	13302	3926
125.9	90.6	0.500	0.100	87.3	67.9	0.890	45	22.2	30.6	7353	9152	1682	12720	3926
115.8	83.3	0.500	0.150	80.3	101.9	0.917	45	30.7	40.0	7077	8415	2361	11696	3926
107.1	77.1	0.500	0.200	74.3	135.8	0.931	45	37.8	46.6	6842	7786	2941	10822	3926
93.2	67.1	0.500	0.300	64.6	203.7	0.945	45	49.3	53.9	6461	6769	3877	9408	3926
82.3	59.2	0.500	0.400	57.0	271.6	0.952	45	58.1	55.7	6165	5981	4598	8314	3926
69.4	49.9	0.500	0.519	48.1	379.3	0.957	45	68.4	51.5	5814	5041	5453	7007	3926

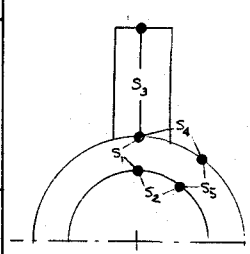

Table conversion to SI units:

°K = °F + 459.67/1.8

centimeter = 2.54 inches

w/(m^2·k) = 5.678 Btu/(h,ft^2,°F)

Table 5

Longitudinal Rectangular Fin
[h_i = 425.8 w/(m^2·k) (75 Btu/hr/ft^2/°F)]

ΔT on Outside Wall (Fin-No Fin) (°F)	ΔT on Inside Wall (Fin-No Fin) (°F)	Fin Height (b) (inches)	Fin Thickness at Base (δo) (inches)	ΔQ With Fin Over Width δo (%)	ΔWeight per Foot of Tube With Finning (%)	Fin Efficiency (η_{fin}) (%)	Internal Heat Transfer Coefficient Btu/hr/ft^2/°F	ΔQ For Tube (%)	ΔWeight for Heat Exchanger Core (%)	STRESSES Radial Under Fin (S_1) (psi)	Inner Circumferential (S_2) (psi)	Fin Radial (S_3) (psi)	Outer Circumferential (S_4) (psi)	Radial Number Fin (S_5) (psi)
169.2	102.5	0.100	0.005	141.8	0.7	0.921	75	1.8	-1.0	11019	11355	689	17084	4557
159.7	96.8	0.100	0.010	133.9	1.4	0.956	75	3.4	-2.1	10658	9776	1328	16128	4557
110.3	66.8	0.100	0.050	92.4	6.8	0.987	75	11.8	-5.8	8770	6750	4665	11137	4557
92.4	56.0	0.100	0.075	77.4	10.2	0.990	75	14.8	-6.1	8085	5654	5873	9328	4557
79.4	48.1	0.100	0.100	66.6	13.6	0.991	75	17.0	-5.7	7591	4862	6743	8022	4557
62.0	37.6	0.100	0.150	52.0	20.4	0.992	75	19.9	-3.5	6926	3796	7913	6263	4557
50.8	30.8	0.100	0.200	42.6	27.2	0.992	75	21.7	-0.4	6498	3110	8662	5131	4557
37.2	22.6	0.100	0.300	31.2	40.7	0.991	75	23.8	7.2	5979	2279	9562	3759	4557
29.3	17.7	0.100	0.400	24.5	54.3	0.991	75	25.0	15.7	5675	1792	10081	2956	4557
122.4	74.2	0.100	0.037	102.6	5.1	0.985	75	9.7	-5.2	9232	7491	3849	12359	4557
173.5	105.2	0.200	0.005	145.5	1.4	0.757	75	1.9	-0.5	11185	10621	313	17523	4557
168.3	102.0	0.200	0.010	141.1	2.7	0.855	75	3.6	-1.0	10987	10303	658	16999	4557
136.0	82.4	0.200	0.050	114.0	13.6	0.960	75	14.5	-2.9	9751	8323	2840	13732	4557
121.4	73.6	0.200	0.075	101.8	20.4	0.970	75	19.4	-3.0	9194	7430	3826	12258	4557
109.6	66.4	0.200	0.100	91.9	27.2	0.975	75	23.4	-2.6	8743	6708	4621	11067	4557
91.7	55.6	0.200	0.150	76.9	40.7	0.980	75	29.4	-0.6	8061	5615	5824	9263	4557
78.8	47.8	0.200	0.200	66.1	54.3	0.982	75	33.7	2.4	7568	4825	6691	7960	4557
61.5	37.2	0.200	0.300	51.5	81.5	0.983	75	39.3	10.1	6903	3759	7853	6202	4557
50.2	30.4	0.200	0.400	42.1	108.6	0.984	75	42.9	19.2	6475	3073	8595	5070	4557
92.0	55.8	0.200	0.149	77.2	40.5	0.979	75	29.3	-0.5	8073	5634	5803	9295	4557
174.6	105.8	0.300	0.005	146.4	2.0	0.600	75	1.9	0.1	11227	10689	174	17634	4557
170.9	103.6	0.300	0.010	143.3	4.1	0.735	75	3.6	0.3	11087	10464	404	17263	4557
147.0	89.1	0.300	0.050	123.3	20.4	0.920	75	15.7	1.5	10173	9000	2006	14848	4557
135.2	82.0	0.300	0.075	113.4	30.6	0.941	75	21.7	2.3	9723	8277	2803	13656	4557
125.1	75.9	0.300	0.100	104.9	40.7	0.952	75	26.7	3.1	9338	7661	3482	12640	4557
108.9	66.0	0.300	0.150	91.3	61.1	0.963	75	34.9	4.9	8717	6667	4578	10990	4557
96.3	58.4	0.300	0.200	80.8	81.5	0.968	75	41.1	6.8	8238	5898	5423	9731	4557
78.2	47.4	0.300	0.300	65.6	122.2	0.973	75	50.1	10.9	7544	4787	6639	7898	4557
65.7	39.8	0.300	0.400	55.1	163.0	0.975	75	56.1	15.4	7067	4022	7470	6636	4557
73.3	44.4	0.300	0.335	61.5	136.5	0.974	75	52.5	12.5	7358	4489	6964	7405	4557
175.0	106.0	0.400	0.005	146.7	2.7	0.479	75	1.9	0.8	11241	10710	102	17670	4557
172.0	104.2	0.400	0.010	144.2	5.4	0.623	75	3.7	1.6	11128	10529	267	17370	4557
152.9	92.7	0.400	0.050	128.2	27.2	0.872	75	16.3	6.4	10399	9362	1521	15445	4557
143.1	86.7	0.400	0.075	120.0	40.7	0.906	75	22.9	8.5	10024	8761	2182	14453	4557
134.5	81.5	0.400	0.100	112.7	54.3	0.923	75	28.7	10.0	9694	8232	2765	13581	4557
120.0	72.7	0.400	0.150	100.6	81.5	0.942	75	38.4	11.8	9140	7343	3745	12115	4557
108.2	65.6	0.400	0.200	90.7	108.6	0.951	75	46.2	12.2	8692	6626	4535	10931	4557
90.4	54.8	0.400	0.300	75.8	163.0	0.960	75	57.9	10.6	8013	5537	5729	9135	4557
77.6	47.0	0.400	0.400	65.1	217.3	0.964	75	66.3	7.0	7512	4750	6588	7837	4557
60.5	36.7	0.400	0.596	50.7	323.6	0.967	75	77.0	-2.4	6369	3705	7717	6112	4557
175.1	106.1	0.500	0.005	146.8	3.4	0.393	75	1.9	1.5	11246	10718	61	17683	4557
172.5	104.5	0.500	0.010	144.6	6.8	0.529	75	3.7	2.9	11146	10558	182	17419	4557
156.6	94.8	0.500	0.050	131.2	34.0	0.820	75	16.7	11.6	10535	9578	1200	15803	4557
148.1	89.7	0.500	0.075	124.1	50.9	0.865	75	23.7	15.1	10214	9065	1763	14955	4557
140.5	85.2	0.500	0.100	117.8	67.9	0.890	75	30.0	17.5	9926	8604	2270	14194	4557
127.5	77.3	0.500	0.150	106.9	101.9	0.917	75	40.8	19.4	9430	7808	3146	12882	4557
116.7	70.8	0.500	0.200	97.9	135.8	0.931	75	49.8	18.3	9016	7146	3876	11789	4557
99.7	60.4	0.500	0.300	93.6	203.7	0.945	75	63.9	9.7	8366	6104	5020	10071	4557
86.9	52.7	0.500	0.400	73.9	271.6	0.952	75	74.3	-4.3	7878	5322	5875	8781	4557
51.1	31.0	0.500	0.981	43.9	632.1	0.960	75	$$$$	-111.6	6510	3129	8229	5612	4557

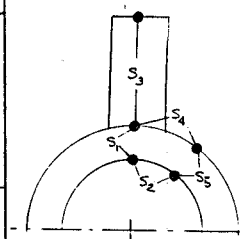

Table conversion to SI units:

°K = °F + 459.67/1.8

centimeter = 2.54 inches

w/(m^2·k) = 5.678 Btu/(h·ft^2·°F)

Table 6

Longitudinal Triangular Fin
[h_i = 85.2 w/(m^2·k) (15 Btu/hr/ft^2/°F)]

ΔT on Outside Wall (Fin-No Fin) (°F)	ΔT on Inside Wall (Fin-No Fin) (°F)	Fin Height (b) (inches)	Fin Thickness at Base (δo) (inches)	ΔQ With Fin Over Width δo (%)	ΔWeight per Foot of Tube With Finning (%)	Fin Efficiency (η_{fin}) (%)	Internal Heat Transfer Coefficient Btu/hr/ft^2/°F	ΔQ For Tube (%)	ΔWeight for Heat Exchanger Core (%)	STRESSES Radial Under Fin (S_1) (psi)	Inner Circumferential (S_2) (psi)	Fin Radial (S_3) (psi)	Outer Circumferential (S_4) (psi)	Radial Number Fin (S_5) (psi)
88.4	78.2	0.100	0.005	42.5	0.3	0.892	15	0.5	-0.2	3306	7897	392	8924	2320
85.2	75.4	0.100	0.010	40.9	0.7	0.942	15	1.0	-0.4	3270	7611	822	8600	2320
62.7	55.4	0.100	0.050	30.1	3.4	0.989	15	3.8	-0.6	3019	5600	3868	6328	2320
51.4	45.5	0.100	0.075	24.7	5.1	0.993	15	4.7	0.1	2894	4597	5390	5195	2320
42.3	37.4	0.100	0.100	20.3	6.8	0.995	15	5.2	1.3	2792	3777	6636	4268	2320
28.9	25.6	0.100	0.150	13.9	10.2	0.997	15	5.3	4.3	2643	2586	8448	2922	2320
20.4	18.1	0.100	0.200	9.8	13.6	0.998	15	5.0	7.9	2548	1824	9609	2061	2320
11.2	9.9	0.100	0.300	5.4	20.4	0.998	15	4.1	15.4	2445	1001	10866	1132	2320
6.9	6.1	0.100	0.400	3.3	27.2	0.999	15	3.4	22.9	2397	615	11458	695	2320
86.9	76.1	0.100	0.009	41.3	0.6	0.934	15	0.9	-0.3	3279	7682	715	8680	2320
80.7	79.4	0.200	0.005	43.1	0.7	0.698	15	0.1	0.1	3321	8015	140	9057	2320
88.0	77.9	0.200	0.010	42.3	1.4	0.812	15	1.1	0.3	3302	7865	348	8887	2320
75.7	67.0	0.200	0.050	36.4	6.8	0.953	15	4.6	1.8	3165	6766	2000	7645	2320
68.7	60.8	0.200	0.075	33.0	10.2	0.969	15	6.3	3.2	3087	6143	2945	6942	2320
62.3	55.2	0.200	0.100	30.0	13.6	0.977	15	7.6	4.9	2016	5571	3817	6295	2320
51.1	45.3	0.200	0.150	24.6	20.4	0.985	15	9.4	9.1	2891	4571	5340	5166	2320
42.0	37.2	0.200	0.200	20.2	27.2	0.989	15	10.3	14.1	2789	3754	6588	4242	2320
28.7	25.4	0.200	0.300	13.8	40.7	0.993	15	10.6	25.9	2641	2568	8404	2902	2320
20.3	17.9	0.200	0.400	9.7	54.3	0.995	15	9.9	39.0	2546	1810	9570	2045	2320
80.1	70.9	0.200	0.035	38.5	4.8	0.934	15	3.4	1.2	3214	7163	1898	8094	2320
90.0	79.6	0.300	0.005	43.3	1.0	0.540	15	0.6	0.5	3324	8044	56	9089	2320
88.6	78.6	0.300	0.010	42.7	2.0	0.676	15	1.1	0.9	3311	7936	176	8968	2320
80.3	71.0	0.300	0.050	38.6	10.2	0.901	15	4.9	4.8	3216	7175	1282	8108	2320
75.3	66.7	0.300	0.075	36.2	15.3	0.931	15	6.9	7.3	3161	6733	1950	7608	2320
70.5	62.5	0.300	0.100	34.0	20.4	0.947	15	8.6	10.0	3108	6314	2588	7134	2320
62.0	54.9	0.300	0.150	29.8	30.6	0.965	15	11.4	15.7	3012	5541	3767	6261	2320
54.3	48.1	0.300	0.200	26.1	40.7	0.974	15	13.3	22.0	2926	4856	4815	5487	2320
41.7	36.9	0.300	0.300	20.1	61.1	0.983	15	15.3	36.4	2786	3731	6541	4216	2320
32.3	28.6	0.300	0.400	15.5	81.5	0.987	15	15.8	52.8	2681	2887	7842	3262	2320
74.6	66.0	0.300	0.079	35.9	16.0	0.934	15	7.2	7.7	3153	6669	2048	3736	2320
90.1	79.8	0.400	0.005	43.3	1.4	0.432	15	0.6	0.8	3326	8055	23	9102	2320
89.1	78.9	0.400	0.010	42.8	2.7	0.563	15	1.1	1.6	3314	7965	93	9000	2320
82.5	73.0	0.400	0.050	39.7	13.6	0.841	15	5.1	7.8	3241	7374	892	8332	2320
78.7	69.6	0.400	0.075	37.8	20.4	0.886	15	7.2	11.7	3198	7031	1404	7945	2320
75.0	66.4	0.400	0.100	36.1	27.2	0.911	15	9.2	15.5	3157	6702	1902	7573	2320
8.0	60.2	0.400	0.150	32.7	40.7	0.938	15	12.5	23.2	3079	6082	2846	6872	2320
61.7	54.6	0.400	0.200	29.6	54.3	0.953	15	15.1	31.0	3008	5512	3718	6228	2320
50.6	44.7	0.400	0.300	24.3	81.5	0.969	15	18.6	47.8	2884	4519	5243	5106	2320
41.5	36.7	0.400	0.400	19.9	108.6	0.977	15	20.3	66.3	2783	3707	6495	4189	2320
69.4	61.4	0.400	0.140	33.4	38.0	0.934	15	11.9	21.6	3094	6202	2662	7008	2320
90.2	79.8	0.500	0.005	43.4	1.7	0.357	15	0.6	1.1	3325	8061	9	9108	2320
89.3	79.0	0.500	0.010	42.9	3.4	0.477	15	1.1	2.3	3316	7979	49	9016	2320
83.7	74.1	0.500	0.050	40.3	17.0	0.779	15	5.1	11.0	3255	7486	646	8459	2320
80.6	71.3	0.500	0.075	38.8	25.5	0.836	15	7.4	16.2	3220	7205	1054	8141	2320
77.6	68.7	0.500	0.100	37.3	34.0	0.870	15	9.5	21.2	3186	6934	1459	7835	2320
71.8	63.5	0.500	0.150	34.5	50.9	0.908	15	13.2	31.0	3121	6417	2240	7251	2320
66.4	58.8	0.500	0.200	31.9	67.9	0.927	15	16.3	40.6	3061	5934	2977	6705	2320
56.7	0.1	0.500	0.300	27.2	101.9	0.951	15	20.8	59.9	2952	5064	4314	5722	2320
58.3	42.7	0.500	0.400	23.2	135.8	0.963	15	23.7	80.0	2859	4317	5468	4878	2320
64.5	57.0	0.500	0.219	20.0	74.3	0.934	15	17.3	44.2	3031	5761	3242	6510	2320

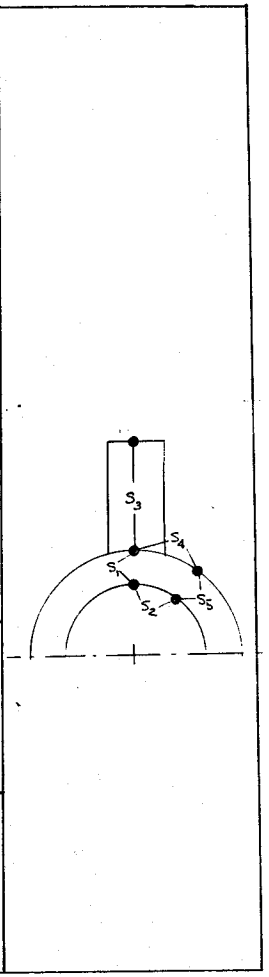

Table conversion to SI units:

°K = °F + 459.67/1.8

centimeter = 2.54 inches

w/(m^2·k) = 5.678 Btu/(h·ft^2·°F)

Table 7

Longitudinal Triangular Fin
[h_i = 255.5 w/(m^2·k) (45 Btu/hr/ft^2/°F)]

ΔT on Outside Wall (Fin-No Fin) (°F)	ΔT on Inside Wall (Fin-No Fin) (°F)	Fin Height (b) (inches)	Fin Thickness at Base (δ_o) (inches)	ΔQ With Fin Over Width δ_o (%)	ΔWeight per Foot of Tube With Finning (%)	Fin Efficiency (η_{fin}) (%)	Internal Heat Transfer Coefficient Btu/hr/ft^2/°F	ΔQ For Tube (%)	Δ Weight for Heat Exchanger Core (%)	STRESSES Radial Under Fin (S_1) (psi)	Inner Circumferential (S_2) (psi)	Fin Radial (S_3) (psi)	Outer Circumferential (S_4) (psi)	Radial Number Fin (S_5) (psi)
146.9	105.7	0.100	0.005	131.8	0.3	0.892	45	1.3	-1.0	7924	10676	939	14838	3926
139.5	100.4	0.100	0.010	96.7	0.7	0.942	45	2.5	-1.8	7721	10136	1914	14087	3926
92.9	66.9	0.100	0.050	64.4	3.4	0.989	45	8.2	-5.1	6455	6753	8269	9385	3926
72.8	52.4	0.100	0.075	50.5	5.1	0.993	45	9.6	-5.0	5908	5294	11003	7358	3926
57.7	41.5	0.100	0.100	40.0	6.8	0.995	45	10.2	-4.1	5497	4194	13066	5830	3926
37.6	27.0	0.100	0.150	26.0	10.2	0.997	45	9.9	-0.8	4948	2730	15817	3795	3926
25.7	18.5	0.100	0.200	17.8	13.6	0.998	45	9.1	3.3	4625	1867	17444	2595	3926
13.7	9.8	0.100	0.300	9.5	20.4	0.998	45	7.2	11.7	4298	993	19098	1380	3926
8.3	6.0	0.100	0.400	5.7	27.2	0.999	45	5.8	19.7	4151	601	19843	835	3926
118.0	84.9	0.100	0.026	81.8	1.8	0.978	45	5.5	-3.8	7138	8578	4852	11922	3926
150.0	107.9	0.200	0.005	104.0	0.7	0.698	45	1.3	-0.7	8008	10902	337	15153	3926
146.1	105.1	0.200	0.010	101.2	1.4	0.812	45	2.6	-1.3	7901	10614	832	14753	3926
118.8	85.5	0.200	0.050	82.3	6.8	0.953	45	10.5	-4.4	7158	8631	4524	11996	3926
104.6	75.3	0.200	0.075	72.5	10.2	0.969	45	13.8	-5.1	6772	7601	6462	10565	3926
92.3	66.4	0.200	0.100	64.0	13.6	0.977	45	16.3	-4.9	6438	6707	8148	9323	3926
72.4	52.1	0.200	0.150	50.1	20.4	0.985	45	19.2	-2.7	5895	5258	10888	7307	3926
57.3	41.2	0.200	0.200	39.7	27.2	0.989	45	20.2	1.4	5486	4165	12958	5789	3926
37.3	26.8	0.200	0.300	25.8	40.7	0.993	45	19.7	13.0	4941	2710	15723	3767	3926
25.5	18.3	0.200	0.400	17.7	54.3	0.995	45	18.0	26.6	4620	1852	17363	2575	3926
90.1	64.8	0.200	0.105	62.4	14.3	0.978	45	16.7	-4.8	5376	6544	8457	9095	3926
150.8	108.5	0.300	0.005	104.5	1.0	0.540	45	1.3	-0.3	8029	10958	136	15231	3926
147.9	106.4	0.300	0.010	102.5	2.0	0.676	45	2.6	-0.6	7952	10751	422	14942	3926
128.6	92.5	0.300	0.050	89.1	10.2	0.901	45	11.3	-2.8	7425	9344	2959	12987	3926
118.0	84.9	0.300	0.075	69.1	15.3	0.931	45	15.6	-2.7	7137	8576	4404	11919	3926
108.4	78.0	0.300	0.100	75.1	20.4	0.947	45	19.1	-2.7	6876	7877	5725	10948	3926
91.7	66.0	0.300	0.150	63.5	30.6	0.965	45	24.3	-2.7	6421	6662	8031	9260	3926
77.8	56.0	0.300	0.200	54.0	40.7	0.974	45	27.5	2.1	6044	5657	9945	7862	3926
56.9	40.9	0.300	0.300	39.4	61.1	0.983	45	30.1	12.6	5474	4135	12853	5747	3926
42.5	30.6	0.300	0.400	29.4	81.5	0.987	45	30.0	27.1	5032	3087	14866	4290	3926
69.3	49.9	0.300	0.236	48.1	48.1	0.978	45	28.9	5.3	5813	5038	11125	7003	3926
151.1	108.7	0.400	0.005	104.7	1.4	0.432	45	1.3	0.0	8038	10980	55	15261	3926
148.7	107.0	0.400	0.010	103.1	2.7	0.563	45	2.6	0.0	7972	10805	223	15018	3926
133.5	96.0	0.400	0.050	92.5	13.6	0.841	45	11.8	0.2	7558	9700	2081	13482	3926
125.1	90.0	0.400	0.075	86.7	20.4	0.886	45	16.6	0.4	7330	9090	3218	12634	3926
117.3	84.4	0.400	0.100	81.3	27.2	0.911	45	20.7	0.8	7117	8522	4287	11845	3926
103.2	74.3	0.400	0.150	71.6	40.7	0.938	45	27.3	2.3	6736	7503	6225	10428	3926
91.1	65.5	0.400	0.200	63.1	54.3	0.953	45	32.1	4.7	6404	6618	7915	9199	3926
71.3	51.3	0.400	0.300	49.4	81.5	0.969	45	37.8	12.9	5868	5185	10666	7206	3926
56.6	40.6	0.400	0.400	39.2	108.6	0.977	45	39.9	25.4	5463	4105	12750	5705	3926
54.0	38.8	0.400	0.420	37.4	114.1	0.978	45	40.0	28.4	5895	3923	13101	5453	3926
151.3	108.8	0.500	0.005	104.8	1.7	0.357	45	1.3	0.3	8042	10991	22	15277	3926
149.1	107.3	0.500	0.010	103.3	3.4	0.477	45	2.6	0.7	7982	10833	118	15056	3926
136.3	98.1	0.500	0.050	94.5	17.0	0.779	45	12.0	2.9	7635	9904	1515	13766	3926
129.3	93.0	0.500	0.075	89.6	25.5	0.836	45	17.1	4.0	7445	9396	2438	13060	3926
122.7	88.3	0.500	0.100	85.1	34.0	0.870	45	21.7	4.9	7266	8920	3327	12397	3926
110.7	79.7	0.500	0.150	76.7	50.9	0.908	45	29.3	6.7	6939	8047	4979	11184	3926
100.0	72.0	0.500	0.200	69.3	67.9	0.929	45	35.3	8.6	6648	7269	6467	10103	3926
82.0	59.0	0.500	0.300	56.8	101.9	0.951	45	43.4	14.0	6156	5955	8996	8277	3926
57.6	48.6	0.500	0.400	46.8	135.8	0.963	45	47.7	20.3	5764	4909	11023	6823	3926
42.6	30.6	0.500	0.650	39.5	222.8	0.978	45	49.3	24.6	5084	3093	14573	4299	3926

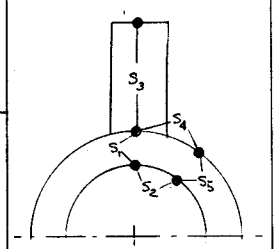

Table conversion to SI units:

°K = °F + 459.67/1.8

centimeters = 2.54 inches

w/(m^2·k) = 5.678 Btu/(h ft^2·°F)

Table 8

Longitudinal Triangular Fin
[h_i = 425.8 w/(m^2·k) (75 Btu/hr/ft_2/°F)]

ΔT on Outside Wall (Fin-No Fin) (°F)	ΔT on Inside Wall (Fin-No Fin) (°F)	Fin Height (b) (inches)	Fin Thickness at base (δ_o) (inches)	ΔQ With Fin Over Width δ_o (%)	Δ Weight per Foot of Tube With Finning (%)	Fin Efficiency (η_{fin}) (%)	Internal Heat Transfer Coefficient Btu/hr/ft^2/°F	ΔQ For Tube (%)	ΔWeight for Heat Exchanger Core (%)	STRESSES: Radial Under Fin (S_1) (psi)	Inner Circumferential (S_2) (psi)	Fin Radial (S_3) (psi)	Outer Circumferential (S_4) (psi)	Radial Number Fin (S_5) (psi)
158.5	102.1	0.100	0.005	141.8	0.3	0.892	75	1.8	-1.5	10995	10316	1303	17020	4557
158.4	96.0	0.100	0.010	132.8	0.7	0.942	75	3.4	-2.7	10609	9698	2668	16001	4557
99.4	60.3	0.100	0.050	88.4	3.4	0.989	75	10.6	-7.6	8356	6088	10704	10044	4557
76.1	46.1	0.100	0.075	63.8	5.1	0.993	75	12.2	-7.7	7463	4656	13898	7682	4557
59.2	35.9	0.100	0.100	49.6	6.8	0.995	75	12.6	-6.7	6818	3623	16206	5977	4557
37.6	22.8	0.100	0.150	31.5	10.2	0.997	75	12.0	-3.1	5994	2303	19159	3800	4557
25.4	15.4	0.100	0.200	21.3	13.6	0.998	75	10.8	1.3	5526	1554	20842	2563	4557
13.3	8.1	0.100	0.300	11.2	20.4	0.998	75	8.5	10.1	5065	815	22508	1344	4557
8.0	4.9	0.100	0.400	6.7	27.2	0.999	75	6.8	18.5	4863	490	23245	809	4557
106.6	64.6	0.100	0.044	89.4	3.0	0.987	75	10.0	-7.3	8631	6528	9723	10770	4557
172.8	104.7	0.200	0.005	144.9	0.7	0.698	75	1.8	-1.2	11159	10579	469	17454	4557
167.4	101.4	0.200	0.010	140.3	1.4	0.812	75	3.6	-2.3	10951	10246	1153	16903	4557
131.3	79.6	0.200	0.050	110.1	6.8	0.953	75	14.0	-8.2	9574	8039	6051	13263	4557
113.6	68.9	0.200	0.075	95.2	10.2	0.969	75	18.2	-9.9	8897	6954	8488	11473	4557
98.7	59.8	0.200	0.100	82.8	13.6	0.977	75	21.1	-10.4	8328	6042	10540	9969	4557
75.5	45.8	0.200	0.150	63.3	20.4	0.985	75	24.2	-8.7	7441	4622	13745	7625	4557
58.7	35.6	0.200	0.200	49.2	27.2	0.989	75	25.1	-4.7	6801	3596	16065	5933	4557
37.3	22.6	0.200	0.300	31.3	40.7	0.993	75	23.9	7.1	5983	2285	19040	3771	4557
25.2	15.3	0.200	0.400	21.1	54.3	0.995	75	21.2	21.2	5518	1541	20741	2542	4557
66.5	40.3	0.200	0.175	55.7	23.8	0.987	75	24.8	-7.0	7096	4069	14995	6713	4557
173.9	105.4	0.300	0.005	145.8	1.0	0.540	75	1.9	-0.9	11200	10644	190	17561	4557
169.9	103.0	0.300	0.010	142.5	2.0	0.676	75	3.6	-1.0	11049	10403	587	17163	4557
144.0	87.3	0.300	0.050	120.7	10.2	0.901	75	15.4	-6.5	10058	8814	4008	14542	4557
130.4	79.0	0.300	0.075	109.3	15.3	0.931	75	20.9	-8.8	9537	7980	5885	13165	4557
118.3	71.7	0.300	0.100	99.2	20.4	0.947	75	25.3	-10.0	9076	7241	7557	11946	4557
93.0	59.4	0.300	0.150	82.1	30.6	0.965	75	31.4	-10.4	8300	5997	10380	9894	4557
81.8	49.6	0.300	0.200	68.6	40.7	0.974	75	34.9	-8.4	7681	5006	12638	8259	4557
58.3	35.3	0.300	0.300	48.9	61.1	0.983	75	37.3	1.0	6784	3568	15927	5887	4557
42.8	25.9	0.300	0.400	35.9	81.5	0.987	75	36.5	15.2	6191	2619	18111	4320	4557
43.6	26.4	0.300	0.394	36.5	80.2	0.987	75	36.6	14.2	6222	2668	17997	4402	4557
174.3	105.6	0.400	0.005	146.1	1.4	0.432	75	1.9	-0.5	11216	10670	77	17604	4557
171.0	103.6	0.400	0.010	143.3	2.7	0.563	75	3.7	-1.0	11089	10466	310	17268	4557
150.4	91.2	0.400	0.050	126.1	13.6	0.841	75	16.1	-4.7	10304	9209	2837	15193	4557
139.4	84.5	0.400	0.075	116.9	20.4	0.886	75	22.3	-6.5	9884	8536	4339	14082	4557
129.4	78.4	0.400	0.100	108.5	27.2	0.911	75	27.6	-8.0	9501	7923	5724	13071	4557
111.9	67.8	0.400	0.150	93.8	40.7	0.938	75	35.8	-9.7	8833	6852	8163	11305	4557
97.2	58.9	0.400	0.200	81.5	54.3	0.953	75	41.5	-9.8	8272	5953	10223	9821	4557
74.4	45.1	0.400	0.300	62.3	81.5	0.969	75	47.6	-5.0	7898	4552	13448	7510	4557
57.8	35.1	0.400	0.400	48.5	108.6	0.977	75	49.4	5.6	6766	3540	15792	5841	4557
29.9	18.1	0.400	0.700	25.1	190.1	0.987	75	44.7	60.4	5700	1832	19789	3022	4557
174.5	105.8	0.500	0.005	146.3	1.7	0.357	75	1.9	-0.2	11224	10683	31	17625	4557
171.5	103.9	0.500	0.010	143.8	3.4	0.477	75	3.7	-0.4	11109	10498	164	17320	4557
154.2	93.4	0.500	0.050	129.3	17.0	0.779	75	16.5	-2.3	10447	9438	2073	15571	4557
144.9	87.8	0.500	0.075	121.5	25.5	0.836	75	23.2	-3.7	10094	8872	3306	14637	4557
136.4	82.7	0.500	0.100	114.4	34.0	0.870	75	29.1	-5.1	9768	8351	4473	13777	4557
121.2	73.5	0.500	0.150	101.6	50.9	0.908	75	38.8	-7.6	9187	7419	6592	12240	4557
108.0	65.5	0.500	0.200	90.6	67.9	0.929	75	46.1	-9.5	8686	6612	8446	10908	4557
86.5	52.4	0.500	0.300	72.5	101.9	0.951	75	55.4	-10.0	7863	5297	11489	8739	4557
70.1	42.5	0.500	0.400	58.8	135.8	0.963	75	59.9	-5.3	7235	4291	13835	7079	4557
21.4	13.0	0.500	1.00	17.9	371.3	0.987	75	49.9	136.0	5374	1309	20910	2160	4557

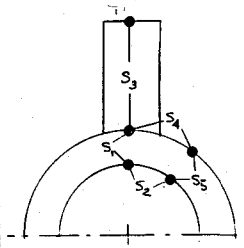

Table conversion to SI units:

°K = °F + 459.7/1.8

centimeters = 2.54 inches

w/(m^2·k) = 5.678 Btu(h·ft^2·°F)

For computer applications, the modified Bessel function has been approximated as shown in Appendix B. This approximation is accurate to at least five places.

By using a constant inside surface area (A_i), the base temperature of the fin can be calculated for both the case with finning as well as without finning. The difference being the maximum temperature on the outer tube surface below the fin minus the comparable temperature in an unfinned tube. This temperature difference is then proportional to the thermal stresss generated, by finning, in the tube. Conduction will tend to diminish these differences from the maximum value calculated and is obviously a function of the material thermal conductivity. Assumptions used in the analysis include:

1. Eight longitudinal fins equally spaced around the tube
2. Tube OD = 2.54 cm (1 in.), ID = 1.27 cm (0.5 in.)
3. Inside and outside heat transfer coefficients = 85.2 w/(m^2·k) (15 Btu/hr/ft^2/°F)
4. Outside fluid temperature = 1366°K (2000°F)
5. Inside fluid temperature = 1200°K (1700°F)
6. Ceramic thermal conductivity = 113.5 w/(m^2·k) (20 Btu/ft^2/°F)
7. Fin thickness: $0.0127 \leq \delta_o \leq 1.01$ cm ($0.005 \leq \delta_o \leq 0.4$ in.)
8. Fin height: $0.254 \leq b \leq 1.27$ cm ($0.1 \leq b \leq 0.5$ in.)

Stress

In order to obtain a better understanding for the magnitude of the temperature differences generated, it is desirable to convert these gradients into equivalent thermal stresses. Figure 28 shows the temperatures calculated by the computer model which can be related to the thermal stresses as indicated below.

Fin gradient (T1 - T2) $[S_3]$

Wall (radial) gradient:	with fin	(T2 - T3)	$\alpha[S_1]$
	without fin	(T4 - T5)	$\alpha[S_5]$
Circumferential gradient:	inside	(T3 - T5)	$\alpha[S_2]$
	outside	(T2 - T4)	$\alpha[S_4]$

where S is the thermal stress induced by the temperature difference.

In a cylindrical vessel under steady state conditions, the thermal stresses produced in a tube as a result of a radial temperature gradient is (Ref. 4):

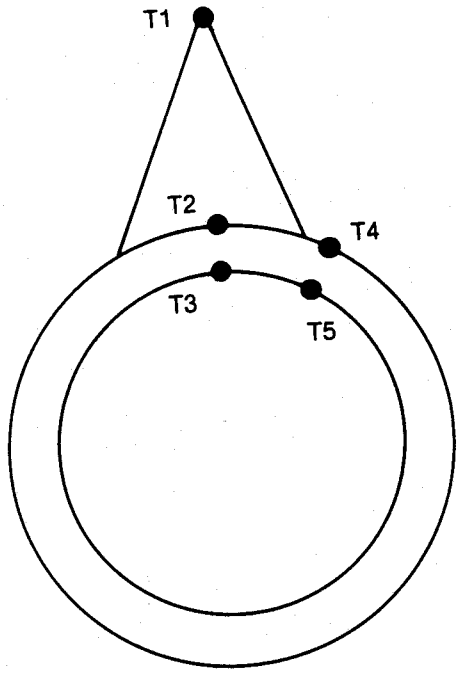

Figure 28.

Fin/Tube Temperature for Calculating Thermal Stresses

$$\sigma = \frac{\alpha E \Delta t}{2(1 - \mu) \log_e (b/a)} \left[1 - \frac{2b^2}{b^2 - a^2} \log_e (b/a)\right] \text{(maximum)}$$

For relatively thin tubes this can be simplified to

$$= \frac{E \Delta t}{2(1 - \mu)}$$

where:
- a = inside radius = 1.27 cm (0.5 in.)
- b = outside radius = 2.54 cm (1.0 in.)
- E = modulus of elasticity = 372 GPa (54 x 10^6 psi)
- t = temperature
- μ = Poisson's ratio = 0.15
- α = coefficient of thermal expansion = 1.38 x 10^{-6}/°K (2.5 x 10^{-6}/°F)

The thermal stresses produced by circumferential temperature gradients around the tube can be estimated as follows (Ref. 5). The stress in a pinned-pinned tube which is held to zero displacment at its midspan due to a circumferential temperature variation can be calculated by

$\sigma = My/I$

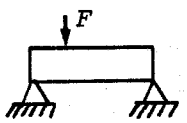

where

- M = PL/4 moment due to point load at center span
- y = $D_0/2$
- δ = $PL^3/48$ E = I tube deflection due to point load at center span
- δ_T = $\alpha L_2/8D = \Delta T$ tube deflection due to circumferential ΔT uniform along tube axis

The boundary condition for this beam is:

$$\delta + \delta_T = 0 \text{ at outer span}$$

Substituting and simplifying yields

$$\sigma = 0.75\ \alpha\Delta T E$$

If the fin thermal stresses are assumed to be produced because the fin is restricted in one direction, then the stress is

$$= E\alpha\Delta T$$

By using the values given before, substituting and rearranging, the equation can be simplified to

tube radial	$\lvert\sigma\rvert$	= 668.3 ΔT kPa (97 ΔT psi)
tube cirumferential	$\lvert\sigma\rvert$	= 695.89 ΔT kPa (101 ΔT psi)
fin	$\lvert\sigma\rvert$	= 930.1 ΔT kPa (135 ΔT psi)

The various thermal stresses calculated are summarized in Figure 29 and are defined as:

S1 = radial stress in tube wall under fin
S2 = circumferential thermal stress on the inside of the tube between a finned and unfinned section of tubing
S3 = fin thermal stress from fin tip to base
S4 = circumferential thermal stress on the outside of the tube between a finned and unfinned section of tube
S5 = radial stress in tube wall with no fin

2.2.13 Discussion of Results

Rectangular Fins

- the thermal stress in the fin decreases with increasing fin thickness
- the thermal stress in the fin decreases with increasing fin height
- The radial and circumferential thermal stresses increase only very slightly with increasing fin height
- the radial and circumferential thermal stresses decrease with increasing fin thickness
- all thermal stresses increase with increasing inside heat transfer coefficients

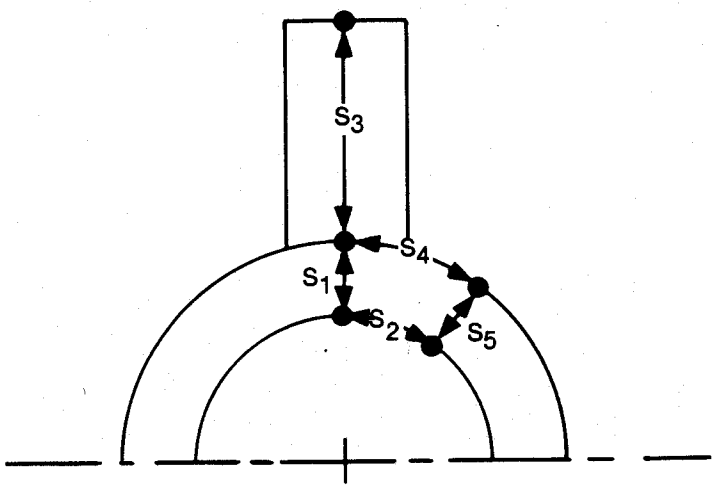

Figure 29.

Thermal Stress Nomenclature

- S4 is usually the maximum stress with S1 becoming the maximum in some cases where the fin thickness is large (>0.2-0.4)

In general, efforts to increase the heat transfer from the surrounding fluid to the internal fluid result in increased thermal stresses within the fin/tube structure simply because the temperature differences must increase to force the heat flow and thereby increase the thermal stresses which are solely a function of the temperature difference.

The triangular fins all exhibit the same trends as delineated for the rectangular fins with the following items noted. The differences are calculated at the same fin geometry (b, δ_o) and heat transfer coefficients [$h_i = h_o$ = 85.2 w/(m^2·k) (15 But/hr/ft^2/°F)].

- Radial stress slightly less in rectangular fin by about 1.3% (S1)
- Circumferential stress slightly less (S2, S4) in rectangular finned tube by about 5%
- Fin stress greatly increased because the fin tip, being triangular, operates near gas temperature thereby creating a large temperature difference between the fin tip and base. Stress (S3) is as much as double at large δ_o while only slightly higher at small base thicknesses δ_o where the triangular fin more closely resembles a rectangular fin.

The advantage of triangular fins is that for about half the weight, the heat transferred is about the same at small δ_o and only 20 percent less at large fin thicknesses making the overall weight to heat transfer more attractive. The disadvantage is that the fin tip operates closer to gas temperature at large δ_o, being about the same at small δ_o.

A further comparison of the thermal stresses between the rectangular and triangular fins is shown in Table 9.

Table 9

Comparison of Thermal Stresses in Rectangular and Triangular Fins

	Rectangular Fins kPa	(psi)	Triangular Fins kPa	(psi)	Δ
S1	21130	3065	20764	3012	-1.73%
S2	41143	5968	38199	5541	-7.15%
S3	11099	1610	25969	3767	+133.97%
S4	46493	6744	43163	6261	-7.16%
S5	15994	2320	15994	2320	0

$h_i = h_o = 85.2$ w/(m^2·k) (15 Btu/hr/ft^2/°F)
$b_o = 0.762$ cm (0.3 in.)
$b_o = 0.382$ cm (0.15 in.)

The analysis assumes that the external heat transfer coefficients remain the same for all fin geometries. This assumption is not necessarily true. As the free flow area between tubes increase, the flow velocity and heat transfer coefficient on the outside of the tube decreases. This can be compensated by decreasing the number of tubes thereby reducing the total flow area and increasing velocity and heat transfer coefficients. This in effect makes the unit longer and changes the overall dimensions of the unit. These effects are analyzed in greater depth in Appendix C. The assumption of constant external heat transfer coefficient with fin geometry is not necessarily incorrect, but its effect can be accommodated by varying the heat exchanger dimension. The overall heat exchanger sizing is very complex and not within the scope of the current analysis.

If the number of tubes is decreased, as indicated above, then the internal heat transfer coefficient also increases for a given flow. This effect can be illustrated simply by assuming that the fouling and wall resistances are small, therefore,

$$\frac{1}{UA} = \frac{1}{h_o A_o} + \frac{1}{h_i A_i}$$

where

U = overall heat transfer coefficient
h = heat transfer coefficient
A = area

subscripts

i = inside
o = outside

If we also assume that $A_o = 5A_i$, then

$$U = (5h_o h_i / 5h_o + h_i)$$

The effect of the internal heat transfer coefficient on the total overall heat transfer coefficient is shown below for a constant external heat transfer coefficient.

h_o		h_i		U		
$w/(m^2 \cdot k)$	$\frac{Btu}{hr \cdot ft^2 \cdot °F}$	$w/(m^2 \cdot k)$	$\frac{Btu}{hr \cdot ft^2 \cdot °F}$	$w/(m^2 \cdot k)$	$\frac{Btu}{hr \cdot ft^2 \cdot °F}$	Change From Baseline (%)
85.2	15	28.4	5	26.6	4.69	-62.5
85.2	15	56.8	10	50.0	8.82	-29.4
85.2	15	85.2	15	71.0	12.50	Baseline
85.2	15	114	20	89.7	15.79	+26.3
85.2	15	142	25	106	18.75	+50.0
85.2	15	170	30	122	21.42	+71.4
85.2	15	199	35	135	23.86	+90.9
85.2	15	256	45	160	28.13	+125.0
85.2	15	426	75	213	37.50	+200.0

This shows that by increasing the internal heat transfer coefficient by six times only increases the overall heat transfer coefficient by a factor of three.

This relates to the overall heat exchanger through the general heat transfer equation

$$Q = UA \Delta T \ell_m$$

or

$$A = \frac{Q}{U \Delta T \ell_m}$$

An increase in the overall heat transfer coefficient (U) by a factor of three will reduce the required area by one-third, assuming that Q and $\Delta T \ell_m$ remain the same. Therefore, increasing the internal heat transfer coefficient from 85.2-426 $w/(m^2 \cdot k)$ (1575 $Btu/hr/ft^2/°F$) with an external heat transfer coefficient of 85.2 $w/(m^2 \cdot k)$ (15 $Btu/hr/ft^2/°F$) and a fin height of 0.300 inch, produces the following effect

- S1 - about a 3 times increase at small δ_o (0.05)
  about a 2 times increase at large δ_o (0.4)
- S2 - about a 25% increase at small δ_o (0.05)
  about a 29% decrease at large δ_o (0.4)
- S3 - about 3 times increase at small δ_o (0.05)
  about 2.5 times increase at large δ_o (0.4)

- S4 - about 2 times increase at small δ_o (0.05)
  about 50% increase at large δ_o (0.4)

- S5 - about double

The net effect from the above is that the thermal stresses all increase with more compact units because the heat fluxes increase which require larger temperature differences (hence larger thermal stresses) to drive the heat flow.

The temperature differences (proportional to thermal stress) for the outside of the tube is shown in Figure 30 for a variety of rectangular fin geometries. The triangular fin results were similar, therefore Figure 30 represents both rectangular and triangular fin temperature difference trends.

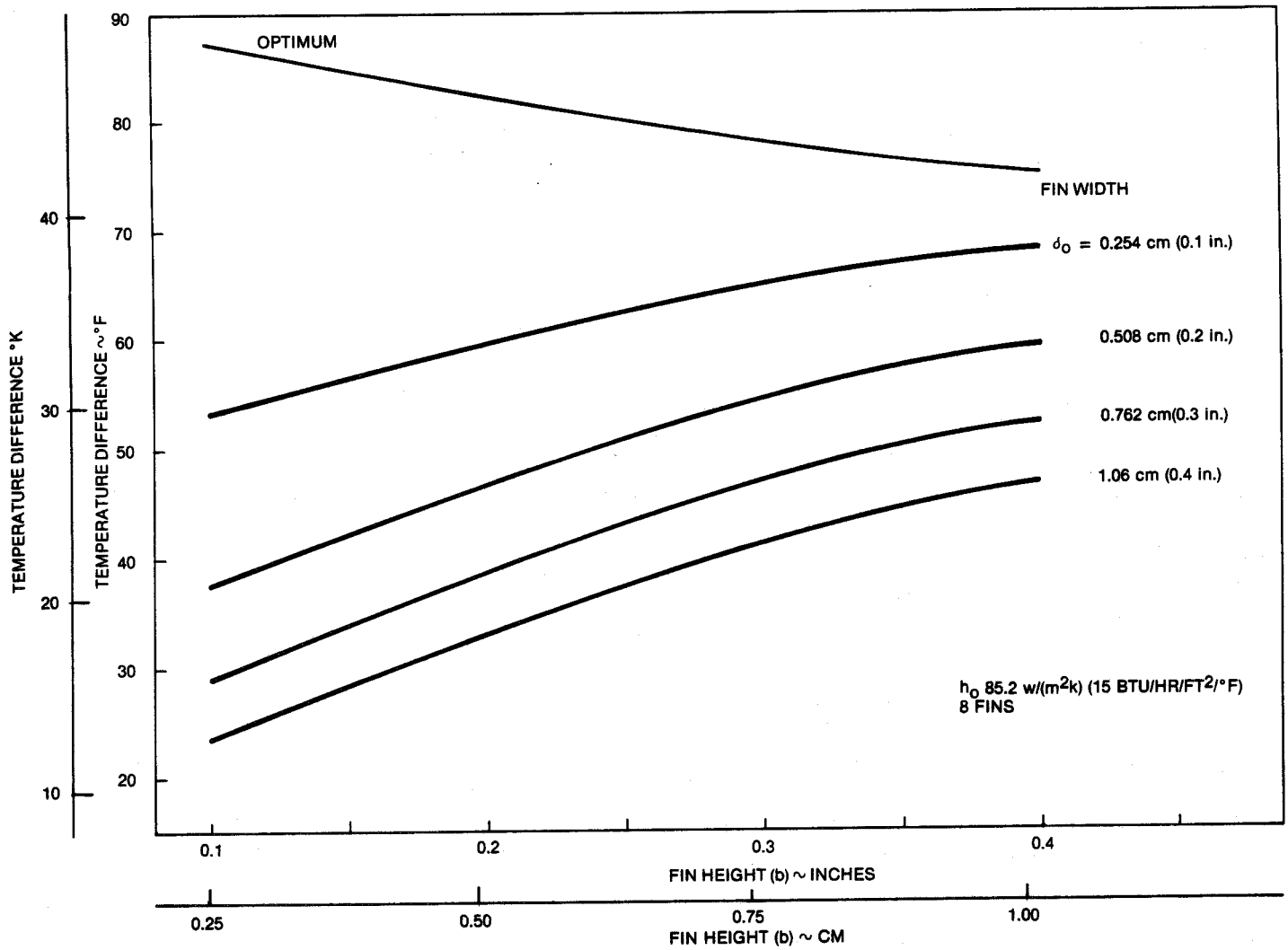

Figure 30. Outside Circumferential Temperature Differences as a Function of Rectangular or Triangular Longitudinal Fin Geometry

The advantages of triangular fins can be seen in Figures 31 and 32 as a lower weight increase for a given increase in heat transfer. If the heat transfer remains the same, as it would in a given application where only the choice of fin type is in question, then the net effect is a reduction in the tube length for a given application since the heat transfer per foot is increasing. Therefore, with the increasing heat transfer per foot of tube, the heat exchanger matrix tube length and thereby volume even though there is a weight A summary of the conditions is given in Table 10.

The conclusion is that triangular fins incur a much lesser weight penalty in transferring the same amount of heat as a rectangular fin.

2.2.14 Test Samples

Two test samples of ceramic finned tubing were purchased for thermal shock testing. These samples, shown in Figures 33 and 34, were chosen to maximize the heat transfer yet minimize the induced thermal stresses. The approximate calculated parameters for these two samples are listed below.

Fin Type	ΔQ* %	Δwt* %	S1 kPa (psi)	S2 kPa (psi)	S3 kPa (psi)	S4 kPa (psi)	S5 kPa (psi)
Rectangular	20.1	115	21095 (3060)	40674 (5900)	10685 (1550)	46870 (6800)	15994 (2320)
Triangular	23.7	80	19716 (2860)	29761 (4317)	37710 (5470)	33642 (4880)	15994 (2320)

[$h_i = h_o$ = 85.2 w/(m^2·k) (15 Btu/hr/ft^2/°F)]

*over unfinned tube

The triangular fin tube appears to have the edge. The heat transfer is up while both the weight and stresses are down when compared to a rectangular finned tube. The fin stress (S3) in the triangular finned tube is greater than the rectangular finned tube because the fin tip temperature operates closer to gas temperatures on the triangular fin.

2.2.15 Conclusions

This study has yielded the following conclusions:

- The concave parabolic is the most efficient fin to use, with the triangular fin coming in a close second, but is less attractive from a manufacturing or handling consideration.
- Triangular fins are more desirable from a performance and weight standpoint than are rectangular fins.

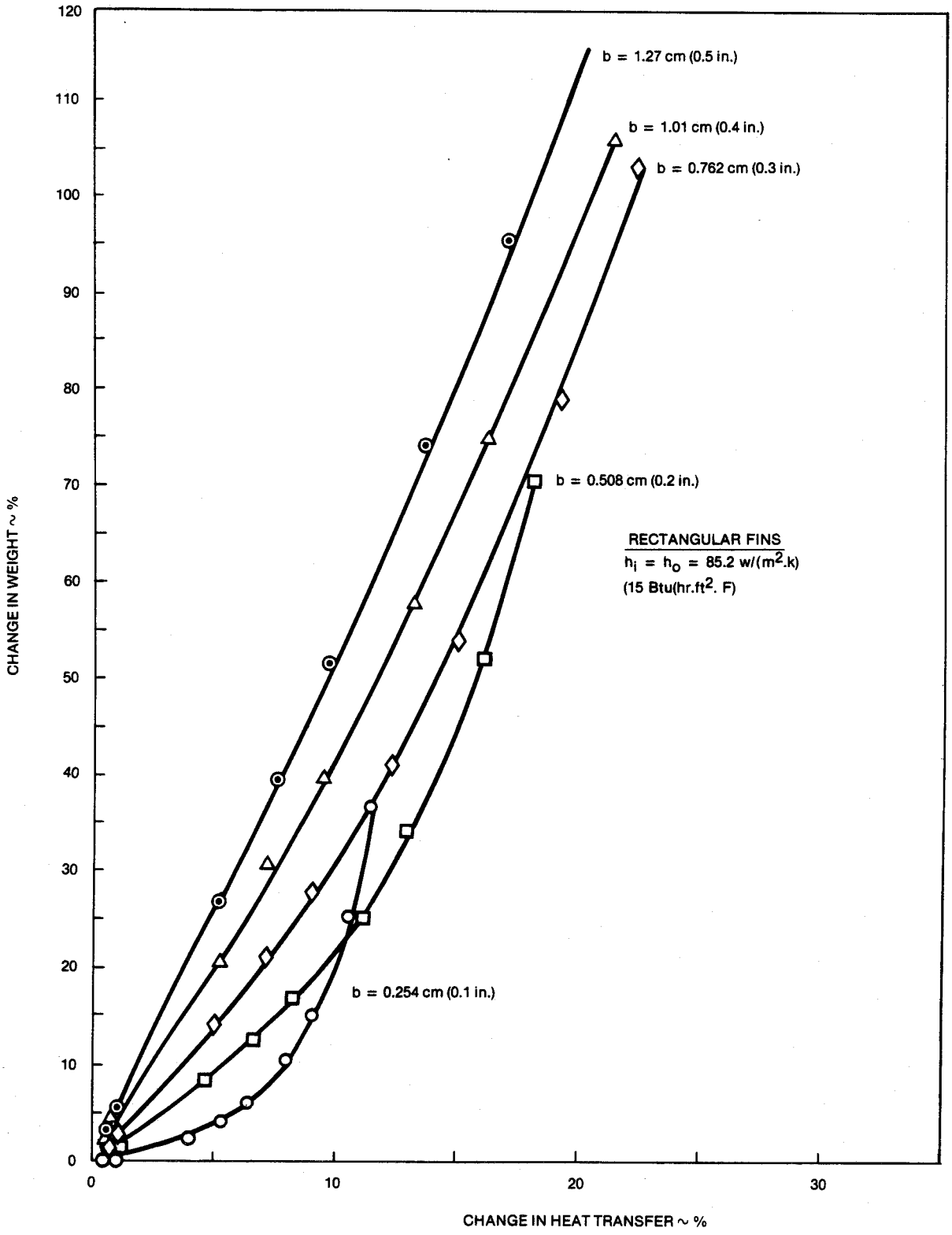

Figure 31. Change in Tubular Weight for Rectangular Fins

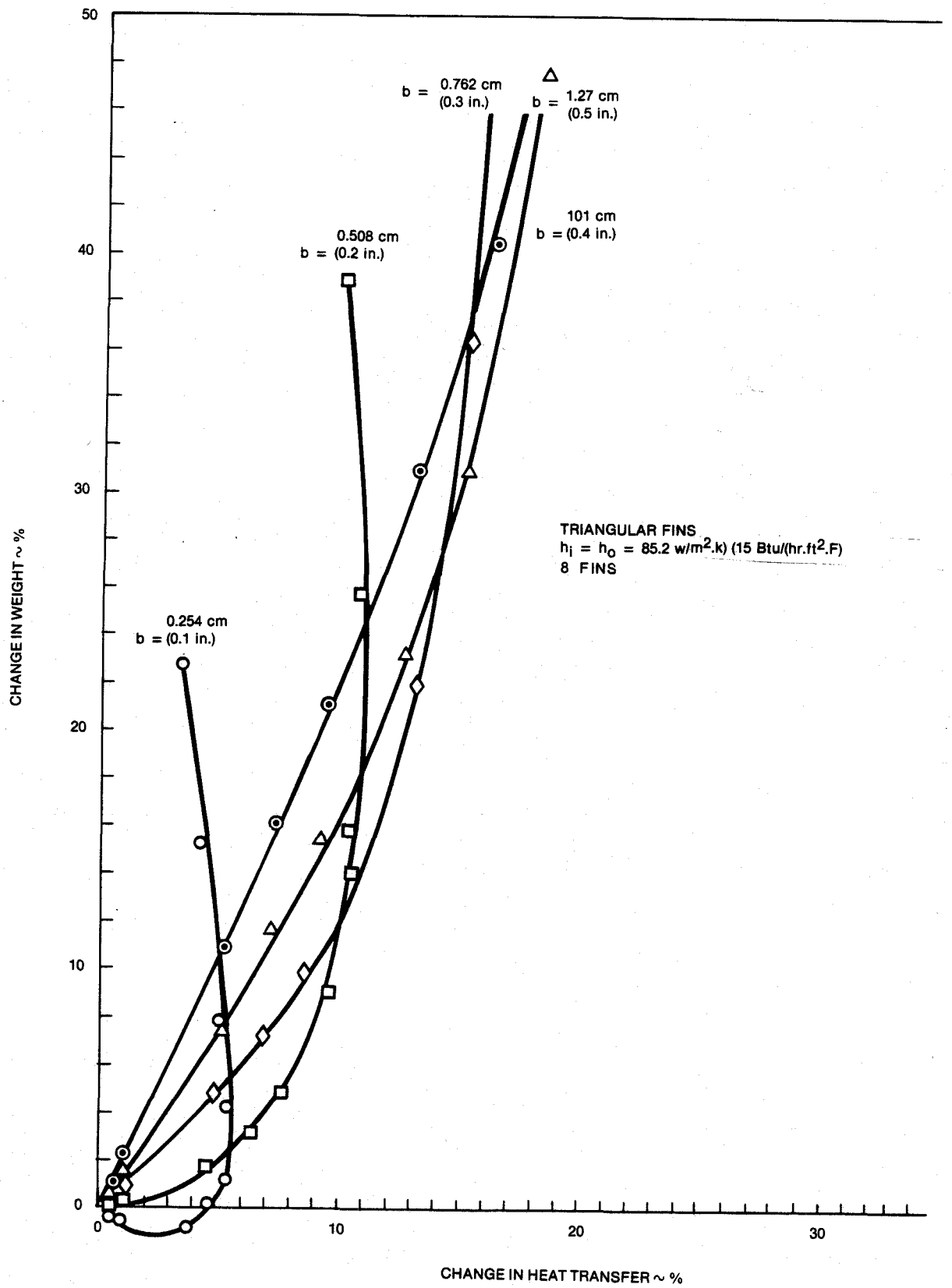

Figure 32. Change in Tubular Weight for Triangular Fins

Table 10

Comparison of Rectangular and Triangular Fins on Heat Exchanger Matrix Weight

Change in Heat Transfer (Q) %	Minimum Change in Matrix Weight for Rectangular Fins %	Minimum Change in Matrix Weight for Triangular Fins %
+1.0	+0.5	-0.4
2.0	1.0	-1.0
3.0	1.6	-1.0
4.0	2.5	-0.4
5.0	3.7	0.4
7.5	8.5	4.9
10.0	19.5	11.6
12.5	31.2	19.2
15.0	45.0	30.9
17.5	65.0	44.0
20.0	85.5	59.6

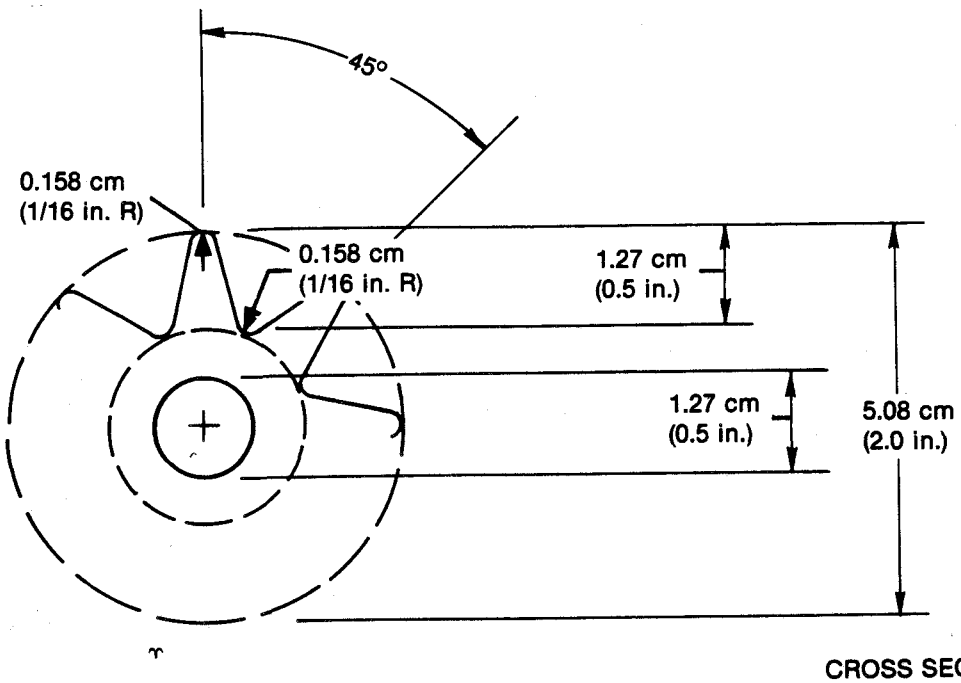

NOTES:
1) LENGTH IS 16.51 ± 6.35 cm (6.5 ± 0.25 in.)
2) CAMBER IS ≤3%
MAT'L IS COORS SC-1

CROSS SECTION FOR
SOLAR TURBINES INCORPORATED
TOLERANCES (INCHES)
DECIMAL ±0.0127 (±.005)
FRACTIONS ±0.039 (±1/64)

Figure 33. Triangular Finned Test Sample

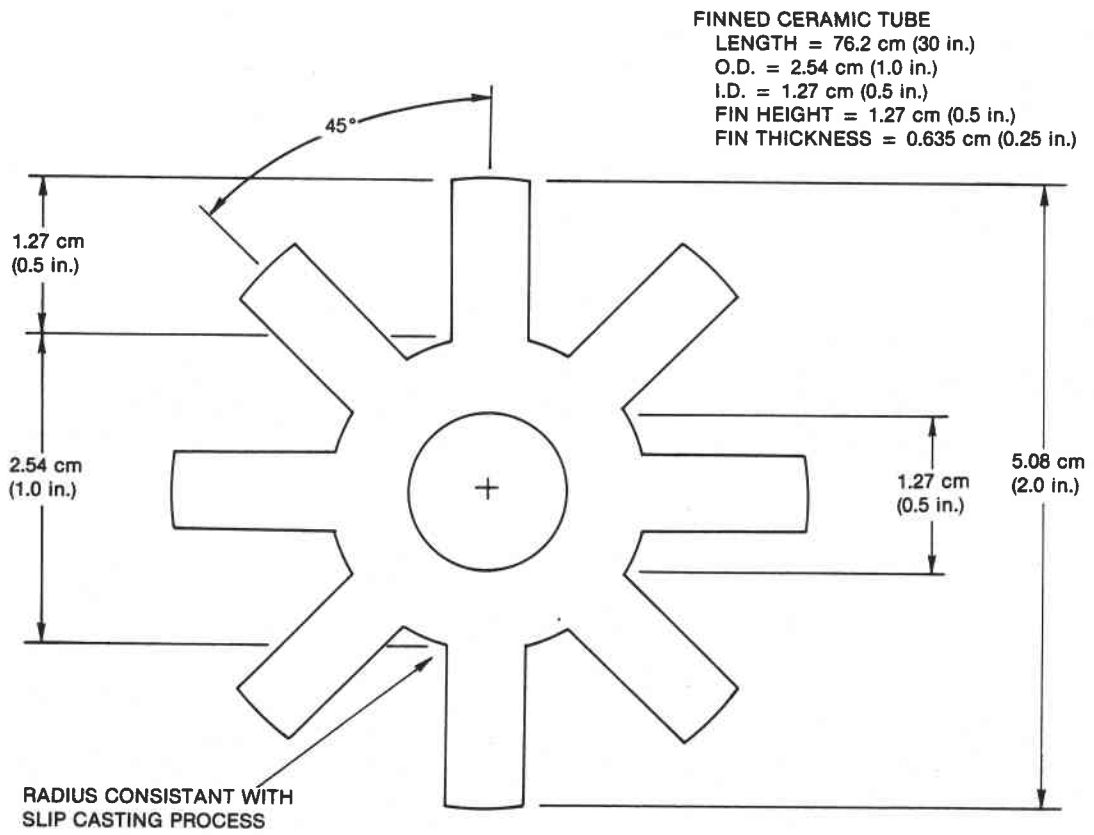

Figure 34. Rectangular Fin Test Sample

- Finning becomes more effective as the internal heat transfer coefficient increases but this also increases the thermal stresses as the temperature differences required for greater heat flow increase.

- Thermal stresses are less in a triangular than in a rectangular fin for the same heat transfer, fin height (b) and fin width at the base (δ_o).

2.2.16 Thermal Shock Tests

Axial finned ceramic tubes were purchased from two vendors. One tube, shown in Figure 35, was a square finned ceramic tube with a 1.27 cm (1/2 in.) ID, a two inch OD and a fin height of 1.27 cm (1/2 in.). There were eight fins equally spaced around the circumference. The second specimen, shown in Figure 36, was a triangular finned ceramic tube with a 1.27 cm (1/2 in.) ID, a 5.08 cm (2 in.) OD and a fin height of 1.14 cm (0.45 in.). This specimen also had eight fins equally spaced around the circumference.

Both axial finned ceramic tube specimens were indirectly heated. Thermocouples were mounted on the tube ID surfaces, the fin tip and the fin base.

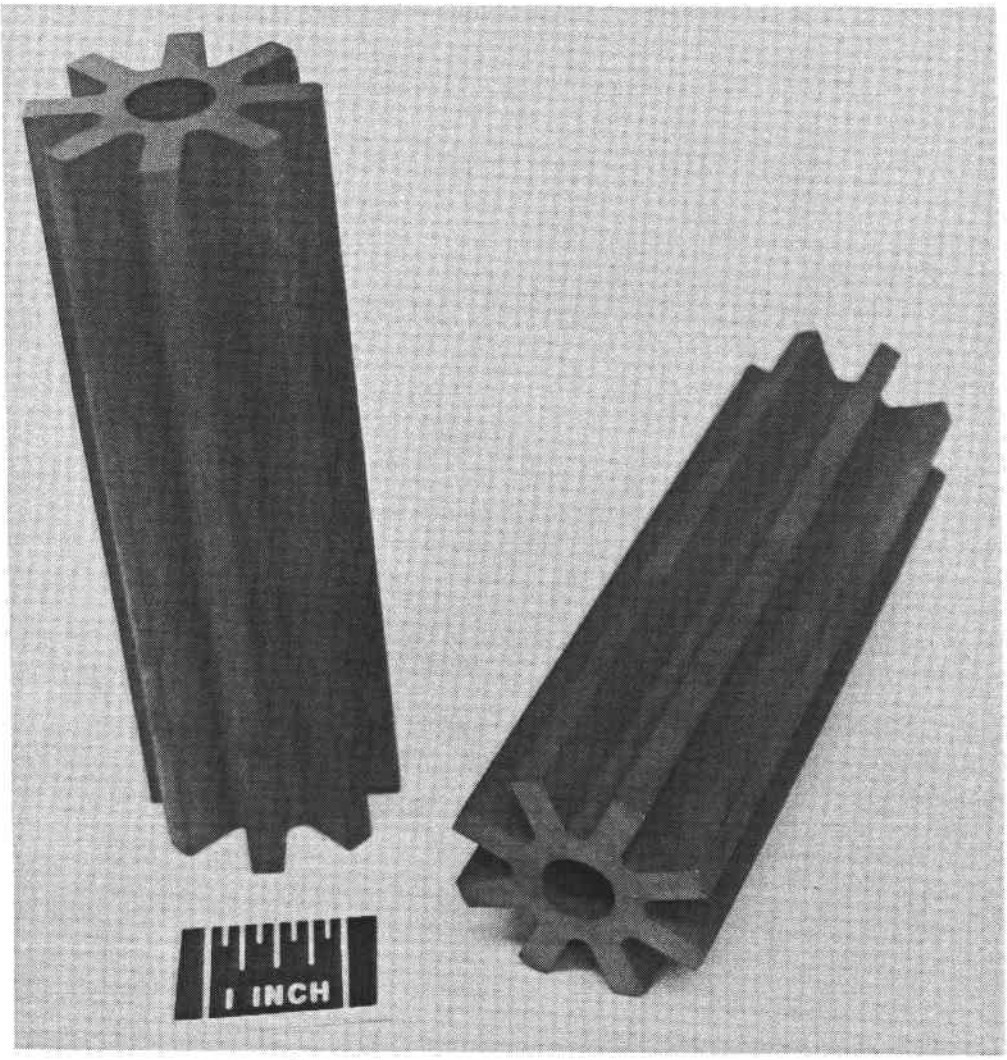

Figure 35. Square Finned Ceramic Tube (NC 430 SiC)

The test results are presented in Figures 37 through 40. Initially the test tubes were heated indirectly with an induction coil (Figs. 37 and 38). In each case, the square finned tubes developed a circumferential hairline fracture, not totally through to the tube ID but extending around the tube following the tube finned surface contour. At no time did the triangular finned tubes develop any fractures.

Then the finned tubes were heated with a susceptor, Figure 41. No damage to the finned tubes were observed.

Besides being desirable from a heat transfer weight view point, it does appear the triangular fin tube has a greater capability of handling thermal stresses.

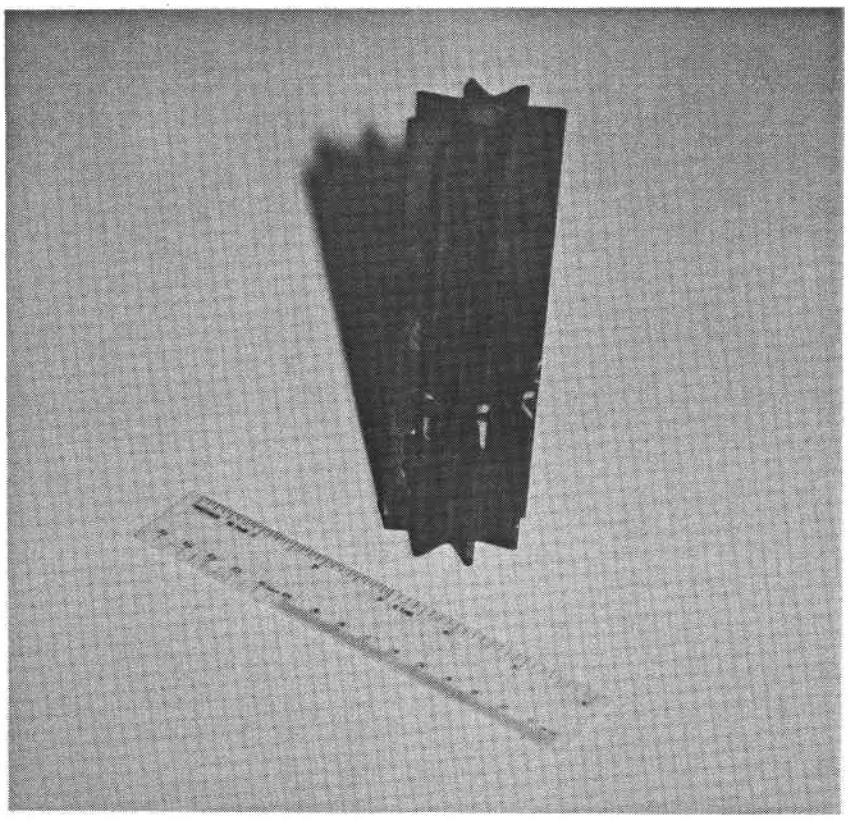

Figure 36. Triangular Finned Ceramic Tube (SC-1 SiC)

The square finned tube square corners, both at the fin tip and base, is believed to cause severe stress concentrations not accounted for in the above analysis.

2.3 ENDURANCE TEST OF THE CERAMIC HEAT EXCHANGER

The design concept that is being tested by this project is shown in Figure 42. Hot gases from a process or combustion chamber enter the top of this unit, flow around the staggered ceramic tubular headers and into the tube bundle. The gases then flow parallel to the tube surfaces, between tubes to the cold end of this air heater at which point it flows around staggered metallic tubular headers and then exits. Cold pressurized air enters the metallic header and is distributed to metallic tubes connected to this header. Air flows up the tube, into the ceramic tubes at or about the mid span of the unit and then into the ceramic header. The hot air flows out of the ceramic header through a ceramic to metal transition into an internally insulated metal header.

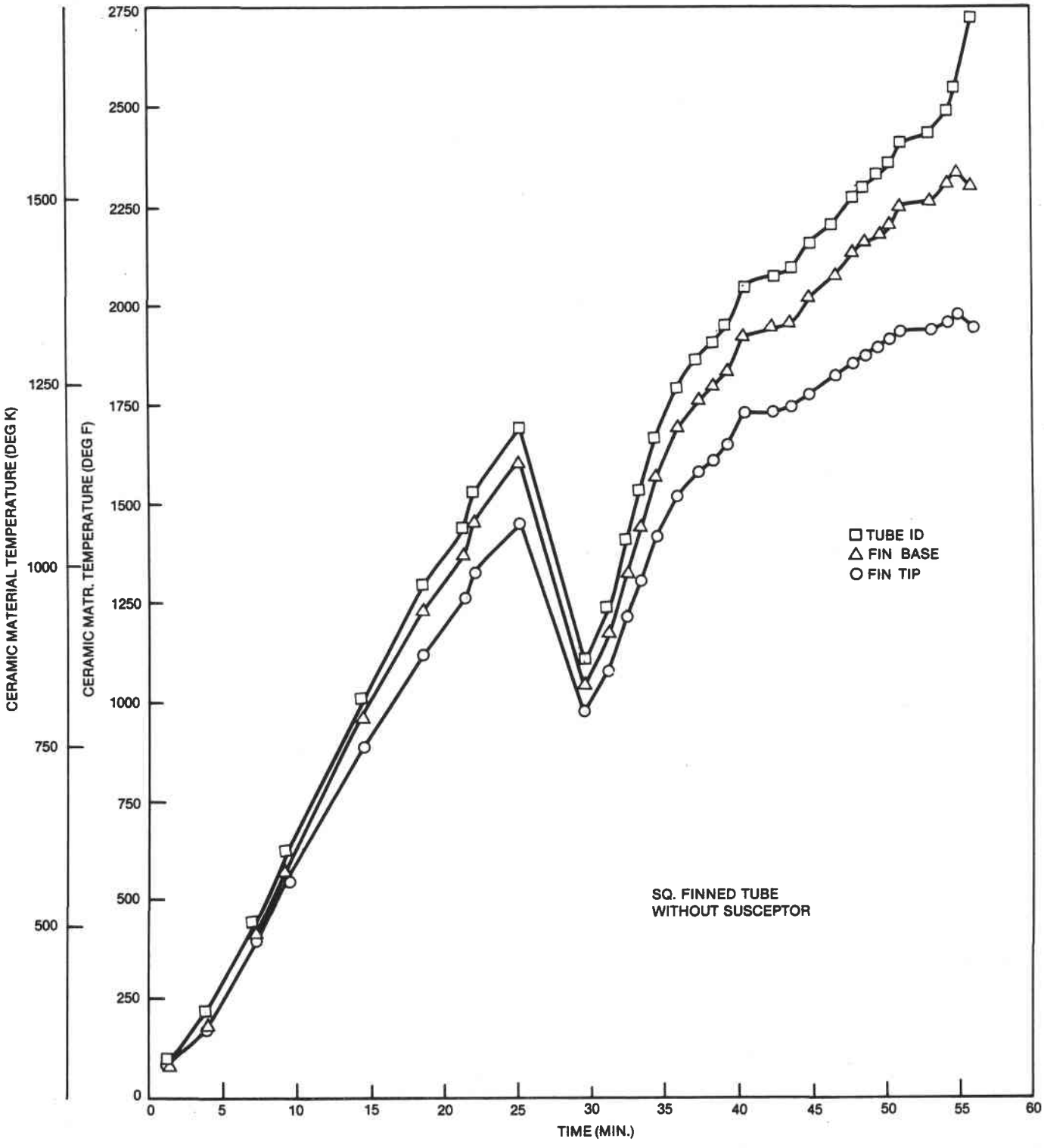

Figure 37. Square Finned Ceramic Tube (Thermal Shock Test Without Susceptor)

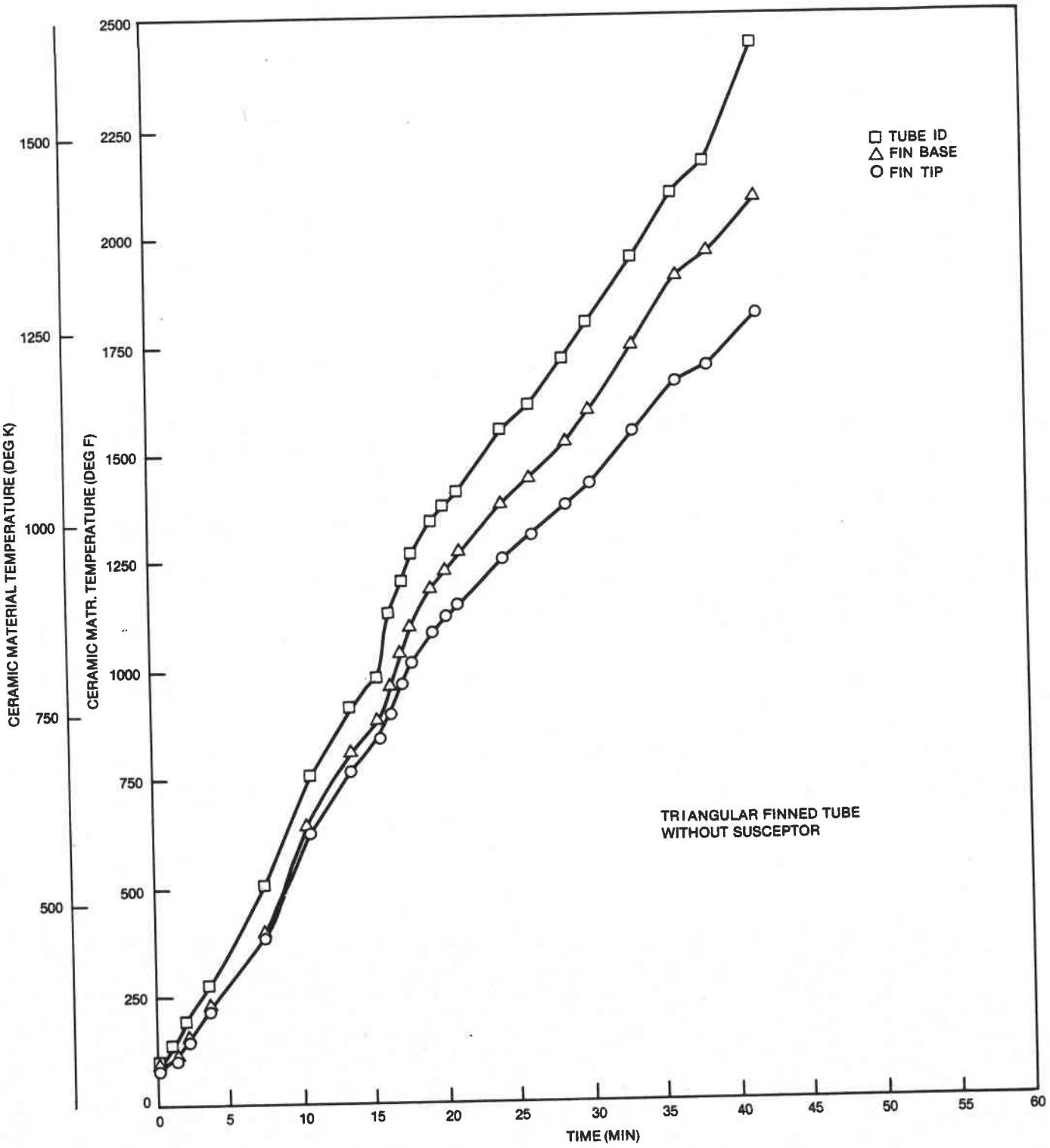

Figure 38. Triangular Finned Ceramic Tube (Thermal Shock Test Without Susceptor)

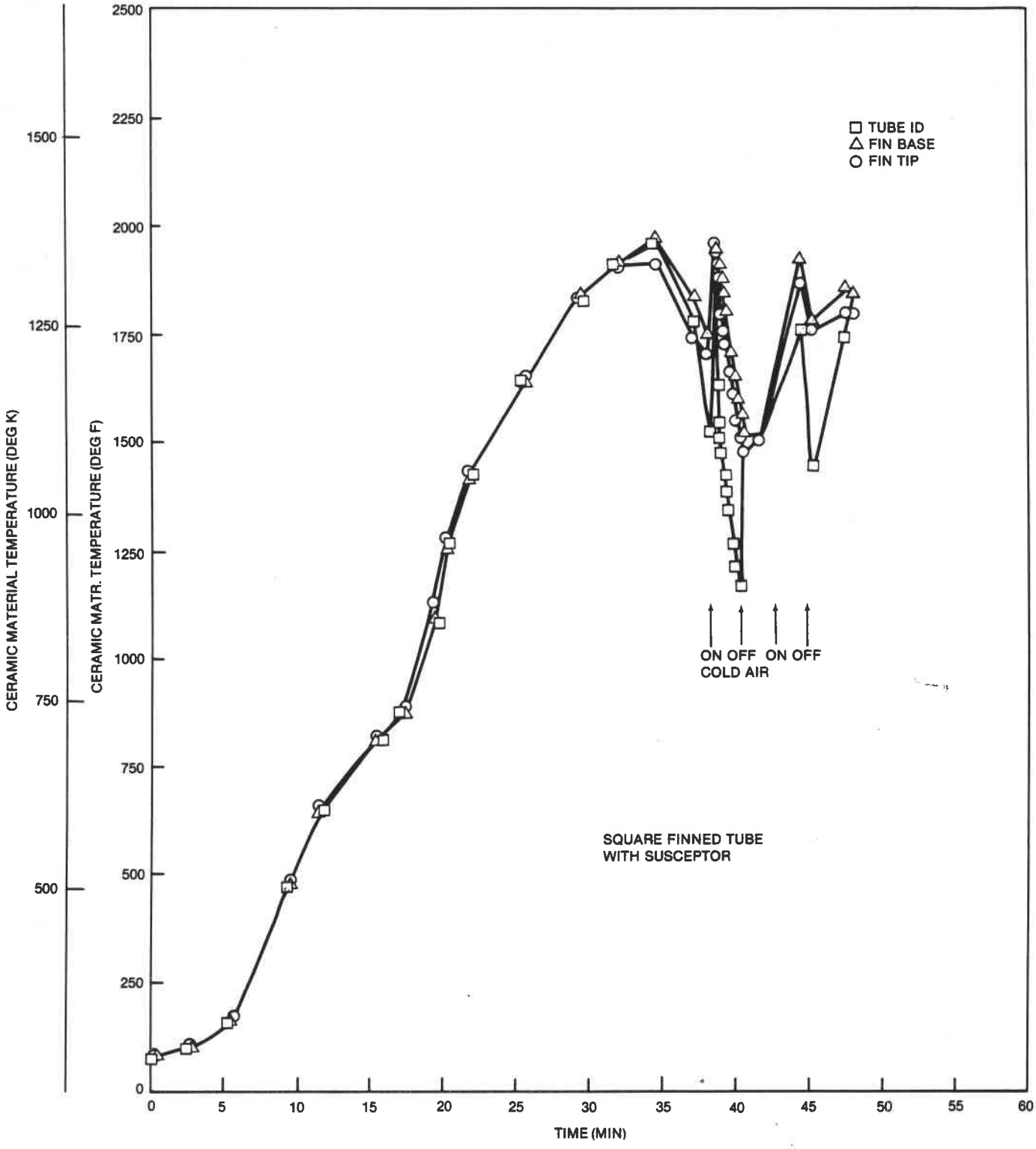

Figure 39. Square Finned Ceramic Tube (Thermal Shock Test With Susceptor)

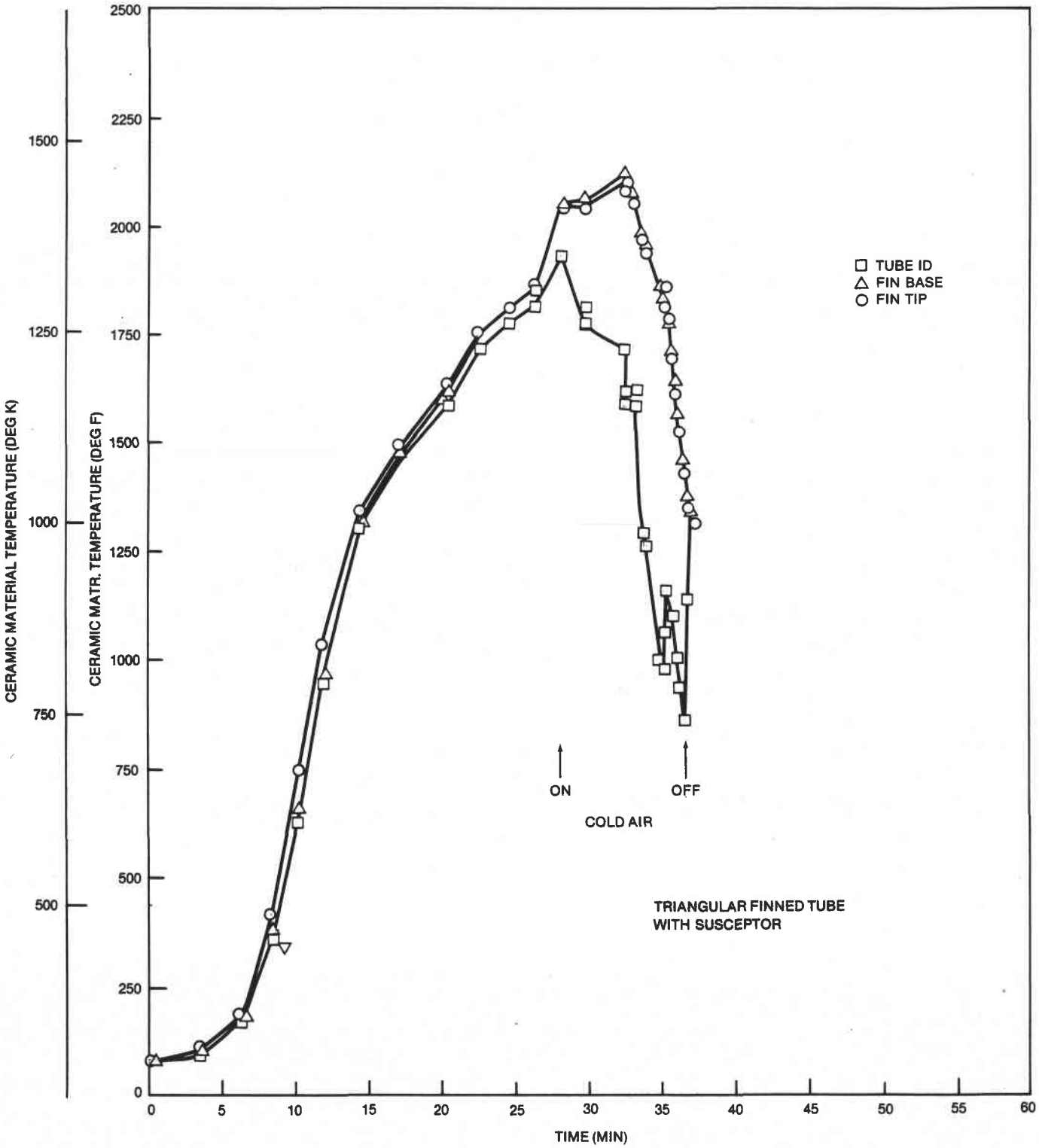

Figure 40. Triangular Finned Ceramic Tube (Thermal Shock Test With Susceptor)

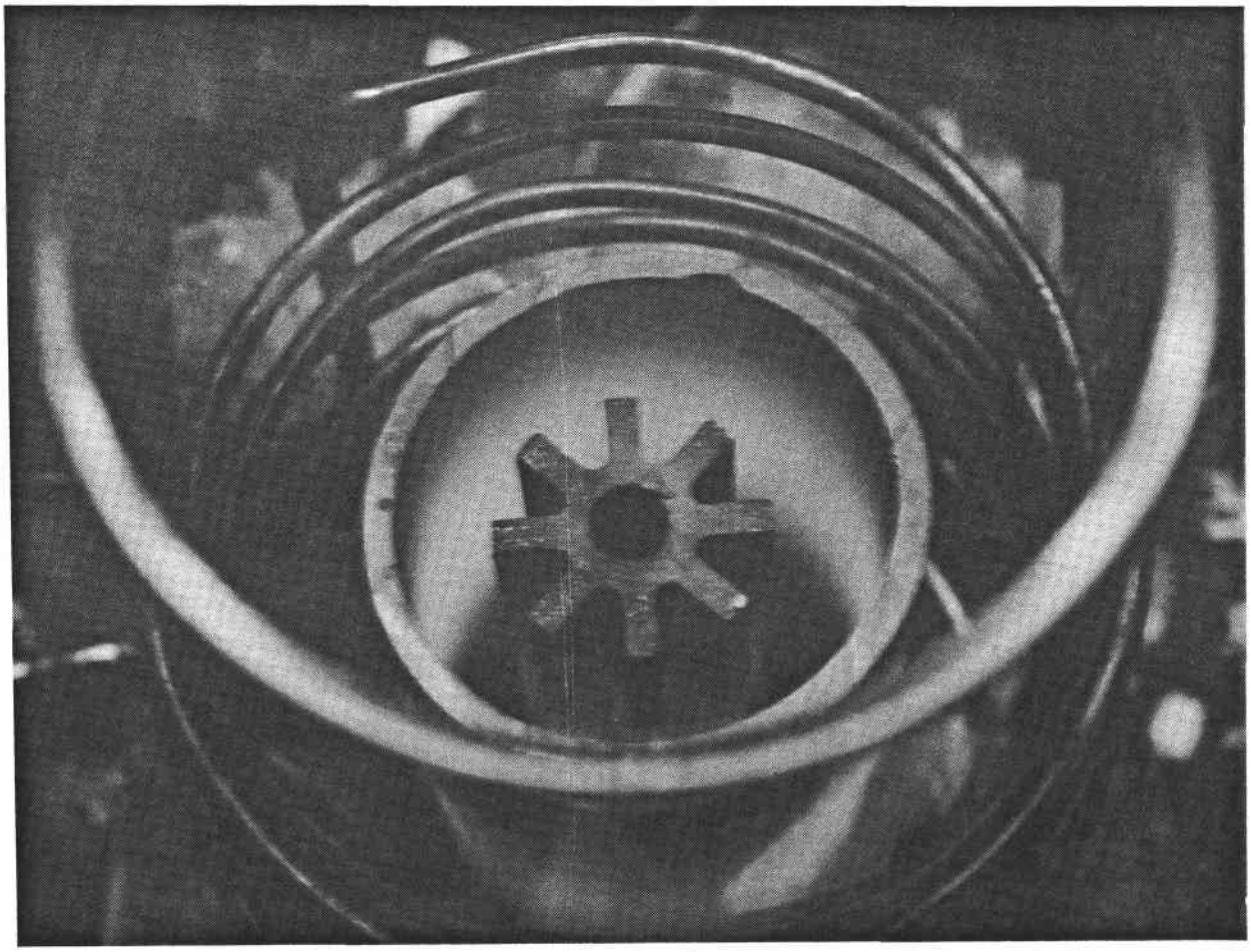

Figure 41. Square Finned Ceramic Tube (Thermal Shock Test)

Solar Turbines Incorporated chose this design concept for the following reasons:

- Minimizes circumferential thermal gradients and strain caused by cross flow
- Eliminates internal air baffles, and therefore, tube to baffle friction joints
- Reduces bending stress in ceramic tubes caused by tube weight over a long horizontal span
- Has potential of reducing flyash accumulations due to lower catch efficiency and self-washing flow
- Minimizes large ceramic tube temperature variations between tubes connected to the same header

Figure 42 illustrates the primary design advanced in this program.

It was decided to construct a modularized slice of this design concept as shown in the shaded area in Figure 42. The ceramic header used in this

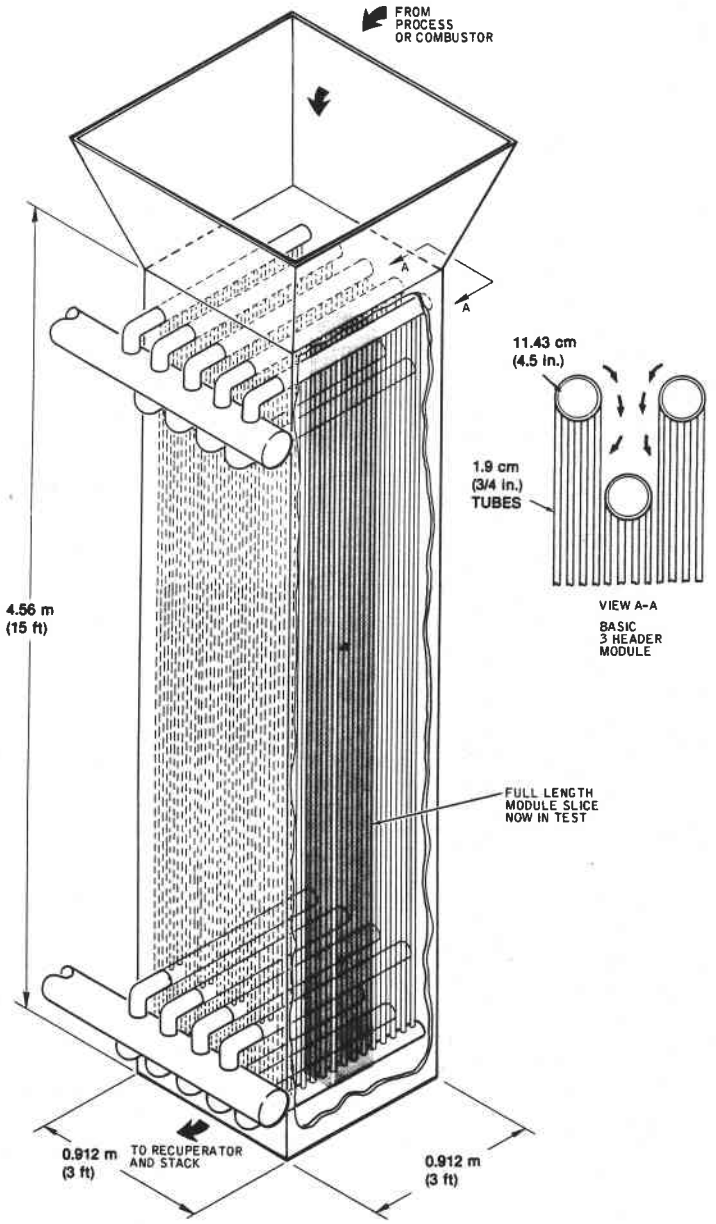

Figure 42. Axial Counter-Flow Heat Exchanger Concept

ceramic heat exchanger module is shown in Figure 43. It is 11.43 cm (4.5 in.) in diameter with 0.635 cm (1/4 in.) walls and is approximately 0.914 m (3 ft) long. The heat exchanger uses 4.57 m (15 ft) long, 2.54 cm (1 in.) OD by 0.635 cm (1/4 in.) wall sintered silicon carbide (NC-430) ceramic tubes (Fig. 44) spaced 0.635 cm (1/4 in.) apart in a triangular matrix. There are 28 ceramic tubes in this test module.

A metal header with an Inconel 625 internally guided bellows was incorporated into the heat exchangers cold end. The header is made from Inconel 800-H material. The Inconel 625 bellows are threaded into the header to give each

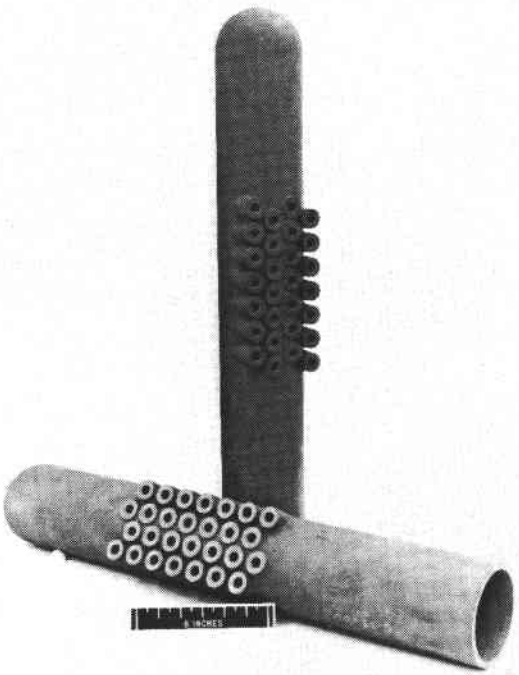

Figure 43. Ceramic Header

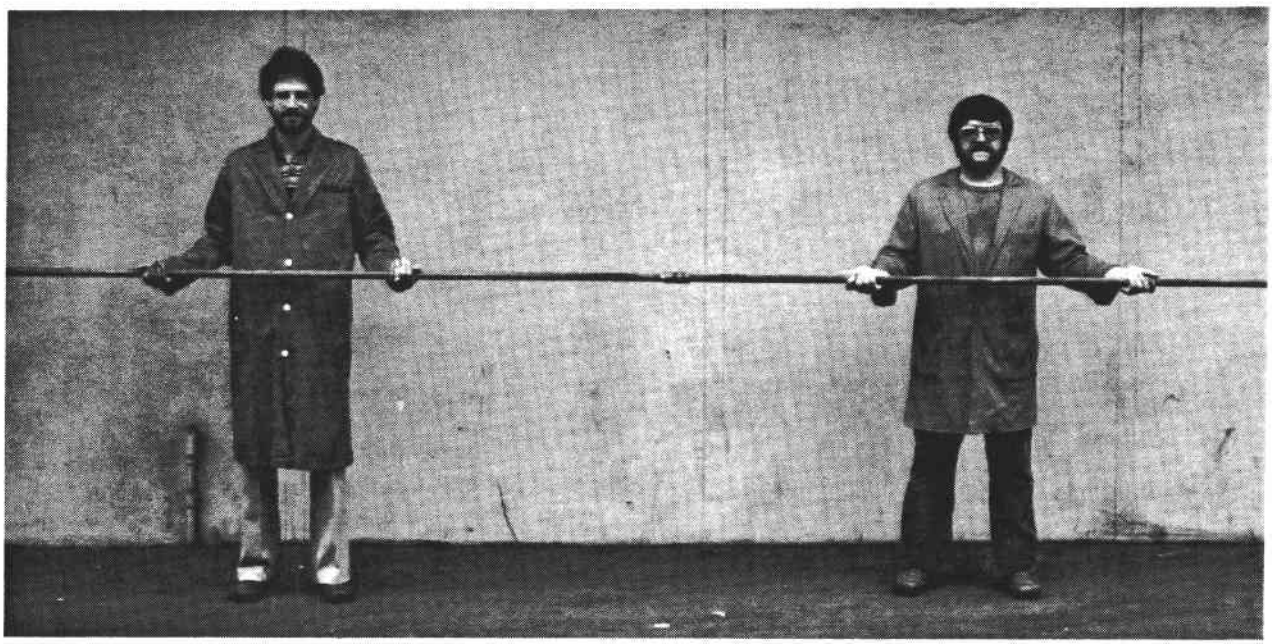

Figure 44. 4.57 Meter (15 ft) Ceramic Tube

bellows individual height adjustment. A top view of the header is shown in Figure 45 and a side view showing a single bellows assembly is shown in Figure 46. The bellows assembly was incorporated into the design to compensate for tube to tube differential expansions. The assembly of the heat exchanger test module was accomplished by providing a spherical compression (ball and socket) joint between the ceramic tubes and the ceramic header and the ceramic tubes and metal header. The spherical joint requires that the ceramic tube be kept in compression to ensure a gas-tight seal between the tubes and headers. This system offers a significant advantage, which is the ability to assemble the heat exchanger and to replace ceramic tubes or headers by simply untensioning the floating header, removing and replacing the desired components and then repositioning the floating header. These features facilitate field repair.

The test module is shown in Figures 47 and 48. Ten hours of operation with an internal pressure of 689 kPa (100 psi) and light oil firing up to 1644°K (2500°F) was successfully completed in 1980. The testing included seven starts and shutdowns and one severe thermal cycle. The thermal cycle consisted of a severe shutdown from maximum operating conditions [1644°K (2500°F) firing temperature and 1478°K (2200°F) air side outlet temperature). Cool

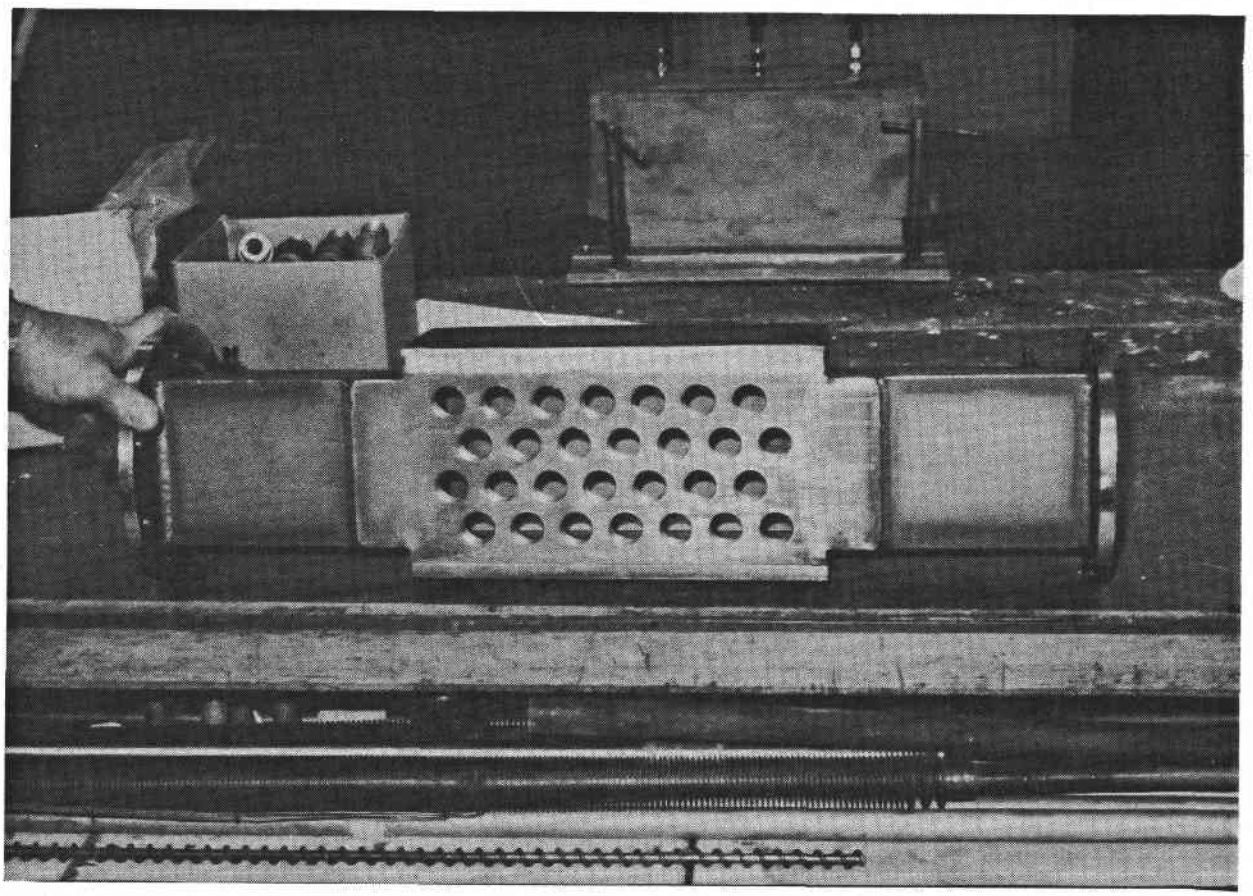

Figure 45. Metal Header (Top View)

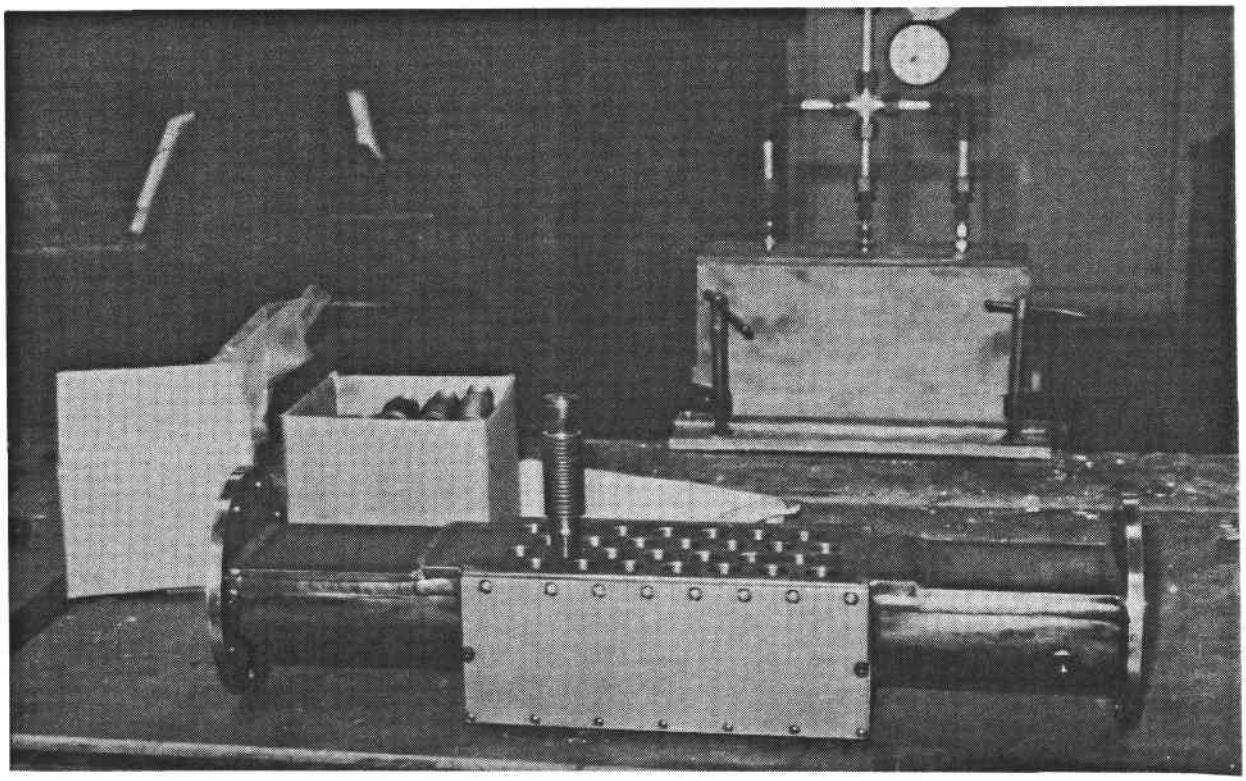

Figure 46. Metal Header (Side View With Bellows)

down rates of 555°K (1000°F) per minute were recorded. A plot of the testing showing firing, inlet and outlet temperatures is presented in Figures 49 and 50.

The ceramic heat exchanger module was moved to a new test facility (Fig. 51). A new outer shell was constructed with a fiber backed refractory lining (Kaocrete 32-C) in order to survive the environment resulting from coal firing this module. The 4.57 m (15 ft) long ceramic tube ball and socket joints were refurbished. The tubes were installed in the new shell and readied for endurance testing. This ceramic heat exchanger module has successfully completed 118 hours of running at temperature and pressure (Fig. 52).

2.3.1 Test Results

The endurance test was concluded after 118 hours. The unit was running steady with very little deviation except for what resulted from the test facility (air supply, fuel supply, etc.). After the system was running steady, leakage was immeasurable. The only leakage in the tube to header joints that occurred was when a thermal cycle occurred. The tube bundle would either expand or contract depending upon the thermal cycle characteristic and the metal header would not completely follow the tube bundle. This was caused by the sealing slide gates between the metal shell and the metal header. Binding in this slide gate would prevent the smooth movement of the metal header. Periodic manual adjustment of the metal header was needed during the test.

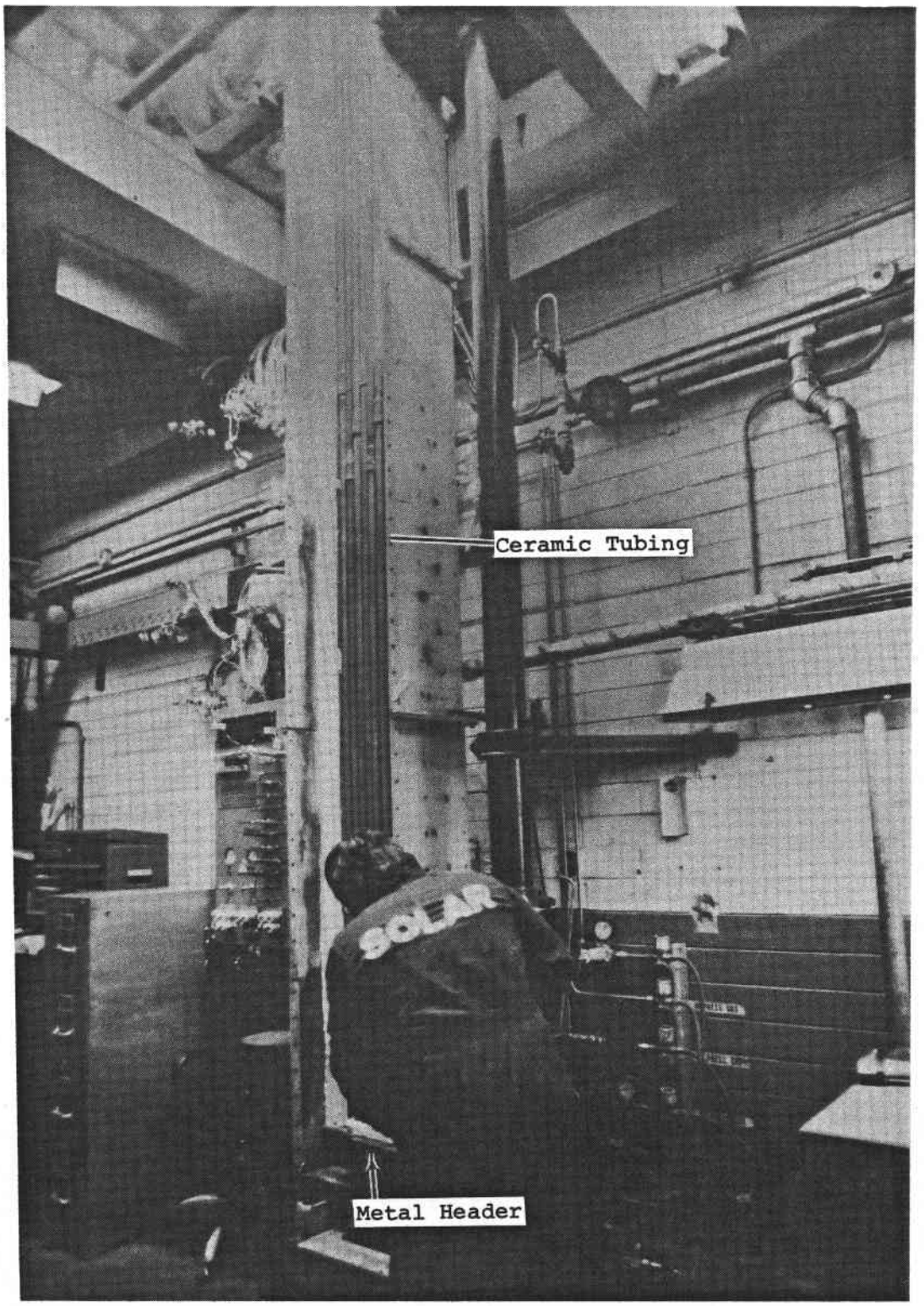

Figure 47. The 4.57 Meter (15 ft) Ceramic Tube Heat Exchanger Module

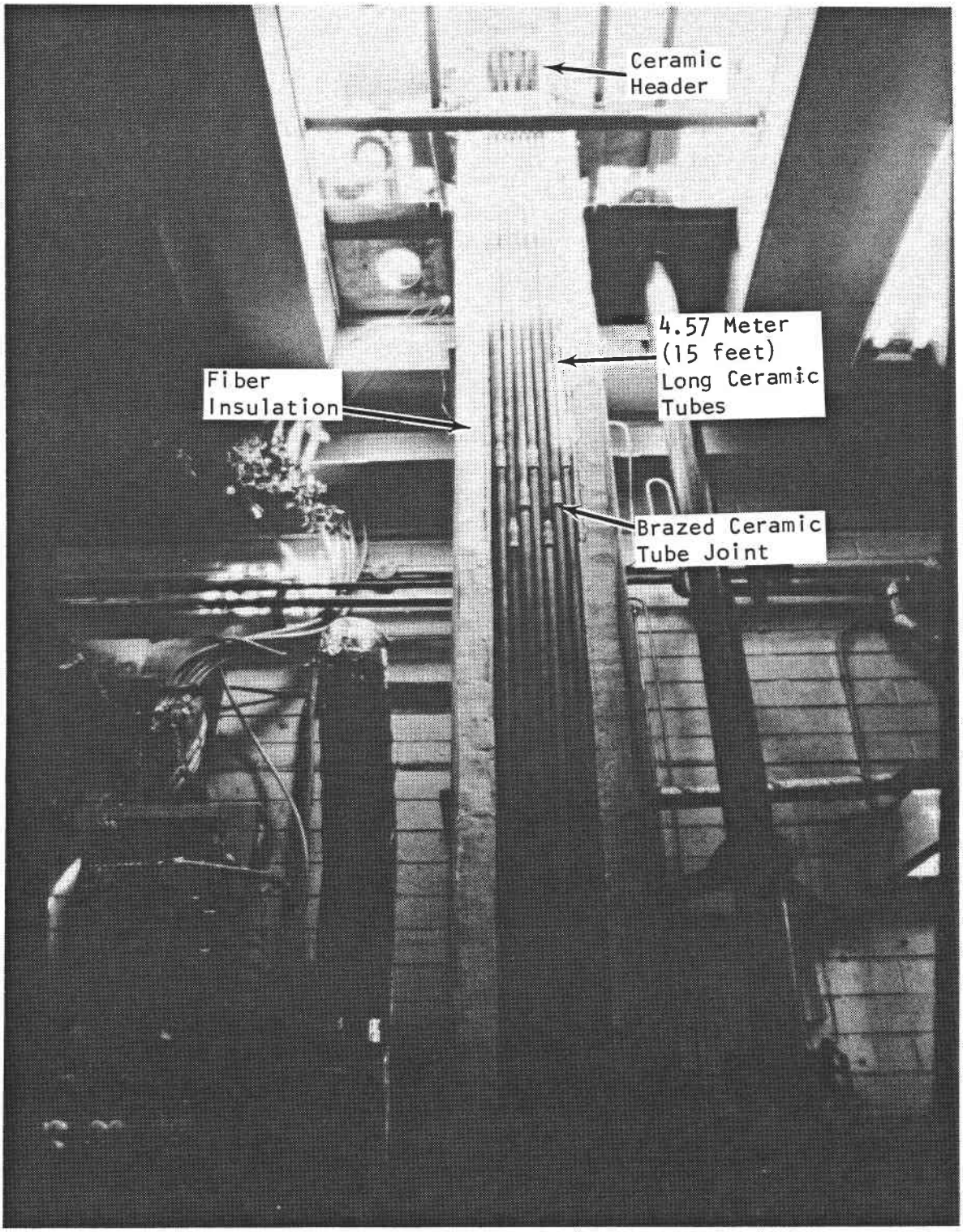

Figure 48. The 4.57 Meter (15 ft) Ceramic Tube Heat Exchanger Module

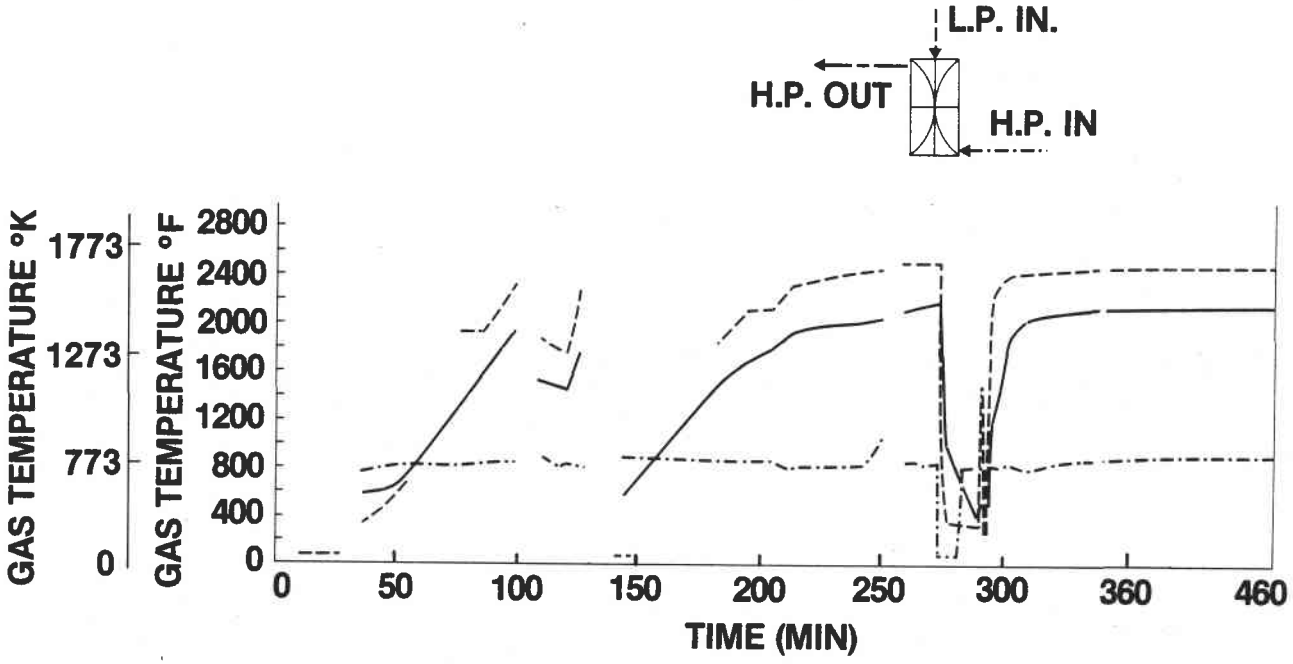

Figure 49. Initial Module Tests

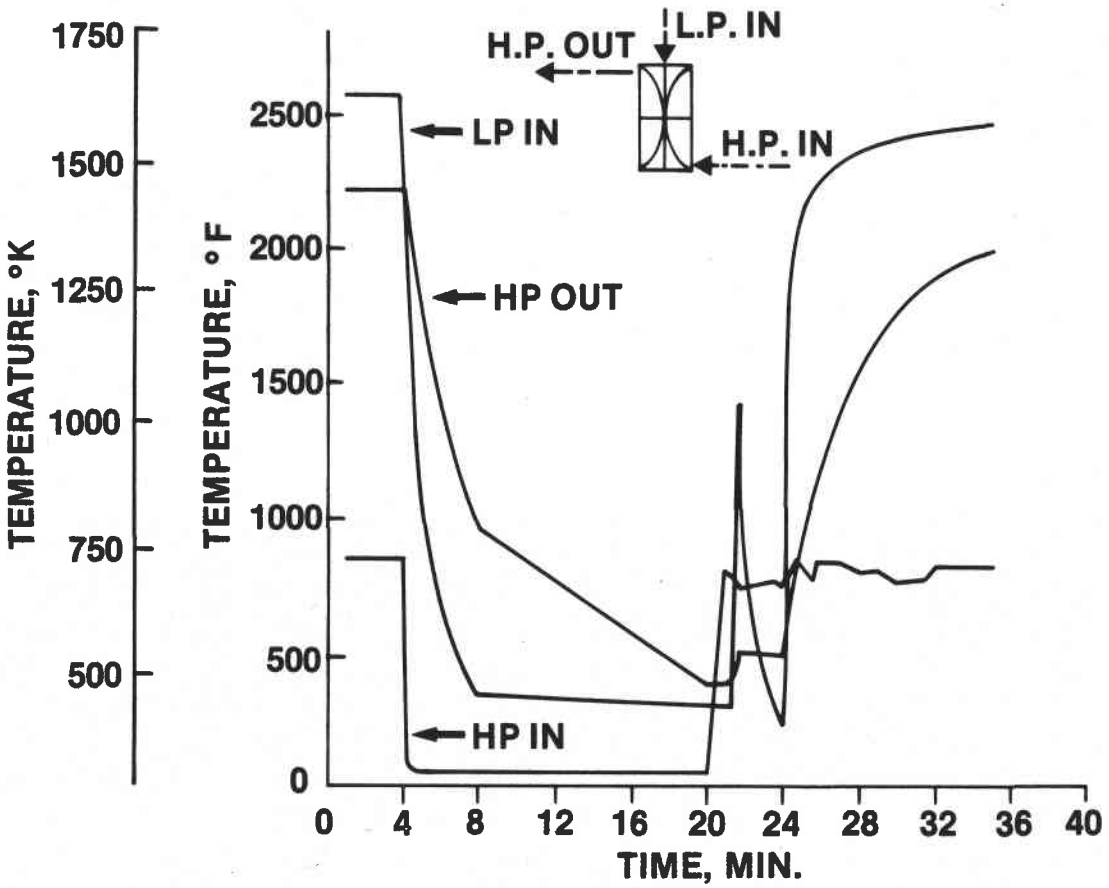

Figure 50. Thermal Transient Plot

Leakage of the low pressure hot gases occurred around the ceramic header. During the period of the test, this caused the shell in the immediate area around the creamic header to distort.

During the 118 hour endurance test, no damage to the ceramics was seen. Inspection of the header, tubing and joints after the test revealed that all were in good condition. Ceramic material temperatures, verified by radiation pyrometry, ranged from 1561°K (2350°F) for the ceramic header to 1478°K (2200°F) for the ceramic tubes at the hot end.

The last three hour test that was performed was at very high temperatures. The firing temperature was 1755°K (2700°F) and the hot air outlet temperature was 1533°K (2300°F). These temperatures were continuing to increase during the test. The ceramic header temperature reached a maximum of 1700-1728°K (2600-2650°F) during this test. About three hours into the test, the ceramic header failed. Upon examination after the test, the ceramic header broken parts had extensive free silicon nodules covering the surfaces (see Figs. 53 and 54). The materials temperature limit, approximately 1700°K (2600°F), had been reached. Free silicon in the ceramic microstructure started to extrude from the material thereby lowering its strength.

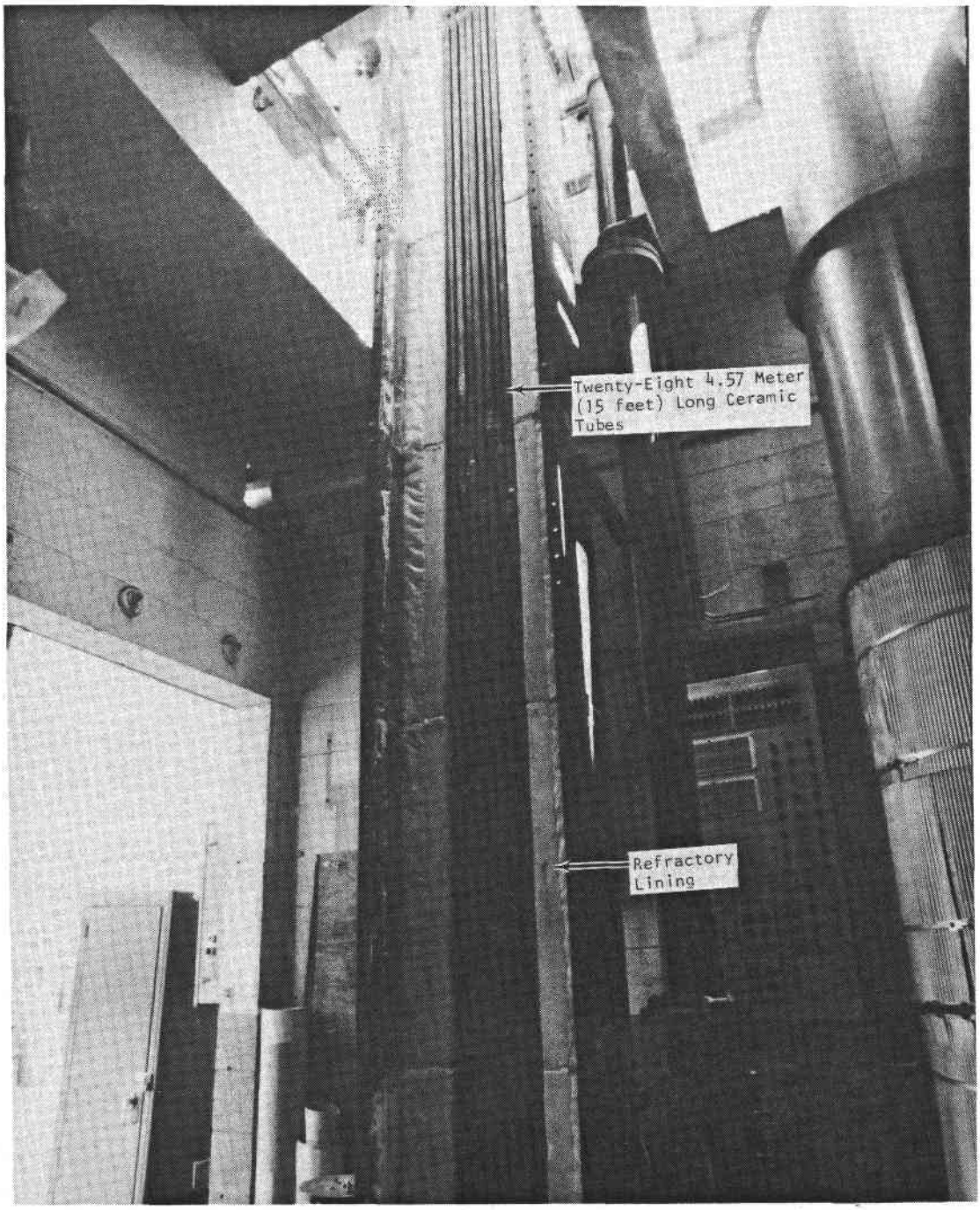

Figure 51. New Test Facility

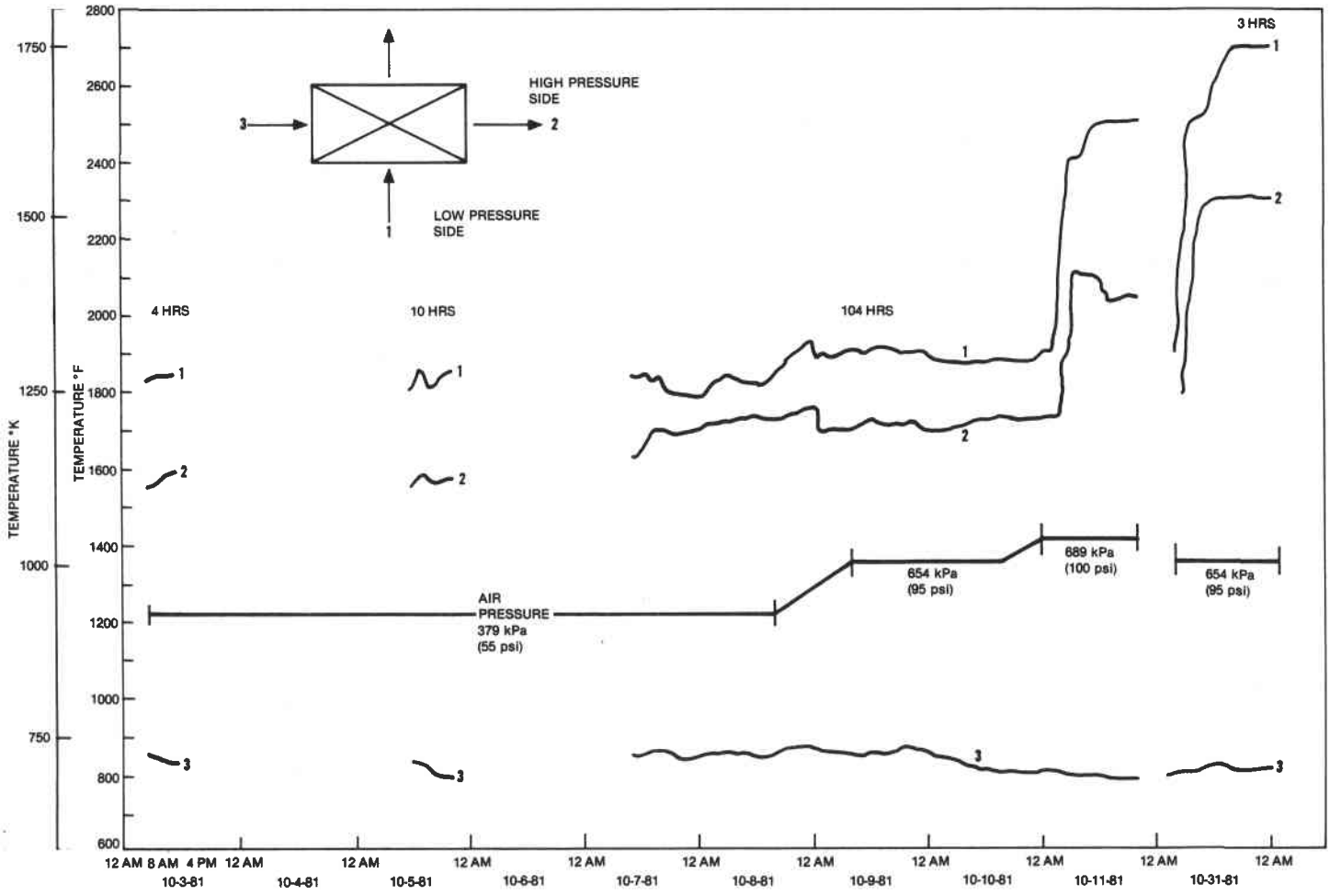

Figure 52. Ceramic Heat Exchanger Endurance Test (Test Conditions) (°K = °F + 459.67/1.8)

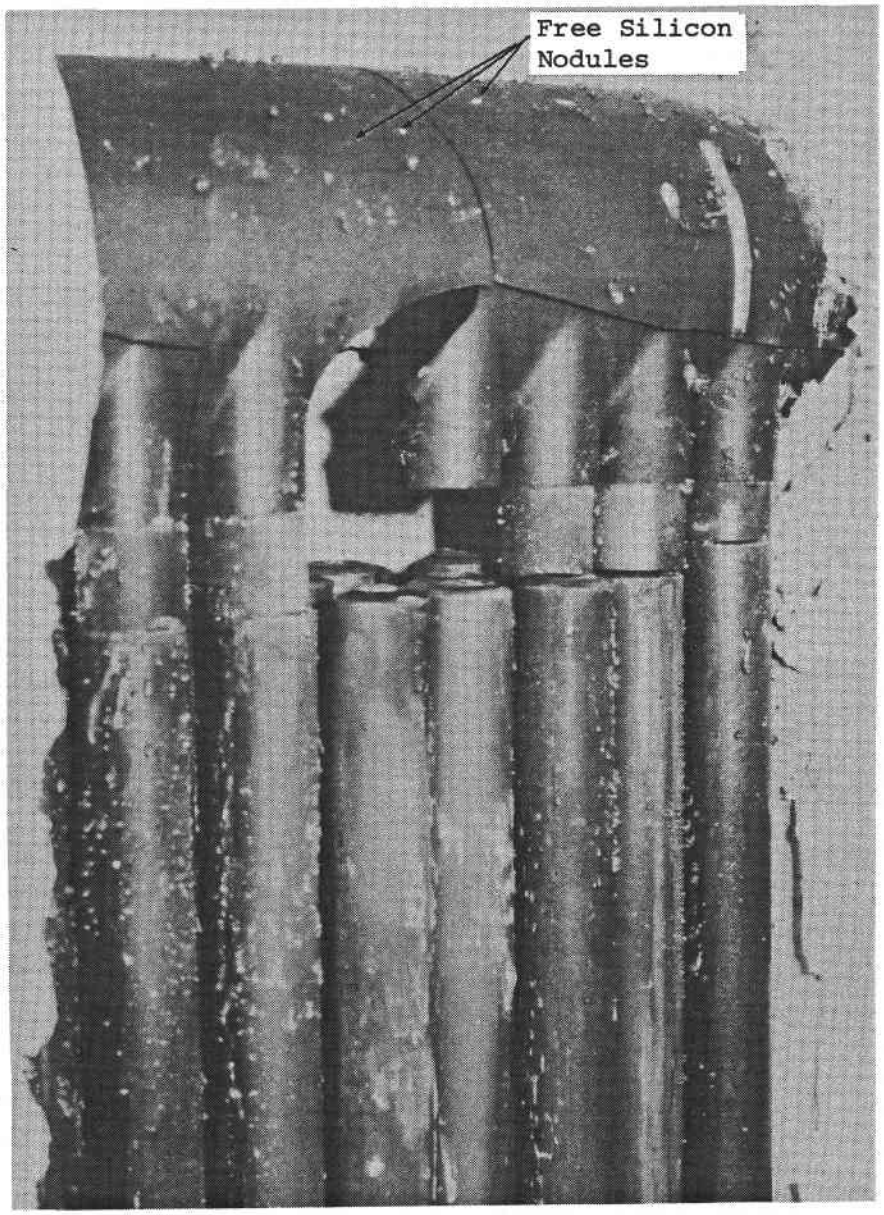

Figure 53. Ceramic Header After Tests Above the Melting Point of Silicon

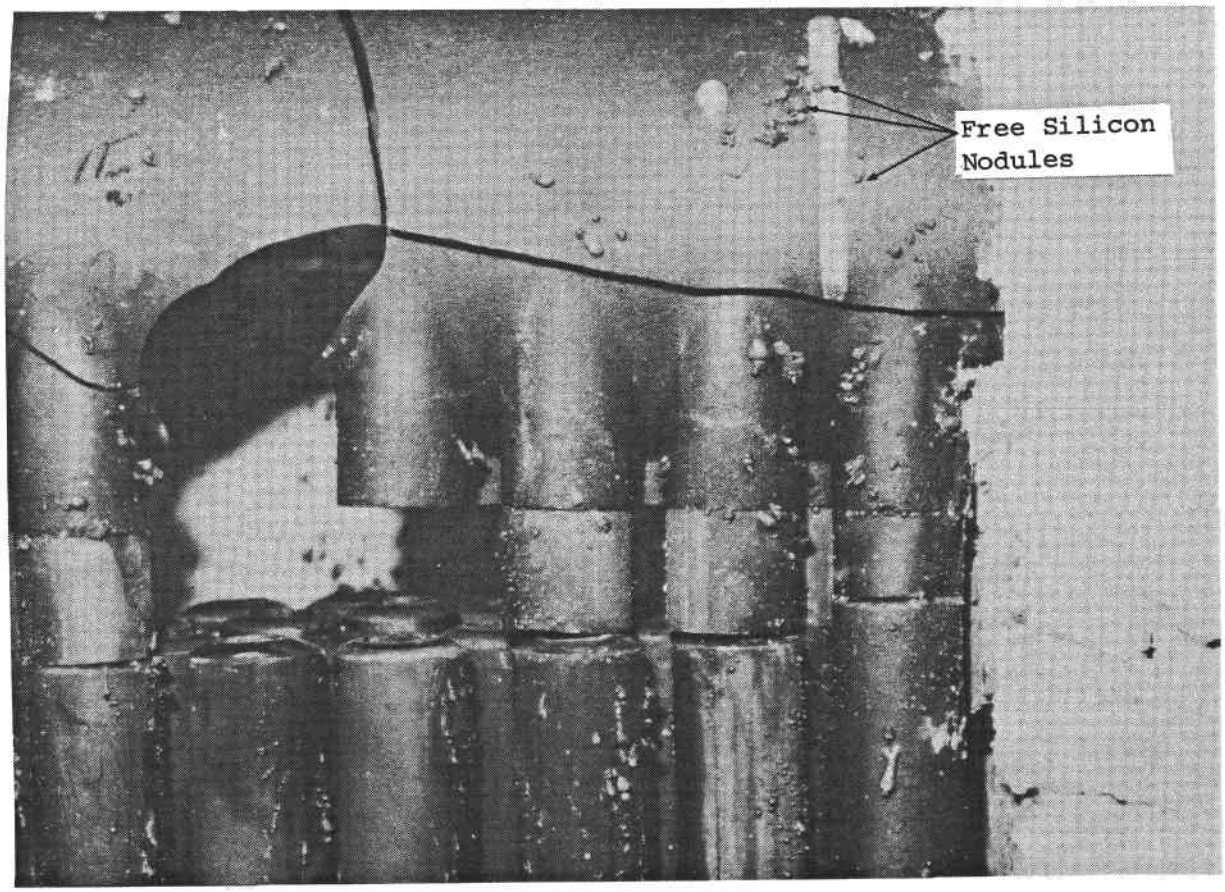

Figure 54. Ceramic Header After Tests Above the Melting Point of Silicon

3

CONCLUSIONS

The accumulation of experience gained on this and Solar's previous DOE ceramic heat exchanger project (contract number EF-7-C-01-2556) has lead Solar to conclude that it is possible to build a pressurized ceramic heat exchanger with the ceramic materials presently available. Allowance for the inherent nature of this material (brittleness) and for the material suppliers' manufacturing state-of-the-art had to be made in order to achieve the goal of this work; the operation of a full-size pressurized ceramic heat exchanger module. This was demonstrated by operating this heat exchanger for a period of time to gain confidence in its operation.

The test module has proven that a bare tube pressurized ceramic heat exchanger is feasible. The fact that 4.57 m (15 ft) ceramic tubes had to be used to transfer the necessary heat did present some difficulties especially in material handling.

It is recommended that the same facility be used to investigate the possibilty of a hybrid metal/ceramic tube design. The metal tubes would extend from the metal header for approximately 1.52 m (5 ft) then mate directly to ceramic tubes. These ceramic axial finned tubes would extend for 3.05 m (10 ft) to a ceramic tubular header. Also as part of this investigation, the header will be directly connected through a ceramic transition to an internally insulated metal duct.

At the conclusion of this work, Solar feels that with the technology that has been acquired since the early 1970's in the use of structural ceramics, the Company would be in a position to enter into a ceramic heat exchanger prototype development project ending with the field testing of a pressurized full size modularized ceramic heat exchanger in an environment suitable for silicon carbide materials.

REFERENCES

1. Moskowitz, S., Weth, G. and Leon, A., "Development of a Coal-Fired Pressurized Bed for Combined Cycle Power Generation", ASME Paper 80-GT-189, presented in New Orleans, LA, March 1980.

2. Schneider, P. J., Conduction Heat Transfer, Addison-Wesley Publishing Company, Inc., Reading, Massachusetts, second printing, 1957, Chapter 4, "Extended Surface".

3. Eckert, E. R. G. and Drake, R. M., Heat and Mass Transfer, McGraw-Hill Book Company, Inc., second edition, New York, 1959.

4. Steam/Its Generation and Use, Babcock & Wilcox, 30th Edition, 1978.

5. Roark, R. J., Formulas for Stress and Strain, McGraw-Hill Book Company, Inc., New York, Third Edition, 1954.

APPENDIX A

FIN EQUATIONS (REF. 1)

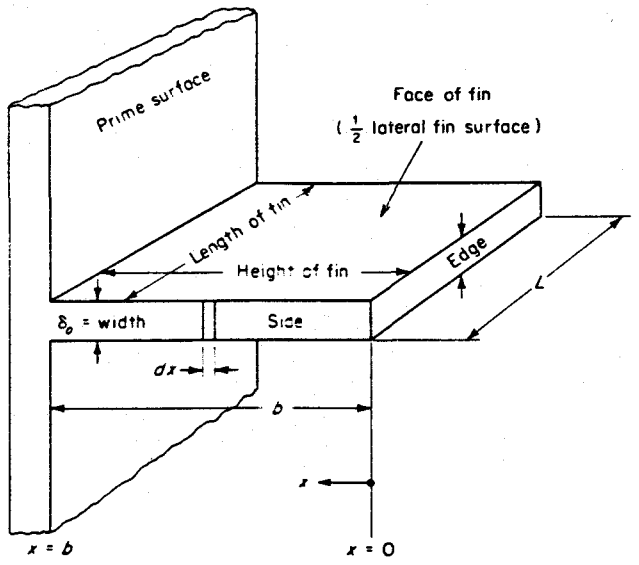

Fig. 1. Terminology and Coordinate System Longitudinal Fin of Rectangular Profile

$$f_2(x) = \frac{\delta_o}{2} \quad (x/b)$$

$$q_o = \frac{2h\theta_o I_1(2mb)}{mI_0(2mb)}$$

$$\eta = \frac{I_1(2mb)}{mbI_0(2mb)}$$

$$\eta \approx \frac{1}{mbI_o(2mb)}$$

$$f_2(x) = \frac{\delta_o}{2} \quad (x/b)^2$$

$$q_o = \frac{k\delta_o\theta_1}{2b}\left[-1 + \sqrt{1 + (2mb)^2}\right]$$

$$\eta = \frac{2}{1 + \sqrt{1 + (2mb)^2}}$$

Simplified

$$q_o = k\delta_o m\theta_o \tanh mb$$

$$\eta = \frac{\tanh mb}{mb}$$

Real Constraints

$$q_o = k\delta_o Lm\theta_o \tanh\left[mb + \left(\frac{h\delta_o}{2k}\right)^{1/2}\right]$$

$$\eta = \frac{\tanh (mb_c)}{mb_c} \qquad b_c = b + \frac{\delta_o}{2}$$

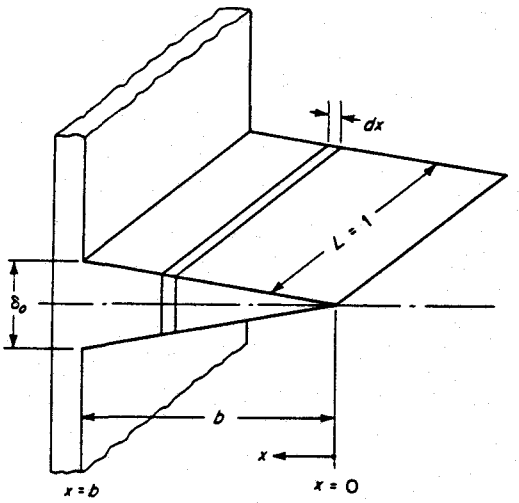

Fig. 2. Longitudinal Fin of Triangular Profile

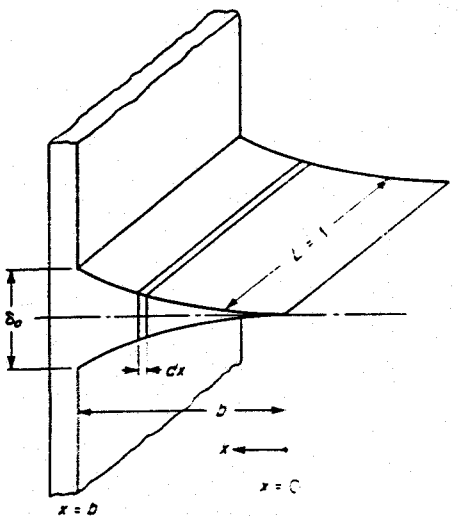

Fig. 3. Longitudinal Fin of Concave Parabolic Profile

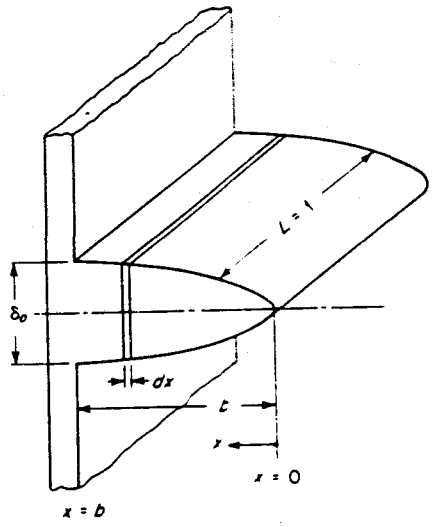

$$f_2(x) = \frac{\delta_o}{2} (x/b)^{1/2}$$

$$q_o = k\delta_o\theta_o m \frac{I_{2/3}\left(\frac{4}{3} mb\right)}{I_{1/3}\left(\frac{4}{3} mb\right)}$$

$$\eta = \frac{1}{mb} \frac{I_{2/3}\left(\frac{4}{3} mb\right)}{I_{1/3}\left(\frac{4}{3} mb\right)}$$

Fig. 4. Longitudinal Fin of Convex Parabolic Profile

Fig. 5. Coordinate System for Longitudinal Radiating Fin of Trapezoidal Profile. The Triangular Profile is a Special Case When $_o = 0$.

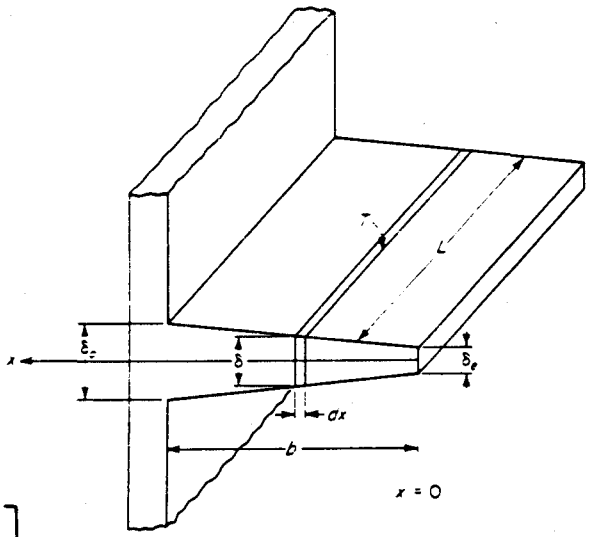

$$q_o = k\theta_o\mu_o \tan K \left[\frac{K_1(\mu_e)I_1(\mu_o) - I_1(\mu_e)K_1(\mu_o)}{I_o(\mu_o)K_1(\mu_e) + I_1(\mu_e)K_1(\mu_o)}\right]$$

$$\eta = \frac{\mu_o}{2K^2 b_c} \left[\frac{K_1(\mu_e)I_1(\mu_o) - I_1(\mu_e)K_1(\mu_o)}{I_o(\mu_o)K_1(\mu_e) + I_1(\mu_e)K_0(\mu_o)}\right]$$

$$K^2 = \frac{h}{k \sin K}$$

$$\mu_e = 2K \left[\frac{\delta_e (1 - \tan K)}{2 \tan K}\right]^{1/2}$$

$$\mu_o = 2K \left[b_c + \frac{\delta_e (1 - \tan K)}{2 \tan K}\right]^{1/2}$$

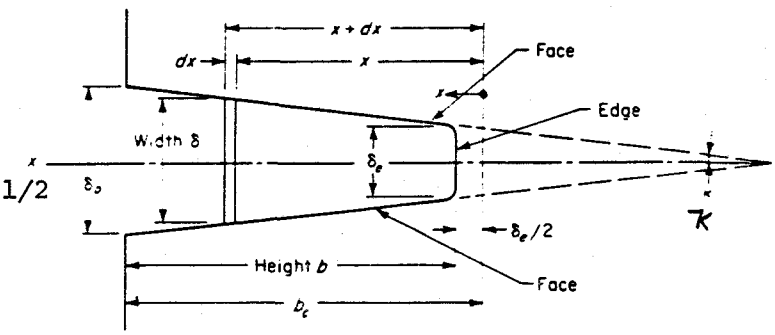

Fig. 6. Terminology and Coordinate System For Longitudinal Fin of Trapezoidal Profile With Edge Heat Loss

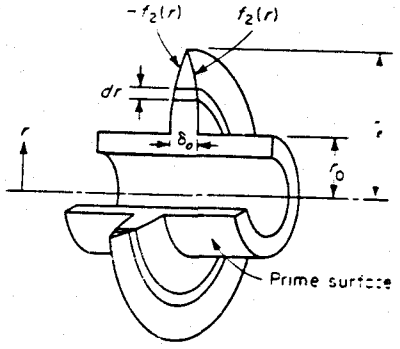

$$d_q = k \frac{d}{dr} \left[(2\pi r)\ 2f_2(r) \frac{d\theta}{dr} \right] dr$$

$$y = f_2(r)$$

Fig. 7. Radial Fin of Arbitirary Profile

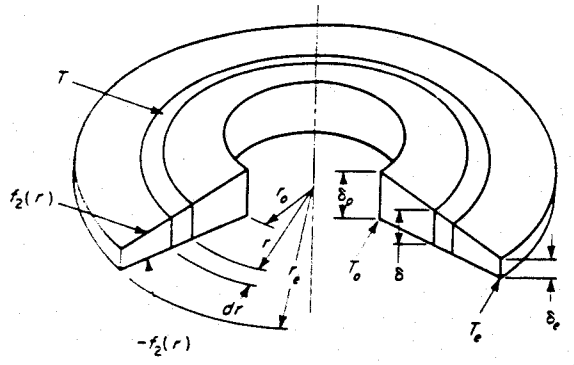

Fig. 8. Coordinate System for Radial Fin of Trapezoidal Profile

$$q_o = 2\pi r_o \delta_o k m \theta_o \left[\frac{I_1(mr_e)\ K_1(mr_o) - K_1(mr_e)\ I_1(mr_o)}{I_o(mr_o)\ K_1(mr_e) + I_1(mr_e)\ K_o(mr_o)} \right]$$

$$\eta = \frac{2r_o}{m(r_e^2 - r_o^2)} \left[\frac{I_1(mr_e)\ K_1(mr_o) - K_1(mr_e)\ I_1(mr_o)}{I_o(mr_o)\ K_1(mr_e) + I_1(mr_e)\ K_o(mr_o)} \right]$$

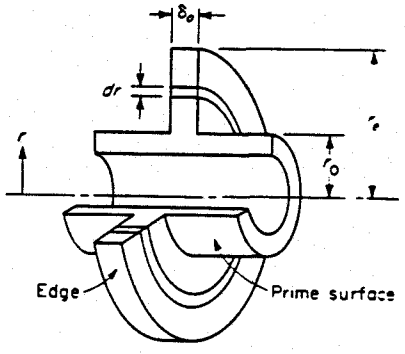

Fig. 9. Radial Fin of Rectangular Profile

$$q_o = 2\pi k r_o \delta_o \theta_o M \; r_o \underbrace{\frac{I_{2/3}(\frac{2}{3} m r_e^{3/2}) \; I_{2/3}(\frac{2}{3} m r_o^{3/2}) - I_{2/3}(\frac{2}{3} m r_e^{2/3}) I_{2/3}(\frac{2}{3} m r_o^{3/2})}{I_{2/3}(\frac{2}{3} m r_e^{3/2}) \; I_{1/3}(\frac{2}{3} m r_o^{3/2}) - I_{2/3}(\frac{2}{3} m r_e^{3/2}) \; I_{1/3}(\frac{2}{3} m r_o^{3/2})}}_{4}$$

$$M^2 = \frac{m^2}{r_o}$$

$$\eta = \frac{2 r_o \; 4}{m(r_e^2 - r_o^2)}$$

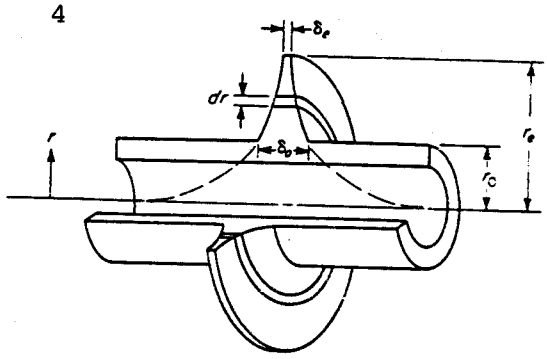

Fig. 10. Radial Fin of Hyperbolic Profile

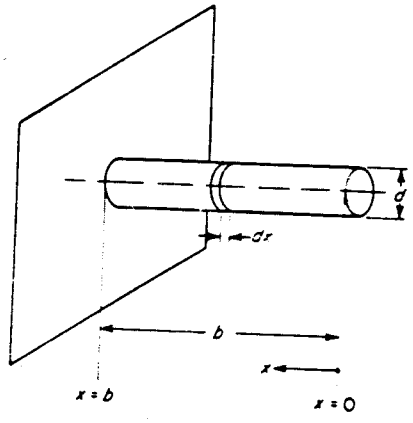

$$q_o = \frac{\pi}{4} k d^2 m \theta_o \tanh mb$$

$$\eta = \frac{\tanh mb}{mb}$$

Fig. 11. Cylindrical Spine

$$q_o = k a_1 a_2 m \theta_o \tanh mb$$

$$\eta = \frac{\tanh mb}{mb}$$

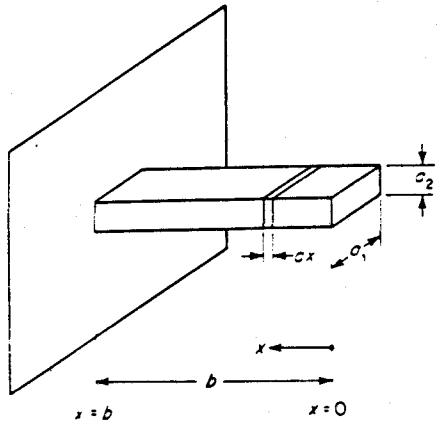

Fig. 12. Rectangular Spine

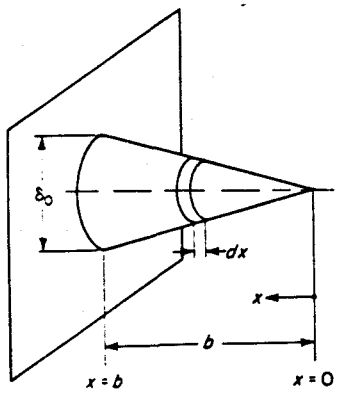

Fig. 13. Conical Spine

$$q_o = \frac{\pi k \delta_o^2 \theta_o M}{4\sqrt{b}} \frac{I_2(2M\sqrt{b})}{I_1(2M\sqrt{b})}$$

$$\eta = \frac{\sqrt{2}\, I_2(2\sqrt{2}\, mb)}{(mb) I_1(2\sqrt{2}\, mb)}$$

$$M = (2m^2 b)^{1/2}$$

$$M = \sqrt{2}\, mb$$

$$q_o = \frac{\pi k \delta_o^2 \theta_o [-3 + (9 + 4M^2)^{1/2}]}{8b}$$

$$\eta = \frac{3}{2m^2 b^2} \left[-\frac{3}{2} + \frac{1}{2}(9 + 4M^2)^{1/2}\right]$$

$$= \frac{2}{1 + (1 + \frac{8}{9} m^2 b^2)^{1/2}}$$

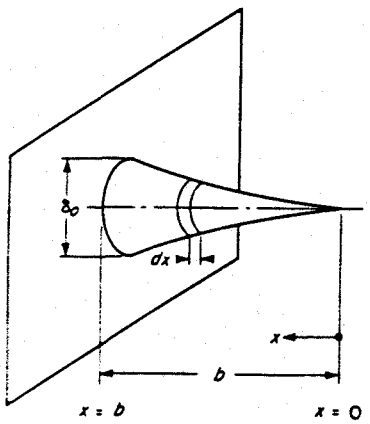

Fig. 14. Spine of Concave Parabolic Profile

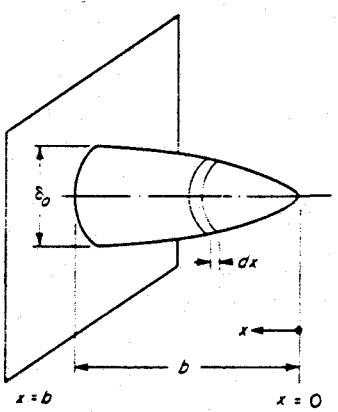

Fig. 15. Spine of Convex Parabolic Profile

$$q_o = \frac{2}{4} k\pi \delta_o^2 \theta_o m \left[\frac{I_1\left(\frac{4}{3}\sqrt{2}\, mb\right)}{I_0\left(\frac{4}{3}\sqrt{2}\, mb\right)}\right]$$

$$\eta = \frac{1}{(2\ \ 2/3)mb} \left[\frac{I_1\left(\frac{4}{3}\sqrt{2}\, mb\right)}{I_0\left(\frac{4}{3}\sqrt{2}\, mb\right)}\right]$$

APPENDIX B

MODIFIED BESSEL FUNCTION APPROXIMATION

To find $I_o(x)$, modified Bessel function of order zero, the following was used for computer solution. From definition

$$I_o(x) = \sum_{m=0}^{\infty} \frac{x^{2m+n}}{2^{2m+n}\, m!\, (m+n+1)}$$

now for n = o and the identity that $\Gamma(m+1) = m!$ then substituting

$$I_o(x) = \sum_{m=0}^{\infty} \frac{x^{2m}}{2^{2m}\, m!m!}$$

For computer applications, which gives accuracy to at least five places, the following was used

$$I_o(x) \sum_{m=0}^{10} \frac{x^{2m}}{2^{2m}\, m!m!}$$

APPENDIX C

OUTSIDE HEAT TRANSFER COEFFICIENT CHANGES WITH FIN/TUBE GEOMETRY

Assume turbulent flow that is correlated by the following expression

$$j = \frac{h\ Pr^{2/3}}{G\ C_p} \qquad \frac{0.023}{Re^{0.2}}$$

or

$$h = \frac{0.023\ GC_p}{Pr^{2/3}\ Re^{0.2}}$$

then the ratio of heat transfer coefficients between two geometries is then

$$\frac{h_1}{h_2} = \left(\frac{G_1\ C_{p1}}{Pr_1 Re_1^{0.2}}\right) \quad \left(\frac{Pr_2\ Re_2^{0.2}}{G_2\ C_{p2}}\right)$$

If we assume, for simplification, that the fluid properties are the same in each case, then $Pr_1 = Pr_2$, $\mu_1 = \mu_2$, $C_{p1} = C_{p2}$ then

$$\frac{h_1}{h_2} = \left(\frac{G_1}{Re_1^{0.2}}\right) \quad \left(\frac{Re_2^{0.2}}{G_2}\right)$$

remembering that

$$Re = \frac{G\ D\mu}{\mu}$$

and $G = M/A$

then

$$\frac{h_1}{h_2} = \frac{M_1}{A_1\left(\frac{M_1\ D\mu_1}{A_1\ \mu_1}\right)^{0.2}} \quad \frac{A_2\left(\frac{M_2\ D\mu_2}{A_2\ 2}\right)^{0.2}}{M_2}$$

$$\frac{h_1}{h_2} = \left[\frac{M_1\ A_1^{0.2}}{A_1\ M_1^{0.2}\ D\mu_1^{0.2}}\right] \left[\frac{A_2\ M_2^{0.2} D\mu_2^{0.2}}{M_2\ A_2^{0.2}}\right]$$

$$\frac{h_1}{h_2} = \left(\frac{M_1^{0.8}}{A_1^{0.8}\ D\mu_1^{0.2}}\right) \left(\frac{A_2^{0.8}\ D\mu_2^{0.2}}{M_2^{0.8}}\right)$$

if the total flow available is the same in each case, the above reduces to

$$\frac{h_1}{h_2} = \left(\frac{A_2 D\mu_2^{0.2}}{A_1 D\mu_1^{0.2}} \right)$$

if the total free flow area outside the tubes is simply a multiple of the number of tubes then

$$\frac{h_1}{h_2} = \frac{N_{t2}\ a_2\ D\mu_2^{0.2}}{N_{t1}\ a_1\ D\mu_1^{0.2}}$$

where a is the area associated with a single tube.

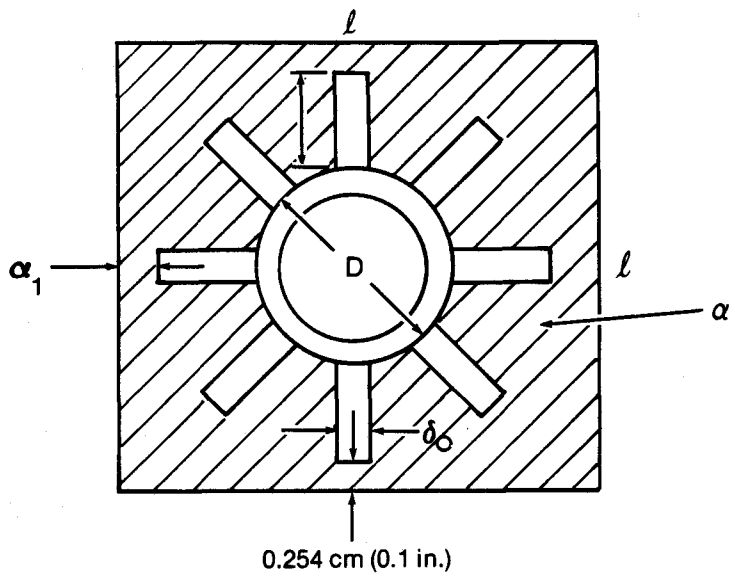

Figure C-1. Tube Geometry

The outside hydraulic diameter is equal to

$$D = 4r = 4L \frac{A_c}{A_s} \qquad \frac{\text{free flow area}}{\text{surface area}}$$

$$A_s = \underbrace{(\pi DL - N_f \delta_o L)}_{\text{tube}} + \underbrace{N_f (2bL + \delta_o L)}_{\text{fins}} = L(\pi D + 2N_f b)$$

The total area is

$$A_T = \ell^2 = (D + 2b + 0.2)^2$$

and the area occupied by the fin tubing is

$$A_{FT} = \frac{\pi D^2}{4} + N_f b \delta_o$$

the free flow area is then

$$A_c = a\,(D + 2L + 0.2)^2 - \frac{\pi D^2}{4} - N_f b \delta_o$$

the hydraulic diameter is therefore

$$D_M = 4L\,\frac{A_c}{A_s} = \frac{4[(D + 2b + 0.2)^2 - \pi D^2/4 - N_f b\,\delta_o]}{(\pi D + 2N_f b)}$$

Now an expression for the heat transfer ratio can be given in terms of the system geometry. This is (remembering that $A_c = a$) and taking a unit length (L = 1)

$$\frac{h_1}{h_2} = \frac{N_2 a_2 D_2^{0.2}}{N_1 a_1 D_1^{0.2}} = \frac{N_2\,A_{c2}}{N_1\,A_{c1}}\;\frac{\left(4L\,\dfrac{A_{c2}}{A_{s2}}\right)^{0.2}}{\left(4L\,\dfrac{A_{c1}}{A_{s1}}\right)^{0.2}}$$

and

$$\frac{h_1}{h_2} = \left(\frac{N_2\,A_{c2}^{1.2}}{A_{s2}^{0.2}}\right)\left(\frac{A_{s1}^{0.2}}{N_1\,A_{c1}^{1.2}}\right)$$

substituting yields

$$\frac{h_1}{h_2} = \left(\frac{N_{t2}}{N_{t1}}\right)\left(\frac{\pi D_1 + 2N_{f1}b_1}{\pi D_2 + 2N_{f2}b_2}\right)^{0.2}\left[\frac{(D_2 + 2b_2 + 0.2)^2 - \pi D_2^2/4 - N_{f2}b_2\delta_{o2}}{(D_1 + 2b_1 - 0.2)^2 - \pi D_1^2/4 - N_{f1}b_1\delta_{o1}}\right]$$

this expression gives the relationship of the heat transfer coefficient for two cases with different fin tube geometries. The above is not free from sizing considerations as the number of tubes in the bundle (N_t) determines the outside flow parameters (Re,h) which in turn governs the bundle length.

This determination is important because the analyses in the text assume a constant outside heat transfer coefficient for all fin/tube geometries analyzed. In reality, with all other things being equal, as the fin height increases, the spacing between the tube increases which in turn increases the free flow area for thegas to pass through. This has the effect of decreasing the outside heat transfer coefficient and he assumption of a constant heat transfer coefficient is invalid. This assumption is only true if the number of tubes in the system is not changed to accommodate larger flow areas. If the number of tubes is changed, however, the geometries and pressure drops of the heat exchanger bundles also is affected.